Technical University of Denmark

Paakitsoq Hydro Power Plant

Thermal Modelling of a Subsurface Permafrozen Tunnel in Rock

August 8, 2016

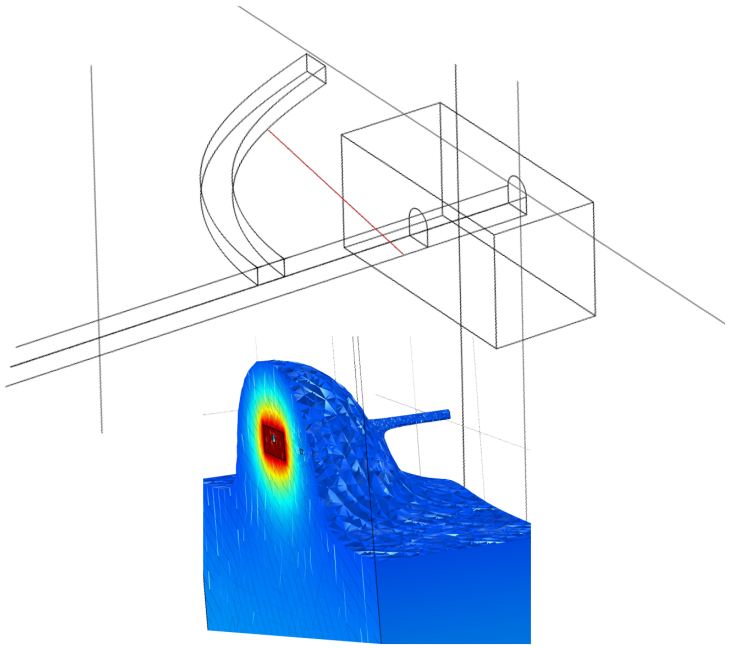

Nils Solheim Smith S123001

Peter Ladefoged S123098

Final Project: Paakitsoq Hydropower Plant
Technical University of Denmark
August 8, 2016

Contents

List of Figures

List of Tables

1 Preface

This report is rated at 20 ECTS points and is a final graduation project for Nils Solheim Smith and Peter Ladefoged. It is written at the Department of Arctic Engineering, Technical University of Denmark.

The authors would first and foremost like to thank their supervisors Thomas Ingeman-Nielsen and Niels Foged for their expertise and guidance. Furthermore a thank you must go out to external supervisor Henrik Mai at NIRAS, for helping to acquire literature for this study.

Also thank you to Egil Borchersen and the rest of the ARTEK administration, for helping in setting up and getting started on this project.

The authors also have to acknowledge the help and effort by client, designer and contractor from the Paakitsoq hydro power project, in regards to this report. Respectively, thank you for time and patience: Nukissiorfiit, Verkís and Istak.

Both group members have contributed equally to the project, whether in regards to data processing and analysis, modelling or writing. All units in this report are given in SI.

Nils Solheim Smith Peter Ladefoged S123001 S123098

2 Resume

This report presents a review of the construction and operation of the Paakitsoq hydropower plant. The plant is located in the Disco Bay Area of Western Greenland.

The report has been produced by data collected from many different sources, both academic literature and data from different interested parties. All site investigations were conducted in the period 1985-1992, by GTO. Later when actual construction began, Istak collected temperature readings as the tunnel was being blasted.

The objective of the report is to present an analysis of the thermal regime, in which the tunnel has been built. To do so, the reader will be given an account of the theoretical principles, concerning the issues at hand. These include knowledge into engineering conditions in the Arctic, geology, rock mechanics, thermodynamics and finite element modelling.

The main task of the report is to examine the disturbances of the thermal regime (expected thawing effects) over time. This includes handling of data from preliminary site investigations and measured data while the project was being constructed.

The first priority of the thermal analysis, is concerned with the presence of permanently frozen rock and the risk of thawing.

The results of this report will mainly be driven by COMSOL Multiphysics - a FEM software. As the authors have no previous experience with COMSOL Multiphysics, or setting up an elaborate modelling scheme, this report is learning process into modelling. Furthermore, modelling results will be validated with substantial analytical analysis.

An initial steady state distribution will first be modelled. This is followed by several transient (time-dependent) models, which will describe the development of thawing over time. The modelling focus will be on the area surrounding the power station, where the largest thaw bulb is expected.

Finally, comparisons of the obtained modelling results and measured temperature data from Istak will be done.

Some of the main conclusions of this report are:

- It is possible to construct and operate a subsurface hydro power plant in a permafrost regime, with emphasis on the necessary considerations.
- Several models of Paakitsoq power plant have been created, which satisfactory mimic the physical reality, specifically of the thermal development.
- The construction period and the operational period of the hydro power plant have been modelled in several time steps. The modelled maximum thaw bulb radius reaching 80 meters.

3 Introduction

This report will analyse the design and construction plan of a small scale hydro power plant. It is located on the western coast of Greenland, north of the town of Ilulissat (Jakobshavn). The area in question is referred to as Paakitsoq.

Within the last few decades several hydro power plants have been planned, designed and constructed throughout Greenland. The idea was to modernize the energy sector and replace vintage fossil fuel systems. In turn, hydro power offers renewable, sustainable and CO_2 neutral energy. The hydro power plant in Paakitsoq was dimensioned to sustain 4600 inhabitants with electricity and heat production. The power station has three turbines, each of which has an effect of 7.5 MW, according to the owner and energy company, Nukissiorfiit. Paakitsoq is fed by two reservoirs, unique for this plant, the main reservoir, lake 187, is fed in direct contact with the inland ice cap.

The construction work commenced in 2011. By blasting a tunnel network, to conduct the water, with a head of 187 meters from lake to sea. The length of the tunnel is approximately 3 km.

In small and isolated societies it is important to have a steady supply of reliable energy. The reason for this being that no coupling of infrastructure exists between towns, which is a natural consequence of their isolation and low populations. Luckily, one of the natural and renewable resources, which Greenland undoubtedly possess is hydro power.

This is due to the differential elevation from mountain terrain to sea level, in which the potential energy may be converted into kinetic energy. In Greenland fresh, surface water from lakes can be used. The fresh water supply, originates from precipitation and melt water from the inland ice cap.

As the climate in Greenland is generally cold, because of its northern latitude, special Arctic conditions exists. The main Arctic condition, that exists in relevance to this report is the occurrence of permafrozen rock and soil. Via preliminary site investigations, made by GTO primarily in the 1980s, it has been concluded that the bedrock surrounding the Paakitsoq hydro power scheme, is underlain with permafrost. This could potentially cause problems, as the water being led through the tunnel system will be close to 0°C. Furthermore, a thaw bulb from the warmth of the power station would develop over time, causing previously undocumented changes in the thermal regime of the mountain.

This report sets out with the main purpose, to conduct research into the field of thermal modelling. To further elaborate; the authors set out to research the effects of construction work and daily operation of the hydro power scheme, on the thermal regime of the surrounding bedrock.

This has led the authors to set up the following questions:

- What is the theory behind thermal physics, permafrost and rock mechanics, driving this report? What considerations must be taken before constructing a hydro power plant in permafrozen rock?
- What analytical solutions exits in the literature and how may these substantiate computer modelling?
- How does a discretization scheme work and what limitations does it entitle, in relevance to finite element modelling?
- How can material parameters be derived, that may best possibly describe a realistic scenario for the initial temperature distribution in the rock?
- What effects have the construction work period had on the initial steady state conditions for an air-filled tunnel?
- How does the construction work thermal regime prediction compare to measured data?
- What effects have daily operation of the power plant, in different time intervals, had on the thaw bulb development?

- What are the future prospects for the Paakitsoq hydro power plant, as a result of the predicted thermal development?

The scope of this report is to investigate the thermal effects of construction work and operation of the Paakitsoq hydropower plant, and to examine the theory behind these developments. The above mentioned statement leads on to the limitations of this report. As the project includes modeling the power plant and its surrounding rock mass in computer software, ome of the model geometry will be simplified and handled axisymmetrical. This is done in order to save computation time. Furthermore it is done to avoid an overly high degree of detail.

The questions of interest have been an undergoing process, meaning that these have been shaped while producing this report. This has given the authors some freedom is shaping the outcome towards the best possible scenario in terms of, what has been possible modelling wise.

4 Locality & Climate

In accordance with Figure 1(a), indicated by the red circle, the hydro power plant of Paakitsoq is located on the western coast of Greenland. The reference coordinates for this locality are given in Table 1. The locality is just north of the Arctic Circle, defined as the latitude 66°33'46", which divides the Northern Temperate Zone from the Arctic. Figure 1(b) is an overview of the Disco Bay Area of Western Greenland. Again the Paakitsoq area is indicated by a red circle. Figure 1(c) is the final zoom-in on the locality.

Table 1: GPS Coordinates for Paakitsoq

Latitude [°:m:s]	Longitude [°:m:s]
69°28'9"N	50°16'40"W

(a) North Atlantic (b) Disco Bay Area (c) Paakitsoq Area

Figure 1: Overview of the locality. (Google, DigitalGlobe).

In terms of climate at the locality, it would be beneficial to determine a n-factor. The n-factor relates air and ground temperature to each other. Thus it is the ratio of air temperature and ground surface temperature. The n-factor becomes especially important, if information in regards to vegetation and/or snow cover is available, as these modifiers have an insulating effect on the underlying thermal regime. However, as no such information is available, the n-factor is disregarded in this report. Instead the authors utilize the fact that ground surface temperature data is available.

Figure 2 shows the mean annual surface temperature of the area in question. Figure 2 is a time dependent temperature graph, based on measurements from borehole K85903 (Section 11). Superimposed over the curves measured from different periods of time, is a sinussoidal curve, which refers to Equation 1, given byAndersland and Anderson (1978). This sinusoidal-wave depicts the time-dependent surface temperature. The annual fluctuations in surface temperature, is thus approximated by Equation 1:

$$T_s = T_g + A_0 \, sin \frac{2\,\pi\,t}{365} \tag{1}$$

where:

T_s = time dependent temperature
T_g = mean annual surface temperature
A_0 = amplitude
t = time

To set T_s with a start value the 1st of January, the sinus term in Equation 1, is replaced with the following expression, Equation 2:

$$- cos \frac{2\pi t}{365} \tag{2}$$

This is the term used to plot the Cosinus-curve in Figure 2. The amplitude is calculated as stated in Equation 3.

$$A_0 = \frac{T_{mean,max} - T_{mean,min}}{2} \tag{3}$$

The input parameters for Equation 1, A_0 and T_g are thus given as 13.9°C and -4.5 °C respectively, based on the temperature data from the aforementioned Borehole K85903.

Furthermore, Figure 2 indicates the freezing and thawing indexes for Paakitsoq. The integral above the 0°isotherm is denoted as the thawing index and the integral below the 0°isotherm is in turn the freezing index.

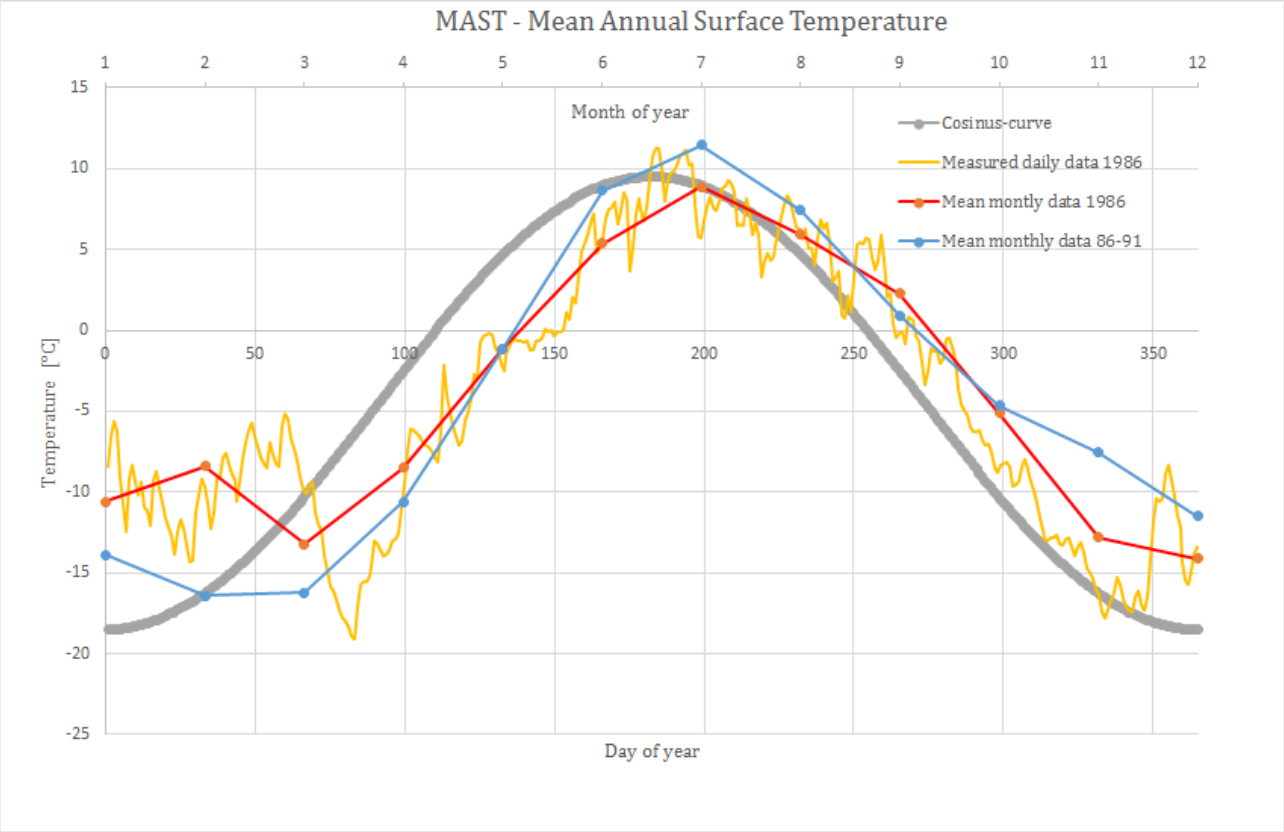

Figure 2: Mean Annual Surface Temperature (MAST) of Paakitsoq area. Data are taken from Borehole K85903.

As seen on Figure 2, mean monthly data for the year 1986, indicates a temperate year with few fluctuations. However, the variation on a daily basis may be larger and sudden temperature drops can be expected.

Mean daily data of 1986 displays quite a sporadic behaviour in the early winter and one can see that the monthly mean for 1986 lies a bit warmer than the mean for all years.

The mean data for all measured years displays a curve more in tune with the cosinusoidal curve than the daily and monthly means, however it seems to be roughly 25 days lagged. In similarity with the other means, the temperature matches well in the summer period, but is slightly warmer in the winter period.

In general throughout this report, the seasonal fluctuations will be neglected. This is elaborated in Section 6, in regards to the depth of zero annual amplitude.

5 Geology

Greenland is home to some of the oldest and most complex geological systems in the world. The orogenesis of the first rocks have been dated back to the beginning of The Archean Eon - 3.8 billion years ago. These oldest rocks of the Earth, are called Amitsoq gneiss. Granitic intrusion of this oldest part of the bedrock are still visible today near the Nuuk region (Henriksen, 2006). Around the eastern to northeastern side of the Disco Bay area in Greenland, the younger part of the bedrock is situated. This area marks the border region from the Nagssugtoqidian orogen to the Rinkian folding/thrust belt, according to Escher et al. (1999):

"Escher & Pulvertaft (1976) proposed that the Paakitsoq fault system formed the tectonic boundary between the Nagssugtoqidian and Rinkian mobile belts. "

Figure 3 is from the database of the geological survey of Denmark and Greenland (GEUS), showing the local geology of the Paaktisoq area.

Figure 3: The local geology of the Paakitsoq area. The location of the hydropower plant is located with an x. The scale legend, lower left hand corner has a magnitude of 6 km (GEUS).

The legend for figure 3, is located in the Appendix, Section 17.

Close to the area in question there is a clear dividing line between a homogeneous Archean granite and an orthogneiss, which is marked with a light yellow signature on Figure 3. Orthogneiss is formed by metamorphosis of igneous rocks. Just below the Paaktitsoq strait the partially deformed igneous granite dated from the Archean is located. This has a pink signature colour in Figure 3.

The orthogneiss is derived from the era Paleoproterozoic, approximately 2500-1600 mya, where the Archean block was folded and reworked with new granitic crustal material. After the Paleoproterozoic era the bedrock of Greenland came to look like it does today. The interior of the island became tectonically stable, a so called craton - or more specifically a shield. After this geological period only the margins of this shield would be structurally deformed.

5.1 Petrological & Structural overview of the Paakitsoq region

As previously stated the host rock of the Paakitsoq complex is based upon a orthogneiss. This orthogneiss has a migmatic composition, meaning that it is a mixture of a banded gneiss, with intrusions of igneous material. The bands of the foliated granodioritic orthogneiss, vary between light and dark colours, due to the mineral composition.

The dark colours are due to the content of sheet silicates, more specifically mica-biotite. Biotite forms flat sheet on the clevage plane and has a brittle nature. The lighter colours in the veins of the rock are caused by a quartz-feldspar intrusive constituent. The foliations may be described as plastic folds, which are caused by metamorphism in depths of 10-40 km at temperatures of 500-800°C (Henriksen, 2006).

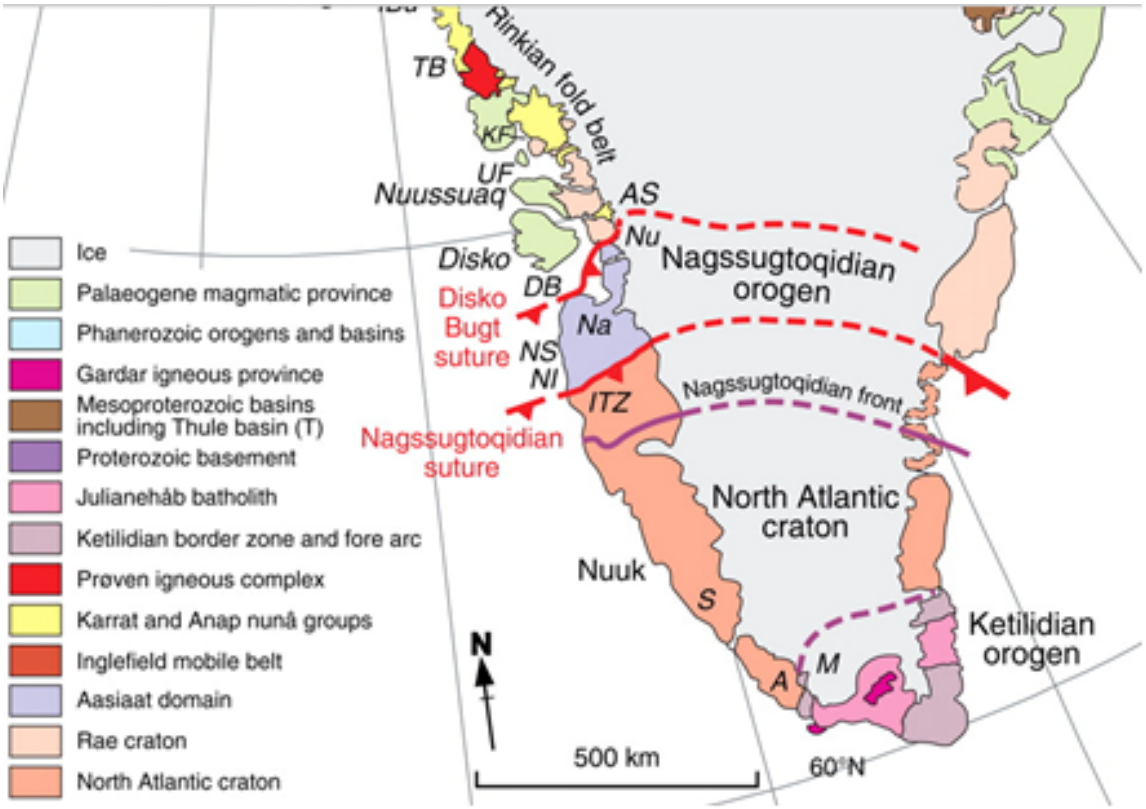

Figure 4: Geological overview of Greenland.

This metamorphism mobilized local melts to form a migmatite texture, called an anatexis procedure. This means that only a portion of the rock was melted at lower temperatures, thus allowing for intrusive veins of igneous materials with a granitic composition.

The wall of rock of the migmatic gneiss may be described as pegmatitic. Along the contact of the host rock and intrusive dike or sill a chill-margin would occur. This indicates more rapid cooling along the edges of the dike or sill and thus decreasing grain sizes.

As seen on Figure 4 the area of Paakitsoq is located within the margins of the Rinkian fold belt and the Nagssugtoqidian orogen.

Figure 5: The expected texture of the Paakitsoq area **SOURCE?!**

Figure 5 **SOURCE?!** shows the typical texture of the migmatitic orthogneiss with intrusive veins of granitic composition in the area. As previously mentioned, the Paakitsoq complex is a boundary layer between the Rinkian and the Nagssugtoqidian mobile belts. Several fault zones runs through this region with a west-northwest to east-southeast trend. Therefore the entire region may be regarded as a shear zone (Escher et al., 1999).

The foliations of the rock strike E-W with a 35-50 °angle towards south (Lennert, 2010). The dip of the foliations will in turn affect the physical thermal properties of the rock. However it should be stated that the above mentioned reference is originates from a student project at DTU. The original source of this information has not been recovered. Thus a critical approach to this statement should be kept in mind.

5.2 Mineral Composition

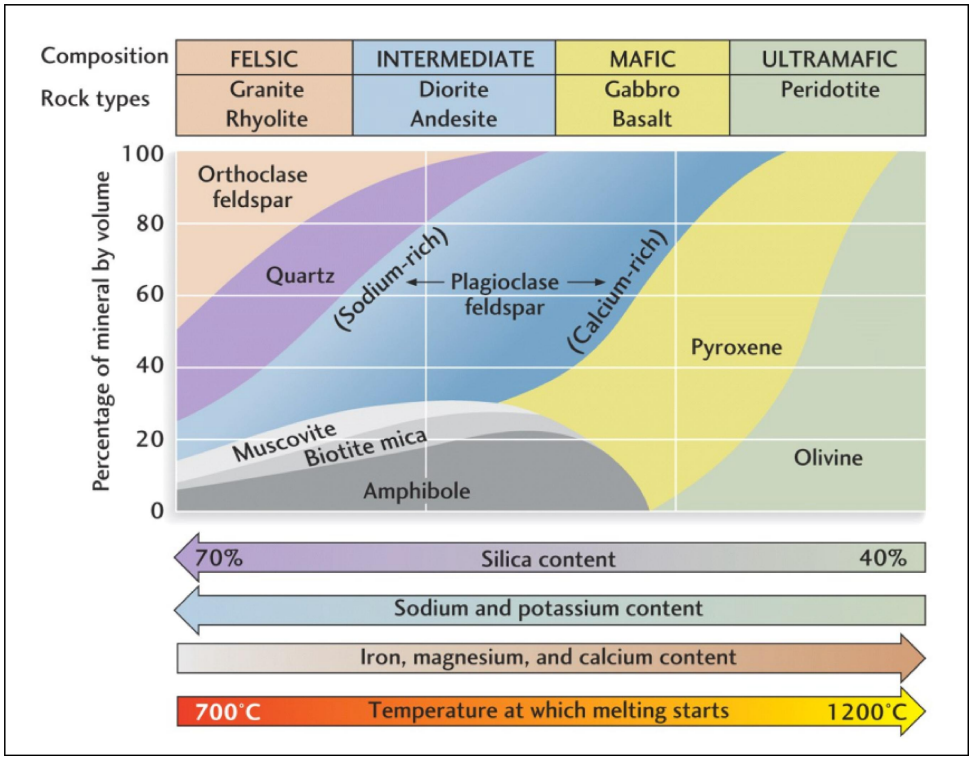

Figure 6: Mineral composition for rock types

The geology of the Paakitsoq area is based upon a host rock of migmatitic, foliated granodioritic to tonalitic orthogneiss (Escher et al., 1999). Even though the migmatic rock is more tonalitic in composition, not much data is available in the literature for tonalite. However granodiorite is more common and has almost identical properties, only differing from each other on plagioclase content. The similarities can be seen on Figure 7. According to Figure 7, both tonalite and granodiorite must have a quartz content over 20%.

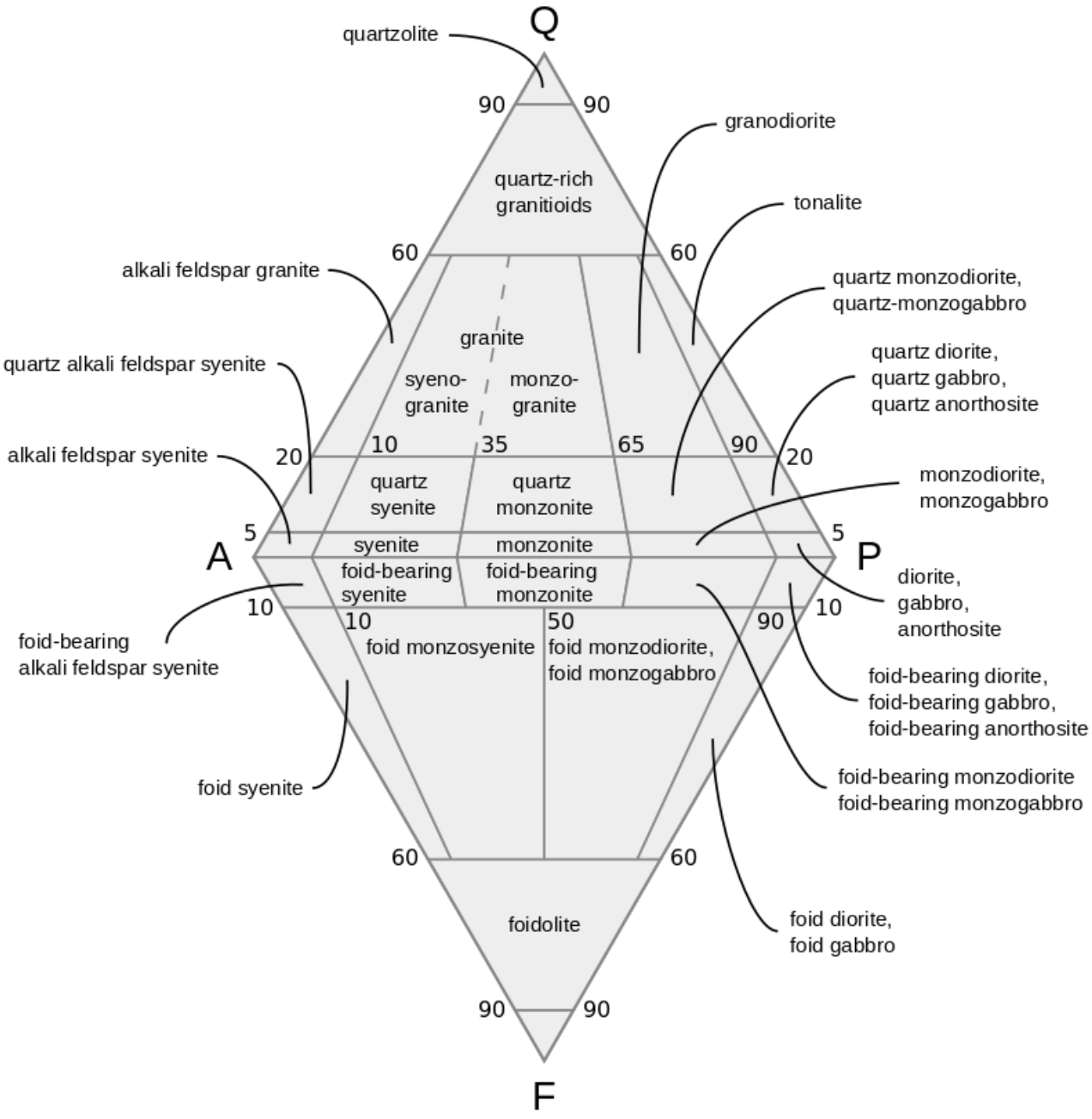

Figure 7: QAPF diagram. The composition of the minerals for granodiorite and tonalite can be seen on the upper right hand corner.

The other constituents of this host rock includes quartz, feldspar, muscovite, biotite and amphibole. This categorizes the rock as having an intermediate composition of intrusive origin (Figure 6). An intermediate composition refers to the grade of metamorphism, the rock has gone through, which is this case is medium. Thus, because of the chemical composition the starting melt of the granodioritic orthogneiss will occur at an approximate interval of 800-950°C. Thus the composition of the rocks

constituents - the minerals - are highly important for the physical properties of a given rock. As a rock type has a higher silica content, its composition becomes more felsic and the density of the rock decreases, as opposed to a rock with heavier elements such as Fe and Mg.

6 Permafrost Theory

Permafrost is considered soil or rock which is perennially frozen, having already remained below zero degrees Celsius for two consecutive years.

6.1 Permafrost Hazards

Whether or not water is present in the strata, does not influence the fact that it is perennially frozen. However, the water content is the driving mechanism regarding settlement or heave induced damages to structures. Permafrost is therefore most critical when it is active in a soil stratigraphy, due to larger pore space and higher water content. Moreover a rock mass can hold a significant amount of water and ice, if the rock is weathered and brittle or has fault zones. Under such circumstances freeze/thaw cycles could damage the rock further and cause instability in the permafrozen rock mass, for instance in regards to slope stability or tunnelling. Permafrost conditions can be neglected and conventional design and construction methods used when foundation materials are stable upon thawing. Such materials include sound rock, free of ice-filled fissures (Johnston, 1981).

Thus, in the case of the Paakitsoq hydropower plant, the problem of permafrost degradation will not cause any stability problems, as the rock is sound and the materials in general are non-frost susceptible (Section 7). Furthermore as stated, the RQD value is for the most part very high, stating a high quality of competent rock. Therefore it should not be expected to find a high porosity and resulting water and ice content.

However Johnston does go on to explain: It must be emphasized that significant amounts of ice are frequently found in all types of bedrock and may occur to depths of 20 or 30 ft or more, not only in sedimentary formations but also in igneous or metamorphic rocks. This ice results from the freezing of surface or ground water, which has percolated or been injected along or into joints, fractures, seams, bedding planes and voids or cavities in the rock. (Johnston, 1981)

The above mentioned reference indicates that even though it is very unlikely, one cannot be indifferent towards the presence of water and ice, even in a solid, competent rock. However one must also expect that with increasing depth into the mountain the fissures will minimize, which can be seen on the drill-log, decreasing the porosity of the rock mass.

6.2 Permafrost Distribution

The distribution of permafrost in the world are often represented in three zones: continuous, discontinuous and sporadic. Figure 8(a) shows the extent of permafrost in the Arctic. Figure 8(b) shows the different permafrost zones on an overview map of the Arctic. The distribution in Greenland is predominantly continuous. Only near the shoreline, on the southern part of the country discontinuous zones of permafrost is found.

The location of the Paakitsoq hydropower plant is according to Section **??** well into the continuous zone, at a latitude of 69°28′09″N. This is also seen from figure 8(b). The continuous zone is characterized by permafrost extending to great depths and few or no taliks.

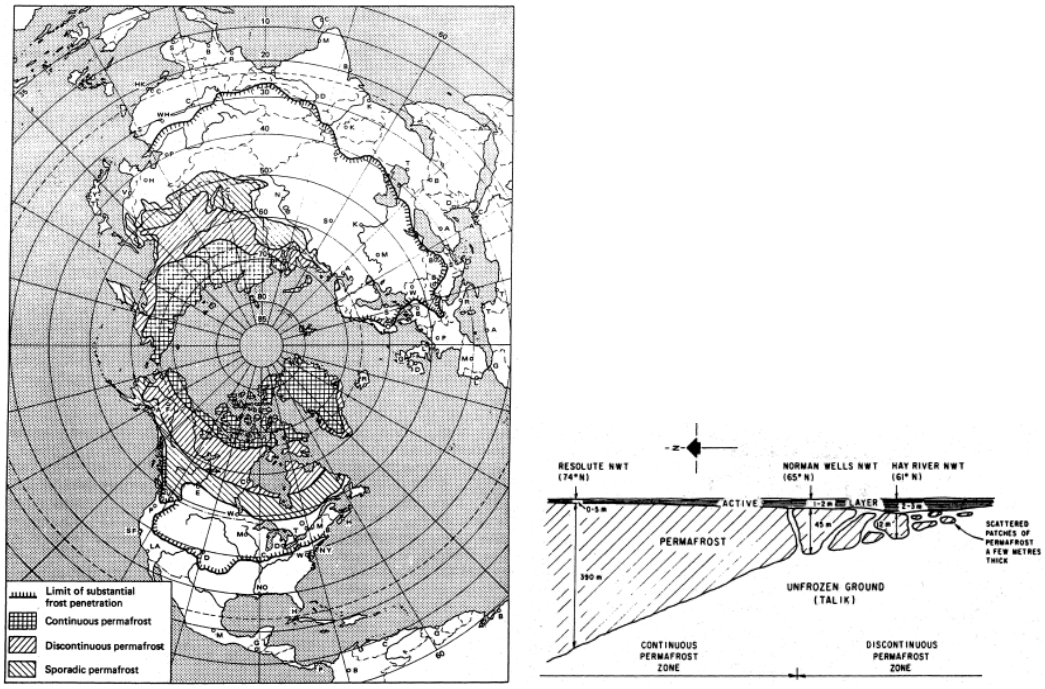

(a) The distribution of permafrost in the Arctic. (b) A schematic representation showing the extent of permafrost.

Figure 8: Overview of permafrost distribution and typical schematics (Andersland and Anderson, 1978)

.

Figure 9 depicts the theoretical permafrost distribution through a rock or soil column. This type of graph is called a trumpet-curve because it shows annual amplitude of temperature (x-axis) as a function of depth. An active layer is indicated near the ground surface. This is the part of the ground that annually thaws and freezes. Just below this border is the permafrost table.

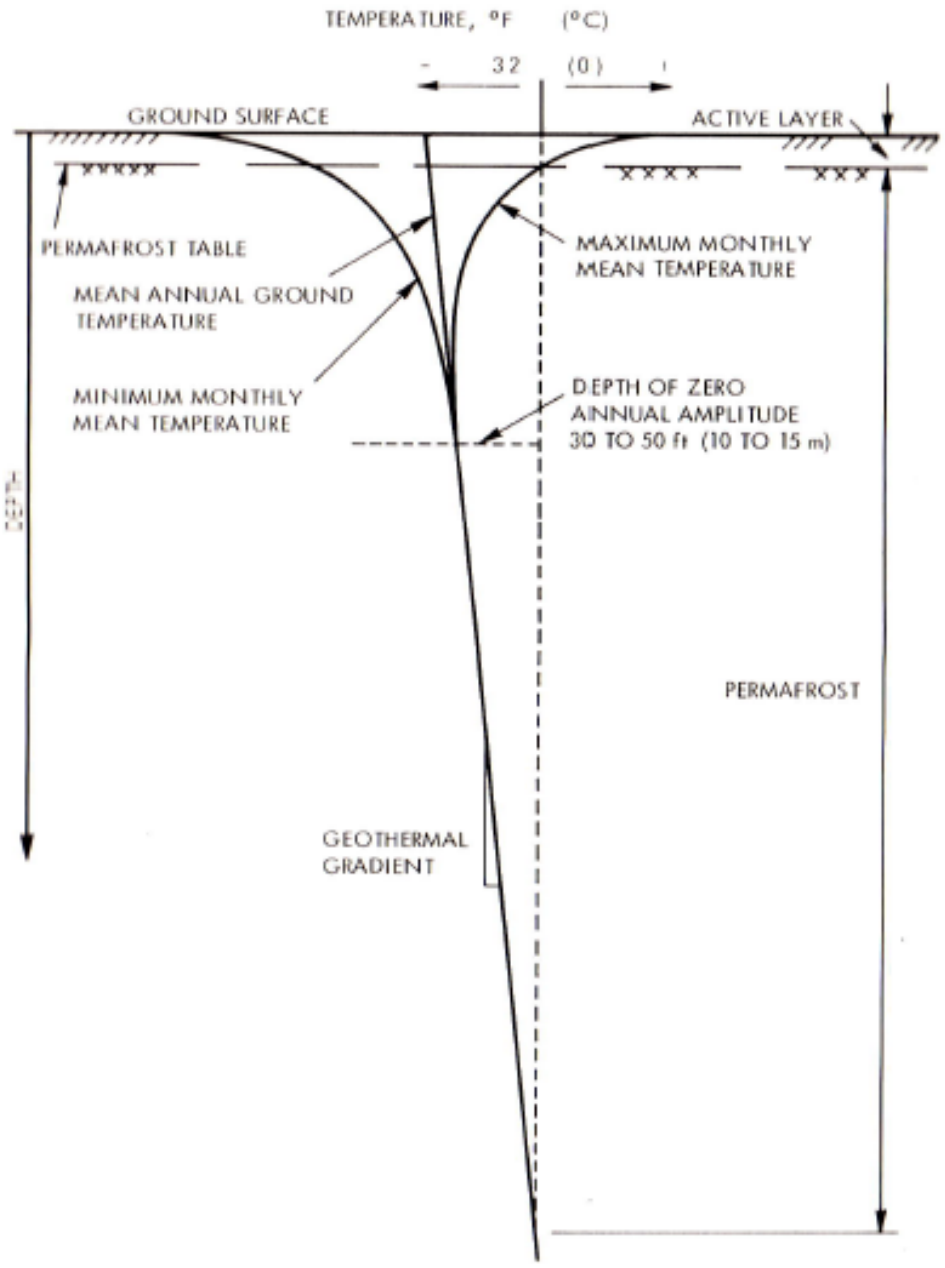

Figure 9: A typical depiction of the ground temperature regime in permafrost (Johnston, 1981)

The amplitude decreases with depth, as the impact of the varying atmospheric temperature decreases. Thus the heat balance becomes stable with depth until the depth of zero annual amplitude. From this depth and downwards the only heat source affecting the permafrost, is the geothermal gradient. Therefore the temperature gradient below this point may be considered constant. The geothermal gradient is a local factor, indicating how much heat is transferred from the center of the Earth towards the surface. This is equivalent to the local heat flux, when considering the product of a given material's thermal conductivity and the in-situ geothermal gradient.

The extension of permafrost is characterized by the intersection of the trumpet curve at the upper and lower boundary with the 0°C-isotherm.

7 Rock Mechanics

7.1 Interpretation of Borehole Data

Available borehole data for this project originates from preliminary site investigations in the 1980s, executed by GTO (Greenlands Technical Organization). These boreholes are aligned in a north-northwest to south-southeast longitudinal profile, approximately following the routing of the tunnel. This includes boreholes near the intake of lake 187 to the interior of the peninsula to the discharge area in the Paakitsoq fiord. Figure 10 shows this overview

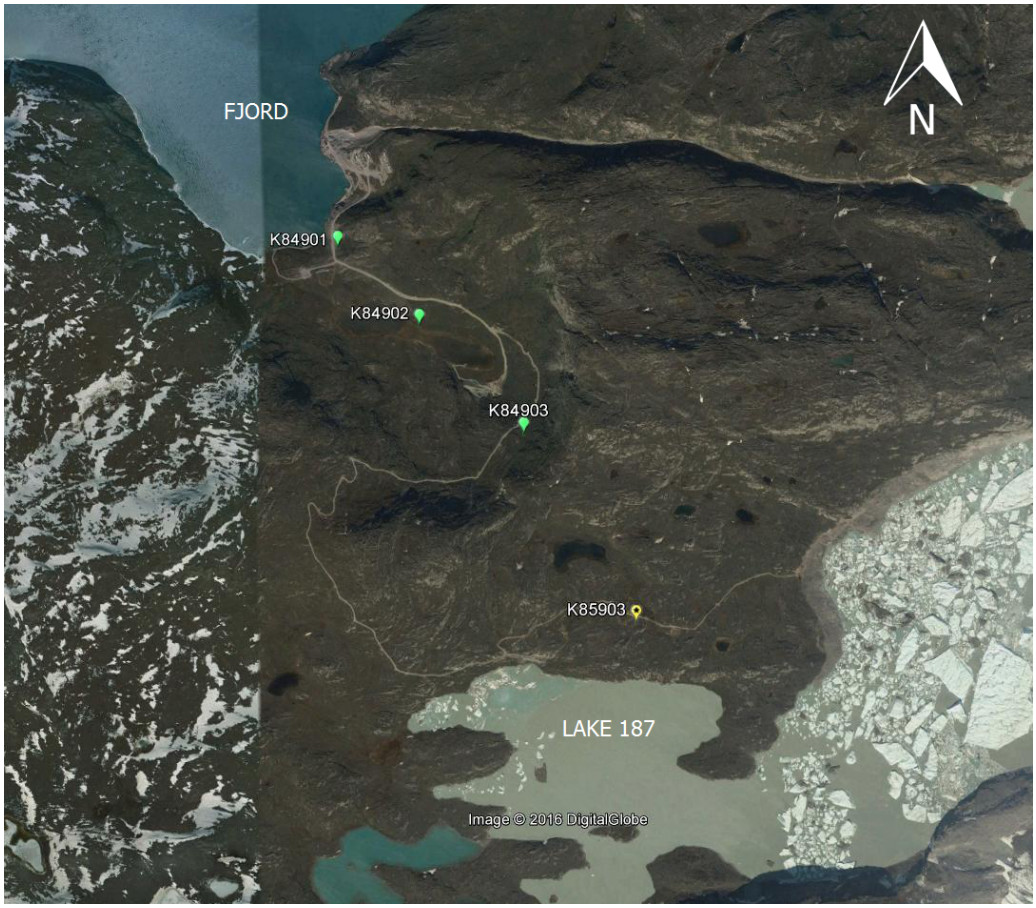

Figure 10: An overview of the boreholes along the tunnel alignment (Google, DigitalGlobe).

In the following sections a brief report of each site-investigation boreholes will be conducted. The most thorough of these reports will be on borehole K85903, as this is the main references for the initial temperature. Furthermore, it is believed to be representative for the stratigraphy of the relative small region - approximately 4 kilometres from lake 187 to the Paakitsoq fiord.

The boreholes are described in order from closest to lake 187 to Paakitsoq fiord. At the end of these descriptions, a summary of the most important lessons from the drill-logs will follow.

7.1.1 K85903

This borehole has a depth of 250 meters with a vertical orientation. It is located at a surface elevation of 239,3 meters.

The host rock is predominantly weakly foliated, coarsed grained, crystaline orthogneiss. This has inclusions of zones with pegmatite and micas, as well as quartz veins. Crushed and fractured zones are dominated by the coarse grained pegmatite.

At a depth of 28 meters in the borehole, a RQD value of 50-25 % has been observed. This zone has a high number of natural joints and fractures occurring more than ten times per meter. Likely due to its proximity to the surface of the rock formation, allowing for climatic weathering effects. For further investigation this and other smaller crushed zones are being disregarded as insignificant data.

Overall an RQD of 100-90 % has been found, with few to no fractures in the range of 0-5 joints/meter. No other data regarding thermal or mechanical properties has been collected for K85903.

7.1.2 K84903

This borehole has a depth of 59 meters with a vertical orientation. It is located at a surface elevation of 135 meters.

As with the previous borehole, K84903 primarily consists of crystaline orthogneiss with inclusions of biotite, and pegmatite zones, also including quartz veins. Foliations occur. The RQD is in the range of 100-90 % and the number of natural cracks are from 0-5 per meter. Thermal and mechanical properties were measured for K84903.

7.1.3 K84902

This borehole has a depth of 59 meters with a vertical orientation. It is located at a surface elevation of 31.6 meters.

The rocktype structure is similar to that of the previous boreholes. The RQD however does tend to be at a lower quality ranging from 100-75 %, with natural occuring cracks of up to 15/m.

It is noted that a layer of moraine has been found in the upper 8 meters of the stratigraphy in this borehole. Thermal and mechanical properties were measured for K84902.

7.1.4 K84901

This borehole has a depth of 73 meters with a dip of 60 °and a strike of 310°N, the resulting vertical depth is 63.2 meters. It is located at a surface elevation of 42.1 meters.

The rocktype structure is similar to the previous descriptives. The RQD is in the range of 100-80 %, with a low degree of naturally occurring cracks.

As with borehole K84902, K84901 includes a layer of moraine, which extends 2 meters near the surface. Thermal and mechanical properties were measured for K84901.

7.2 General comments

Through the above mentioned descriptions of the borehole data, an overview is established, which yields a fairly homogeneous bedrock, where the host rock is weakly-normal foliated orthogneiss with intrusions of micas and quartz veins, as well as occurences of pegmatite along the margins.

Table 2: An overview of the quality and competence of the bedrock

	Point Load Test conducted	RQD [%]	RMR
K85903	No	100-90	Very high
K84903	Yes	100-90	Very high
K84902	Yes	100-75	High
K84901	Yes	100-80	High

Table 2 gives an overview of what rock quality can be expected from each borehole. The most competent rock is located near lake 187 and that the bedrock near the fjord is possibly more weathered and eroded, leading to a lover RQD. As noted in the aforementioned sections, the stretch interpreted by boreholes K84902-K84901, found glacial-postglacial soil in the form of moraine. Thus, glacial tectonics could have had an influence on this portion of the mountain, which is in agreement with the lower elevation. However the results from the point load test does not show any decisive link.

7.3 Point Load Testing

A point load test measures a samples ability to withstand compression until failure. This has been measured in two directions for the core specimens taken at Paakitsoq - diametrally and axially.

Kahraman and Fener (2005) have conducted research into *The effect of porosity on the relation between uniaxial compressive strength and point load index.* The resulting Equation 4 and Equation 5 formulate a relationship between the point load index and UCS, dependent on the range of porosity:

For n<1% - $r^2 = 0.72$

$$UCS = 24.83 \times I_{s(50)} - 39.64 \tag{4}$$

For n>1% - $r^2 = 0.75$

$$UCS = 10.22 \times I_{s(50)} + 24.31 \tag{5}$$

where:

$I_{s(50)}$ = the point load index of a 50 mm equivalent core sample
$I_{s(50)}axial$ = 10-12.5 $[MPa]$
$I_{s(50)}diametral$ = 4.8-7.2 $[MPa]$

As noted the coefficient of determination r^2, is around 0.75 for both formulas, thus indicating a relatively high correlation. Other sources, such as Bieniawski suggest merely a factor of 20-25 times the point load index, in order to obtain the UCS (Kahraman and Fener, 2005).

The range of anisotropy based on the ratios of axial to diametrical compressional strength, for the rock samples at Paakitsoq, is between 1.75 - 2.125.

Based on the relationship between the axial and diametric strength and what is known of the geology of the area, a high variety of anisotropy can be expected, dependent on the direction of the heat flow and foliation of the bedrock. Therefore it should be noted, that it is not possible to account for the anisotropy in the models throughout this report. As it will be stated later on in Section 13, one assumption is that the rock is homogeneous and isotropic.

8 Glaciology and Arctic Lake Conditions

Greenland is covered by an inland ice cap, with most of the coastline ice free. The previous maximum glaciation occurred during the last ice age, the Weichsel era, which lasted from approximately 115,000-11,500 years ago (Henriksen, 2006). From 11,500 years ago until now, the Earth has entered an interglacial period. The dominating period is still Quaternary, while the era has shifted from Pleistocene to Holocene.

Before the retreat of the ice cap to the present day position, it extended a few hundred kilometres beyond the present day coast line. As the ice caps melt, so happens a disturbance in the state of equilibrium between buoyancy from water and weight from land and ice mass. Eustatic changes regards rise and fall in water level. These changes happen relatively rapidly in comparison to isostatic changes, which relate to the rising and sinking of continents. Areas along the coastline of Greenland, would previously have been submerged, but as the landmasses rose the coastline is left with a majestic topography.

According to Mai (2009) an Arctic lake has an average temperature of less than 4°C at any time. An Arctic lake may be fed by both glacial meltwater and/or precipitation.

As seen on Figure 12, during the winter periods the water column is stratified in regards to temperature isotherms. However, as summer comes, heating progresses and ice starts to break. After a few weeks of exposure to wind and sun, the water will become homogenized. This is seen on the bottom of Figure 12. Here for example, the theoretical temperature distribution in the month of August is very uniform, close to 3°C.

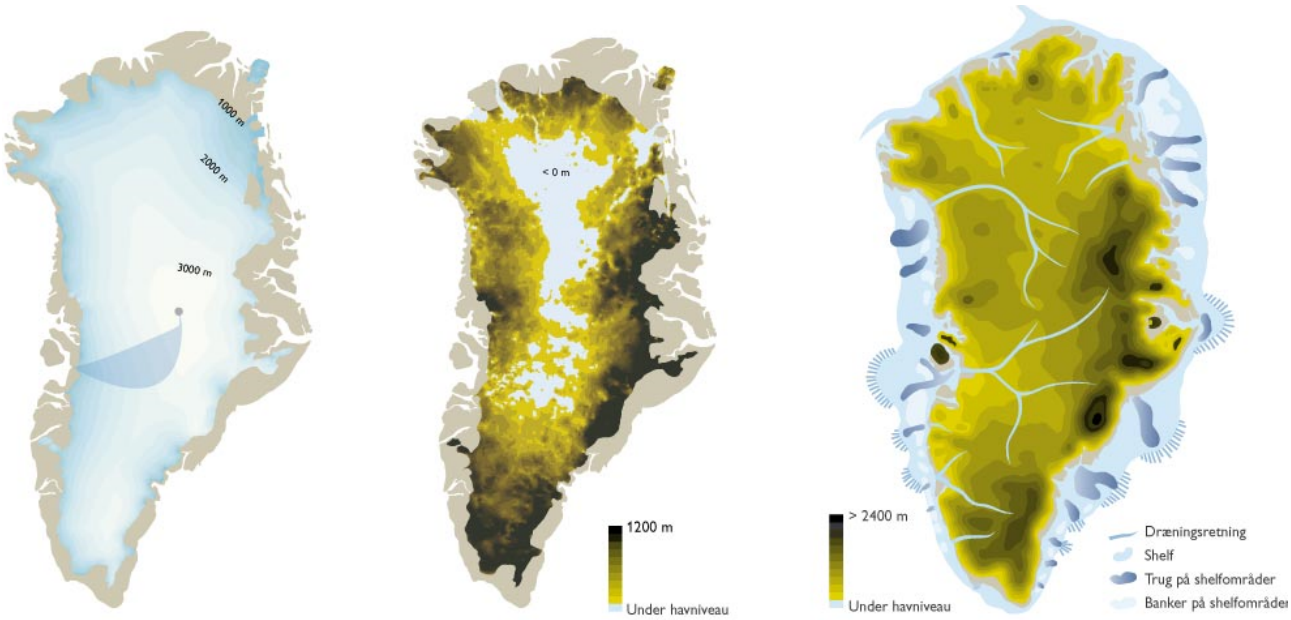

Figure 11: Left: The inland ice cap today. Middle: Topography at the bottom of the ice cap. Right: Greenland without ice cap, corrected for overburden of ice (GEUS).

As previously mentioned, Figure 11 shows the effect of isostatic and eustatic processes. If all the ice melts at one time, the scenario in the middle figure would occur. However after long time isostatic processes would cause a new state of equilibrium, as shown on the right hand figure, consequently raising the continent.

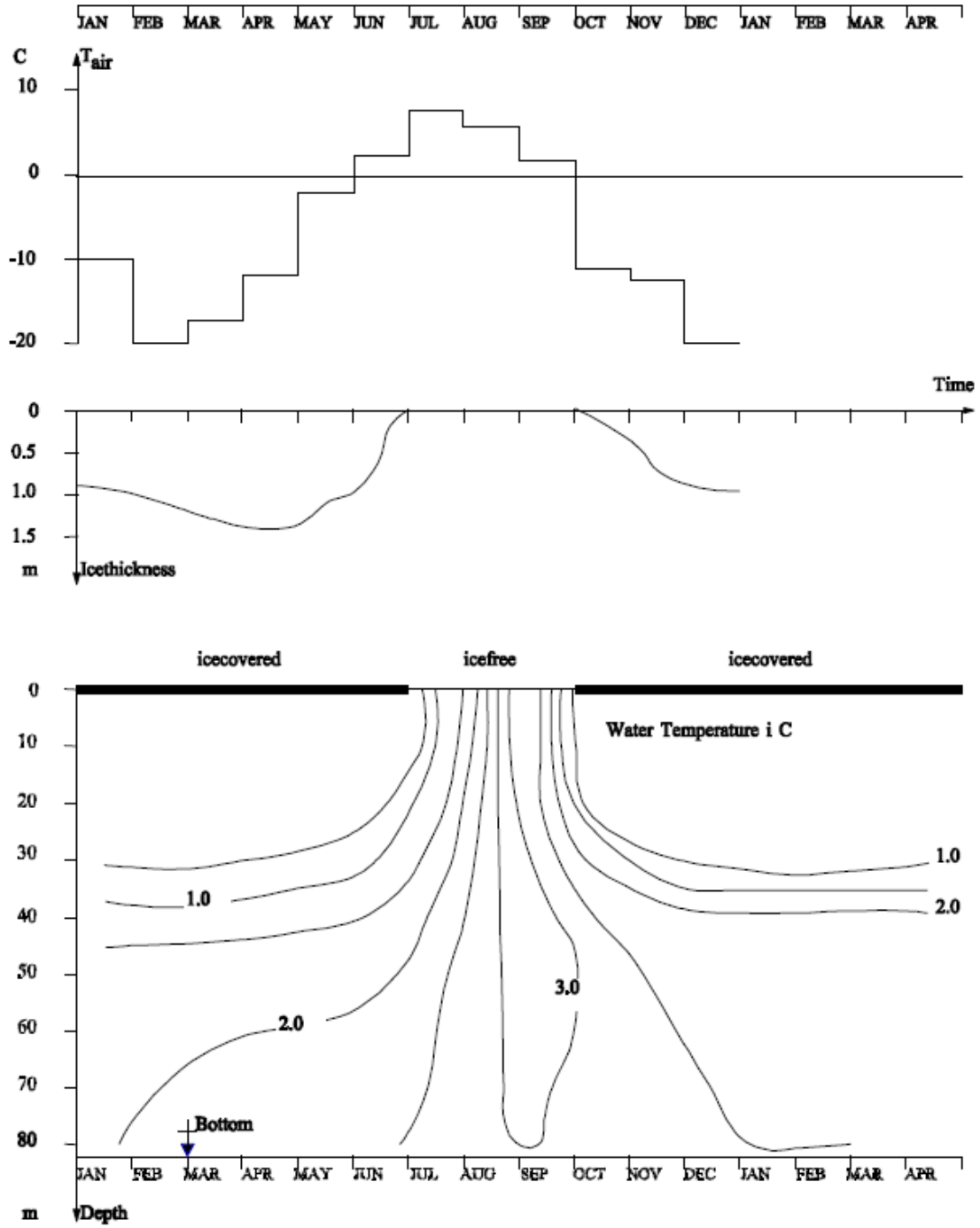

Figure 12: Theoretical temperature and ice cover distribution in an Arctic lake ((Mai, 2009)).

8.1 Paakitsoq Reservoirs

Lake 187, is located near the inland ice cap, and is being fed by a ice tongue. For this reason lake 187 is consistently colder than lake 233, which is only fed by precipitation.

A central condition, which has to be taken into account when designing hydro power schemes in conditions as Paakitsoq, are the available resources. These are in turn subdivided into summer and winter resources. In wintertime, it is important to have sufficient water left in the reservoir, as this has to cover production the entire season, until the lake once again is ice free.

Several design concerns have to be taken into account, when utilizing an Arctic lake as reservoir. Among these are blocking of residual ice, which could also cause damage to utility lines. A more relevant problem for this report however, concerns the presence of supercooled water.

Water close to zero degrees Celsius is introduced into a system of permafrozen rock, there is a real chance ice formation could occur. However, as long as supercooled water is pressurized above the atmospheric pressure, it is not an issue. However, as the water passes the power station the pressure drops, the water could be in risk of freezing.

9 Fluid Mechanics

The following section has been written in accordance with Elger (2013), for a brief overview of fluid mechanical physics, relevant for this report.

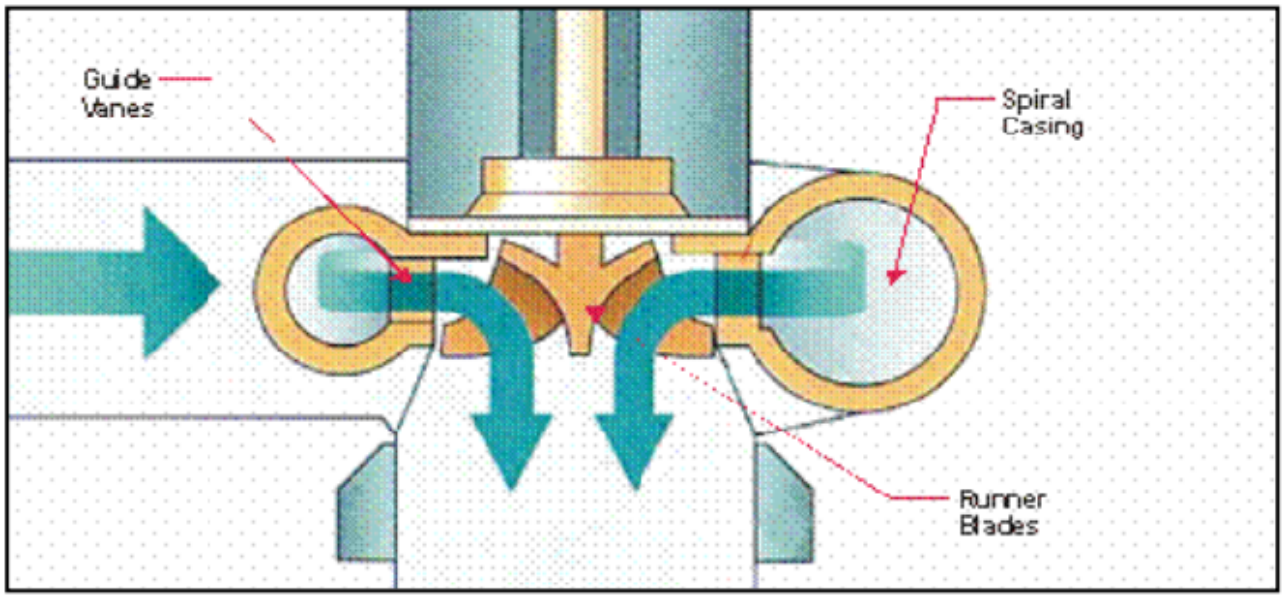

Figure 13: A typical Francis turbine

Figure 13 shows a typical Francis reaction turbine. Three of these are utilized in the Paakitsoq plant. The reaction turbine does not run at atmospheric conditions, opposite the impulse type turbine. The pressure change continuously in the flow through the Francis turbine. The Francis turbine has a mechanical effect of $> 90\%$, while the remaining kinetic energy goes to heating the water through friction.

In this report some assumptions regarding fluid flow has been made. This is particularly important later on, in the modelling section 13 and 14. The Reynolds number determine wheter a flow is laminar, transitional or turbulent, by the ratio of kinetic/viscous forces. According to the Reynolds number (Re), the regime type flow is determined by the following equation:

$$Re = \frac{\rho V D}{\mu} = \frac{1000\frac{kg}{m^3}0.02\frac{m}{s}4.6m}{1.787 \times 10^{-}3Pa \times s} = 51483 \tag{6}$$

where:

ρ = density $[1000kg/m^3]$
V = average water velocity $[0.02m/s]$
D = equivalent pipe diameter $[4.6m]$
μ = dynamic viscosity for water at 0°C $[1.787 \times 10^{-}3Pa \times s]$

The equivalent pipe diameter Equation 16, can be seen in section 12.

From the above Equation 6, it can be determined that the flow in the tunnels will most definitely be considered turbulent. All flow with Re>4000, is considered turbulent. Turbulent flow is defined as non-parallel, non-uniform streamlines in the water column, that consistently cross each other in lateral direction. Furthermore laminar flow is considered a steady, uniform flow, with parallel streamlines, that do not cross each other. Moreover velocity is constant in magnitude and direction. An example of laminar streamlines are depicted on Figure 14.

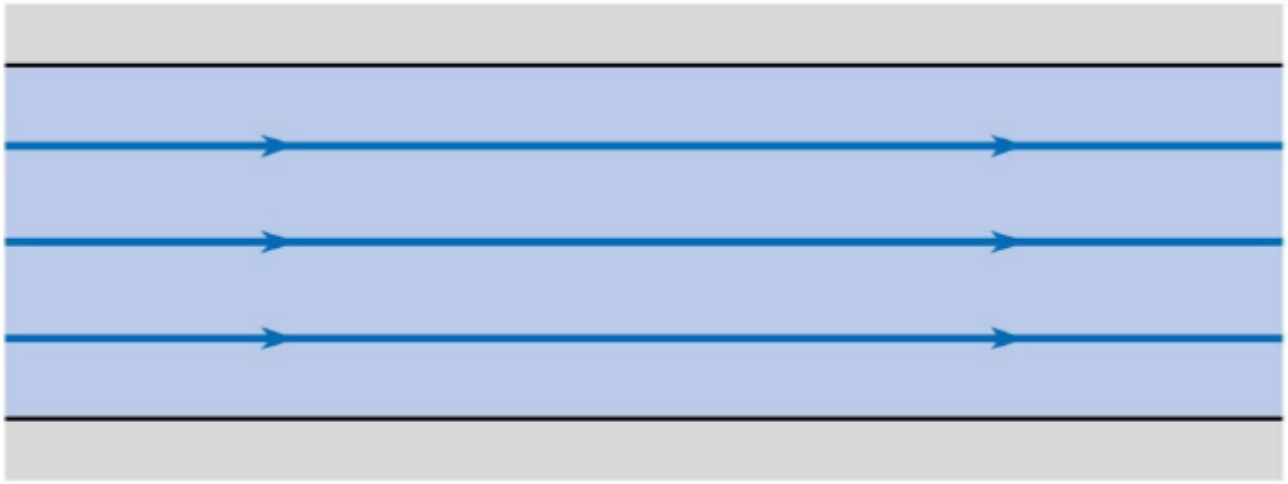

Figure 14: Idealized steady, uniform and laminar flow. (Source: Elger (2013).)

As turbulent flow is much more difficult to work with, in terms of future modelling, this fact will be disregarded and a laminar flow will be adopted. Other basic assumptions regarding laminar flow are incompressibility and that it is inviscid.

For all future intends and purposes, the water flow in this report, will be assumed laminar.

The power available from water can be expressed in the following:

$$P = \rho Q g h \eta \tag{7}$$

where:

P = power generated $[W]$
Q = water flow $[m^3/s]$
g = acceleration of gravity $[9.81 m/s^2]$
h = hydraulic head $[187m]$
η = efficiency [0-1]

With an efficiency of 90% and a minimum flow rate of $1/3 m^3/s$ it means that the power plant will have a minimum effect of 0.55 MW. If the remaining energy goes to heating the water, this will give a minimum effect of 61 kW. At most this effect in the power station, given to heating the intake water would be 750 kW, at maximum production of 7.5 MW. This means that the minimum and maximum temperature increase

Furthermore, a topic not discussed elaborately in this report, is the thermal interaction between tunnel wall and water. In previous reports studied by the authors by GEO and Verkís, amongst others, a scheme has been made, which includes thermal energy transferred from water to rock (cold to warm). This includes the thermal energy of the water, frictional energy lost over the length of the tunnel, energy gained to water in power station and freezing point depression due to pressurized water.

With an effect as mentioned above the energy, which the water will gain through the power station, is equal to:

$$\Delta\theta = \frac{P}{C_{p_water} \times Q} = \frac{61kW}{4187 \frac{kJ}{kgK} \frac{1}{3} \frac{m^3}{s}} = 0.044°C \tag{8}$$

10 Heat Transfer Theory

In order to assess the thermal development of the bedrock, one must first understand the concepts of thermal energy and the transfer of energy. Firstly, heat transfer is the transition of thermal energy, either through a body or from one body to another.

At the basis of heat transfer theory lies the general laws of thermodynamics, where the first law of thermodynamics constitutes energy conservation. This is the main principle behind the constant energy of a system, meaning that in a closed system, energy merely changes form. Consequentially, the sum of a heat flux at the boundary and the generated heat of a system is equal to the change of the internal energy of the system, (i.e., temperature). Furthermore, the thermal development is governed by the 2nd law of thermodynamics, expressed as the natural direction of energy flow or the heat flux. Direction of heat flux will always be from hot to cold, the law postulates that the flow of energy as heat through a system boundary will always be in the direction of lower temperature or along the negative temperature gradient (Kothandaraman, 2006). A common term in the language of heat transfer theory is heat flux, defined as the amount of energy that is transferred through a material per unit time, typically given in W/m^2.

Heat transfer in rocks and soil occur through three main processes, radiation, convection and conduction. In terms of this project, focus is on heat transfer through conduction and convection. The portion of heat transferred by radiation within the ground usually comprises less than a few percent of the value of the total heat flux (Yershov, 1998), and can thus be neglected.

10.1 Convection

Convection is the transfer of thermal energy through the flow of gas or a liquid. Convection is of high relevance in terms of the heat transfer through the water-bearing tunnels of the Paakitsoq hydropower plant, where the arctic lake conditions of intake water lie close to freezing temperature and later must pass through permafrost bedrock. In scrutiny, the heat transfer is in fact a combination of conduction and flow, where the water flowing along the tunnel alters temperature due to conduction with the bedrock walls. This will induce mass-movement of fluid as the colder denser fluid will sink - thus a convective process within the fluid. The steady-state heat flux per unit time due to convection, i.e., movement of pore fluid, is given by Equation 9, from Andersland and Anderson (1978):

$$Q_{conv} = c_0 \, \rho_0 \, V_0 \, \frac{\Delta \Theta}{\Delta X} \, A \tag{9}$$

where:

Q_{conv} = convective heat flow per unit time $[W/m]$
c_0 = specific heat capacity $[J/kg\,K]$
ρ_0 = the density of fluid $[kg/m^3]$
Θ = temperature $[K]$
x = distance $[m]$
A = area $[m^2]$

In regards to this project, the main convective energy transfer to be taken in consideration concerns the boundary of air above the bedrock. Here, the temperature of the atmosphere interacts with the surface of the bedrock. If the surface is warmer than the air above it, the air next to the surface has a lower density than higher layers and the warm air has a tendency to rise. This density profile is unstable and, for a large enough temperature difference, convection currents will arise (Andersland and Ladanyi, 2004). Thus resulting in a convective heat transfer between atmosphere and bedrock.

10.2 Conduction

The main and most basic mechanism of heat transfer in ground is conduction. Heat is conducted through a medium as a result of atomic and molecular vibrations in the crystal lattice, the intensity of which increase with temperature (Yershov, 1998). As water is of higher thermal conductivity than most soil and rock materials, and air is among the lowest conductive materials, naturally the saturation is of high importance in regards to the conductivity of soils. In this project, the material in question is a granitic gneiss, implicating a higher dependence on the conductivity of its inherent minerals compared to the contents of its pores.

The steady rate of heat transfer in a material by conduction is given by Fourier's law, Equation 10 (Andersland and Anderson, 1978)):

$$Q_c = -k \frac{\Delta T}{\Delta x} A \tag{10}$$

where:

Q_c = heat flow per unit time $[W]$
k = thermal conductivity $[W/mK]$
Θ = temperature $[K]$
x = distance $[m]$
A = area $[m^2]$

The negative prefix for the equation is in order to comply with the 2nd law of thermodynamics and the direction of warm to cold heat flux. Furthermore, the aforementioned heat flux, can be derived from Equation 10, rewritten as Q/A, seen in Equation 11:

$$q = \frac{Q_c}{A} = -k \frac{\Delta T}{\Delta x} \tag{11}$$

10.3 Phase Change

Central to this project is the development of ice. During phase-change at a constant temperature there is energy released or absorbed, known as latent heat. The volumetric latent heat of fusion has a dominant role in thermal calculations and represents on a volume basis the amount of heat that must be supplied to a soil below 0°C to change ice into water (Andersland and Anderson, 1978). The latent heat can be calculated by Equation 12.

$$L = \rho_d \, w(1 - w_u) \, L' \tag{12}$$

where:

L = volumetric latent heat $[J/kg]$
ρ_d = dry density $[kg/m^3]$
w = water content
w_u = unfrozen water content
L' = latent heat of water $[333 \times 10^3 J/kg]$

10.4 Material Parameters

For convection, Equation 9, the key thermal material-parameter is the heat capacity. Heat capacity relates to the amount of energy required to raise the temperature of the unit mass by one kelvin. For this project, the fluid and gas in question is water and air, where the heat capacity is well defined through decades of empirical measurement.

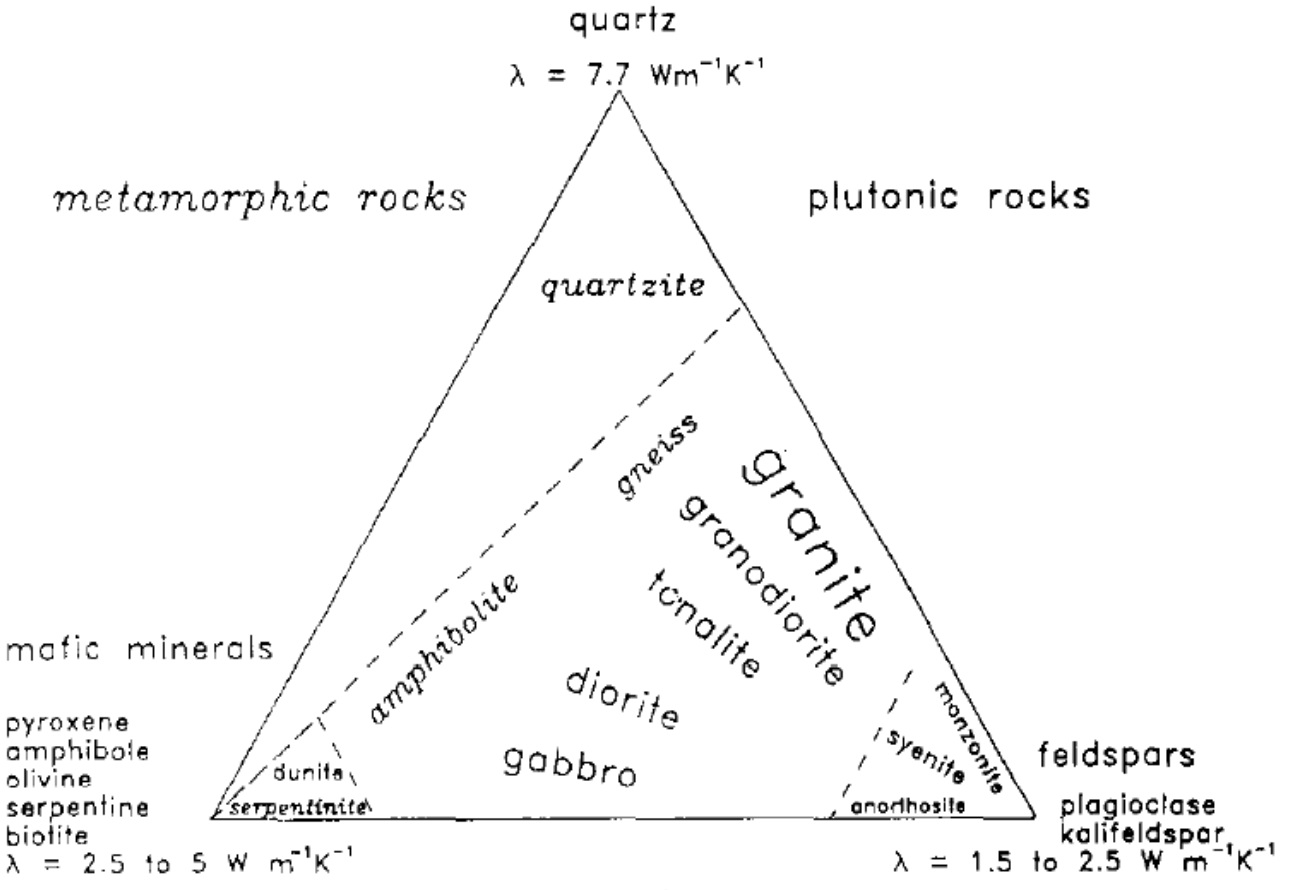

Figure 15: Thermal conductivity of intrusive igneous and metamorphic rocks, dependent on mineral composition.

As seen in Equation 10, the most central parameter for heat transfer by conduction, and thus most central for the transfer of heat in bedrock, is the thermal conductivity of the material. The conductance of heat for a material is defined as the rate of energy transfer through a thickness of material due to the difference in temperature on each side of the unit thickness.

Andersland and Ladanyi (2004) denotes granite as having a thermal conductivity varying from 1.7–4.0 W/m K and heat capacity at 800 J/kg K. For a pure quartz the thermal conductivity is given at 8.4 W/m K and heat capacity is given as 733 J/kg K. As shown, the material parameters of rocks can vary greatly depending on a few factors. Firstly, the mineral composition of the rock is highly influential, as the different minerals have vastly different conductance. Clauser and Huenges (1995) developed a chart to illustrate the thermal conductivity of different rocks, depending on the composition of individual minerals. This chart is seen on figure 15.

The charts on figure 15, are based on many different research results on micro- and macroscopic scale, giving a semi-quantitative way to look at the thermal conductivity of different rock groups and classes. Note that the italic text in the figure is in regards to metamorphic rocks, while bold text, is in regards to plutonic rocks. Per figure 15, the largest contribution from any given mineral, in regards to thermal conductivity, originates from quartz content. Per Figure 6 in comparison with the before mentioned thermal conductivity figure, they correlate well together. Thus by approximating 25-30% quartz, with a predominantly felsic composition, into Figure 15, the output will be an orthogneissic, tonalite-granodiorite.

Another factor of the values of thermal conductivity is the foliation of minerals. Not essential in the case of granite or volcanic rocks, but in metamorphosed and banded rocks such as gneiss, the crystal structure of the minerals in the bedrock are influential on the thermal conductivity. Furthermore, a point for discussion is the fact that thermal conductivity on a specific site is typically measured or

calculated through a vertical borehole, utilizing a thermal conductivity acting in the same direction. However, the anisotropy of non igneous rocks entails that the thermal conductivity is anisotropic, which can give way for varying properties.

The geothermal gradient of the earth is a primary factor in the thermal state of the bedrock, especially in permafrost regions, where the permafrost depth can be described as a boundary between the atmospheric temperatures frost depth and the geothermal heat flux from the core of the earth. The geothermal heat flux, which is effectively the product of the geothermal gradient and the corresponding thermal conductivity of the earth materials at depth, provide the basal boundary condition to practically all thermal calculations related to the ground-temperature regime (Andersland and Anderson, 1978). Typically, the gradient is defined as change of temperature per unit depth or as previously mentioned heat flux $[W/m^2]$.

In order to calculate the latent heat, one must obtain a value for the water content. In this project, the rock lies buried 100-200 meters below the surface, at a height close to mean sea level. From this the authors assume that the pores are water filled. Water saturation close to the water table, could also be assisted by capillary action.

The water content is then dependant on the porosity of the material. Porosity of the rock in question has not been measured specifically, however a range of porosities can be estimated from several other research papers - see section 12.

11 Temperature Measurements

11.1 Site Investigations

Data from borehole K84901, K84902 and K84903 was acquired from Asiaq's archives. These site investigation boreholes were installed with thermistor-strings, however they were not installed with a data-logger and required manual reading. The data was measured manually in a period from 25/09/1984 until 28/09/1988. As the boreholes are located in a relatively remote area, measurements have only been carried out between three to six times per year. The resulting data is therefore irregular in terms of continuity. Measurements have been taken in three different depths for 901 and 902 boreholes, while borehole 903 has five depths of measurement, all measure to a maximum vertical depth of 60 meters from the surface. In addition to these boreholes, the water temperature of the two intake lakes were also monitored.

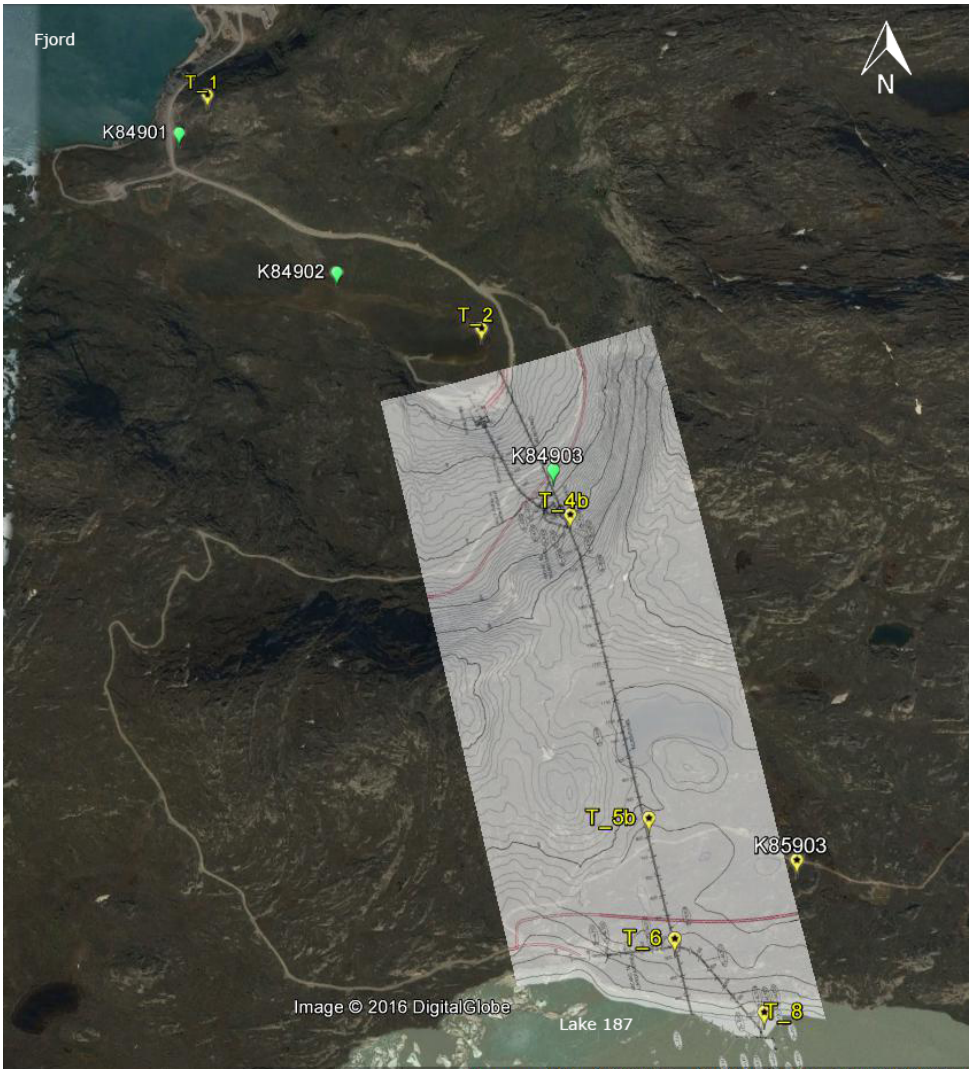

Figure 16: An overview of the tunnel and different measurement points, with blueprints overlain (Google, DigitalGlobe).

Furthermore, during site investigations one deep borehole was drilled 250 meters deep ending at roughly -12 m.a.s.l. This borehole, K85903, was installed with an automatic data-logger which was maintained from December 1985 until August 1992. The data from this borehole is the most detailed account of the reference temperature for the area and has been used to calculate the geothermal flux of the area. An overview of the boreholes and thermistor positions can be seen in Figure 16.

For all the temperature measurements made during the site-investigations, the thermistor strings in use were of the type Pt-500 resistance thermometers. Kern-Hansen (1990) argues that the thermistor strings installed in the above-mentioned boreholes maintain an error of ±0.04°C.

11.1.1 Data processing

Original data from the site investigations were used to define the boundary conditions, which is explained in further detail with regards to the modelling in section 13.

Original measurement data from the site-investigations were received in text format from the supervisor of this project. The data was organized in order to summarize the development for each of the measured depths. Firstly, minimum and maximum temperatures for each month and depth were found. Secondly, the mean temperature for every day was noted. Due to fluctuating measurement times, the data had to be analysed in order to remove months with missing data. For calculations of the mean temperature, months which were not fully represented were removed from the mean. For the trumpet curve, most of the data was used, unless more than half of the month was missing. For every depth of measurement, the minimum and maximum temperatures for each month over the years were found. This monthly value was averaged over the seven years of measurements and then used as the mean monthly minimum and maximum temperature for the trumpet curve.

11.1.2 Results

The trumpet curve is seen in Figure 17. One can see that the depth of zero annual amplitude is met at roughly 15 meters depth. Here the standard deviation from the yearly mean temperature is 0.16 °C. However to be on the safe side, the gradient is calculated from a depth of 50 meters to the bottom of the borehole.

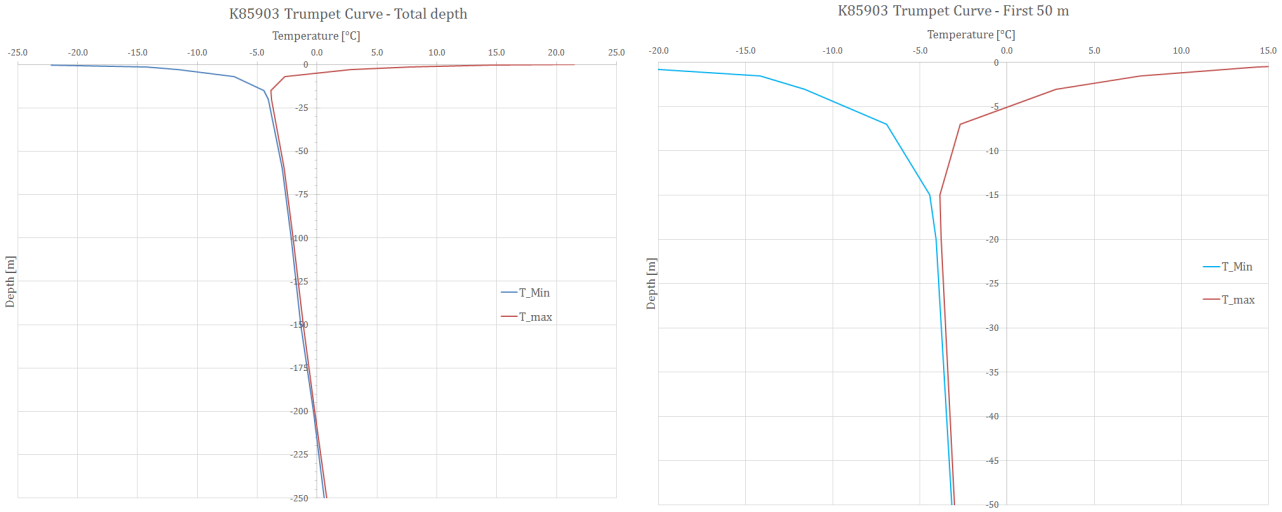

Figure 17: Trumpet curve based on temperature data from borehole K85903. Left figure displaying full depth, while figure on the right shows the first 50 meters.

Also interpreted from the temperature measurements from borehole K85903, is the geothermal gradient. As seen in Figure 17, the gradient of the slope from 50 meters, the depth of zero annual amplitude, down to the total depth 250 m. The slope of this range gives the inherent geothermal flux coming from the core of the earth, calculated and found to be 1.86°C per 100 meters (Figure 18). This result is in good coherence with previous measurements and design factors used for the Paakitsoq project. Whilst the trumpet curve is based on the minimum and maximum temperatures, the geothermal gradient is based on the mean temperatures. The result in Figure 18 is found through the linear trendline for the mean temperatures from 60 meters down to 250 meters.

*****The data in use is available in appendix***

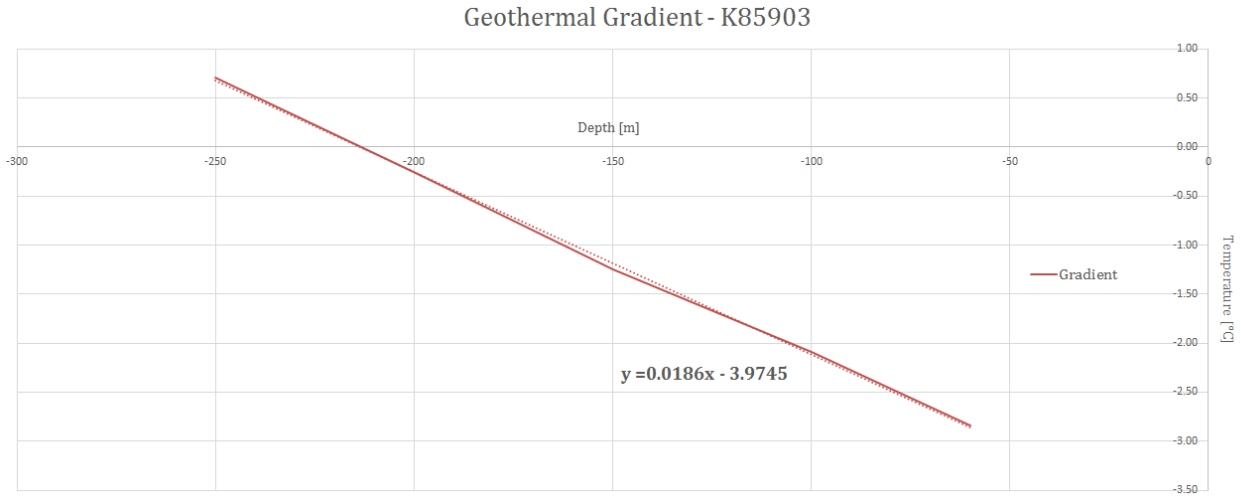

Figure 18: Geothermal gradient calculated from borehole K85903, for depth 15**** meters to 250 meters, where annual amplitude is zeroed.

11.2 Construction and Operation Period

During construction of the Paakitsoq Hydropower Plant, the main contractor Ístak installed 11 borehole thermistor strings in the walls of the tunnels under construction. The thermistors were installed in 63 mm boreholes drilled as close to horizontal as possible from the middle of the tunnel wall. The sensors are placed in a plastic tube inside the boreholes. Once placed correctly, the boreholes are then grouted and completed with a steel box at the tunnel wall. According to Ìstaks report regarding temperature measurements, the thermometers were calibrated before use and have an accuracy of ±0.1°C (Ístak, 2012). Positions of the different boreholes can be seen in Figure 19.

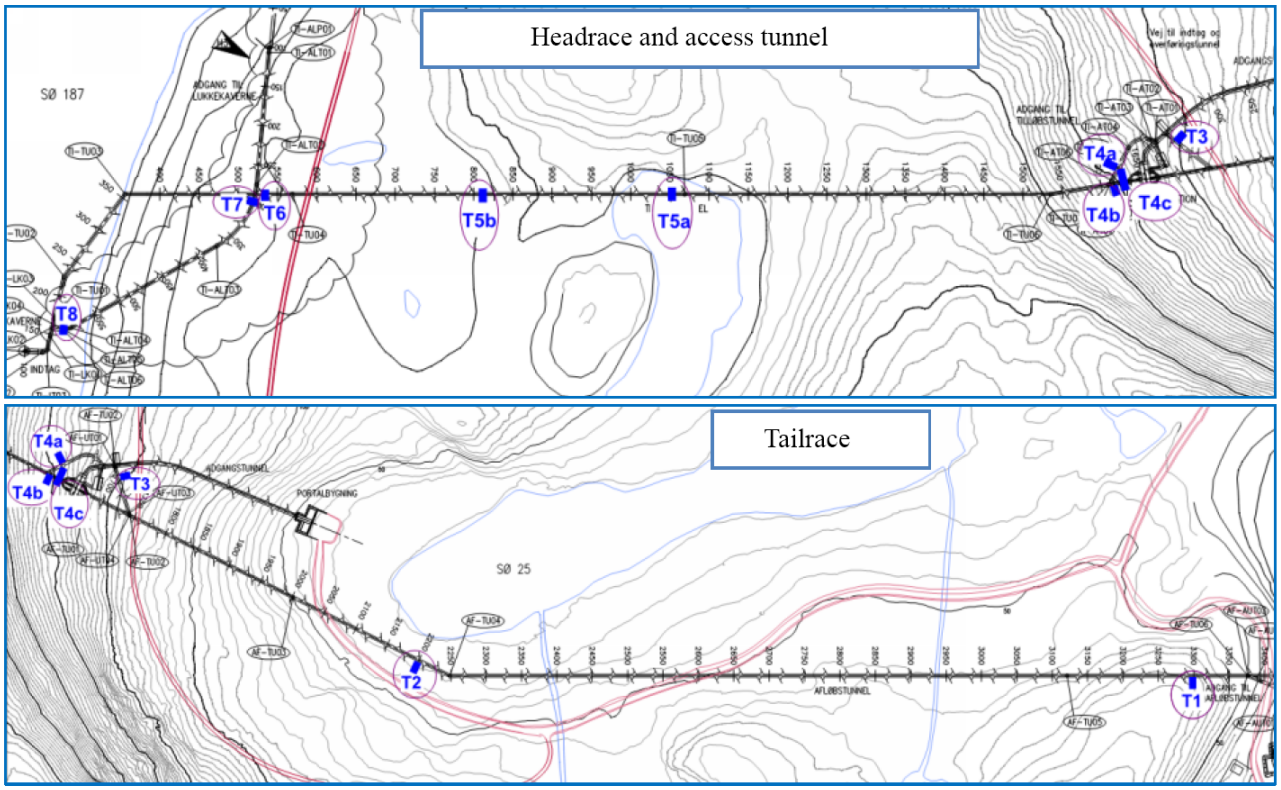

Figure 19: An overview of the tunnel and different measurement points, courtesy of Ístak (2012)

In general, the thermistors were installed at a depth of 0.5, 3 and 6 meters. On several boreholes surrounding the power station, strings with four measuring depths were installed, at 0.5, 2, 4 and 6 meters. On the measuring point 4c, which is drilled from an access tunnel over the water intake tunnel, the borehole is 26 meters long and runs over the intake, thus providing an image of the intake-tunnel's effect on the surrounding rock.

The data received from Ístak has been measured manually during the construction period. As some of the boreholes are located in water bearing tunnels, they were not accessible after the tunnels were water-filled. However, many of the remaining boreholes are still accessible and can continually be monitored.

Lastly, the thermistor strings that remain possible to monitor have been left in the control of Nukissiorfiit - the client and operator of the power plant. Measurements have been noted on five different occasions from December 2012 to January 2014, and thus provide an inconsistent foundation for further analysis.

Ístak and Nukissiorfiit's data has been imported and combined into one document for the available boreholes. The development of temperature as a function of time for every measurement point gives a solid picture of the temperature development and the effect of the water bearing tunnel underneath. The data is available in appendix 20.

11.2.1 Results

Firstly, the results for borehole 4B gives a expected image of how the rock mass reacts to temperature change in the tunnel. This borehole is drilled slightly in front of power station, in the water bearing head race tunnel. This means that the temperature measurements were stopped shortly before the tunnel was water filled. The results can be seen plotted on Figure 20.

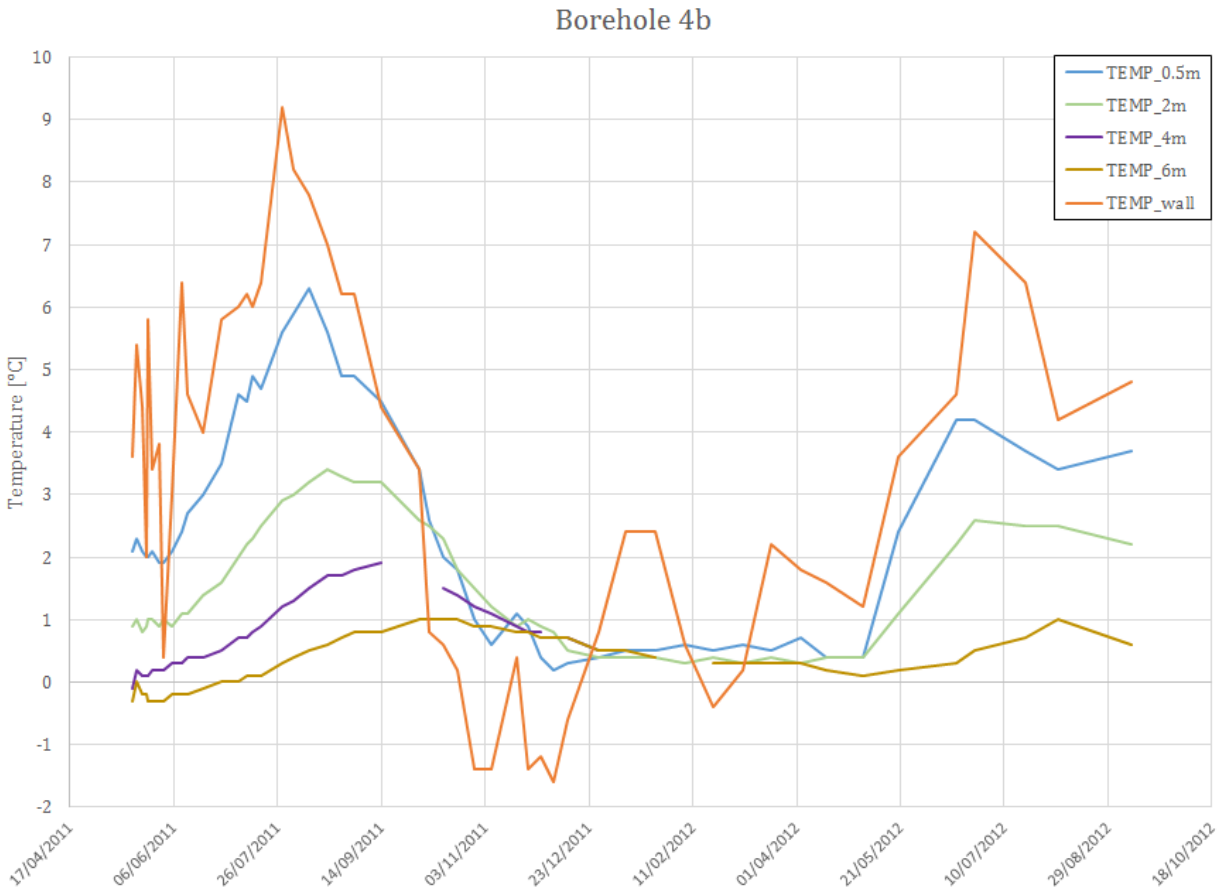

Figure 20: Temperature development of borehole 4b plotted for every depth over time.

One can see the relation between the wall temperature and the slight lag and dampened amplitude shown at deeper measurement spots. One can see a temperature increase from the beginning, as construction was going on. From December 2011, work was paused, which can be seen as the temperature drops and stabilizes around 0.5 °C. Finally one can see the temperature rise again, as work was resumed from April 2012. It is also interesting to note the slight amplitude of the measurement spot at 6 meters depth, indicating that the heat transfer from construction period has had little effect at this distance.

Naturally, this is a question of temperature difference and time. However, it is interesting to note that with the minute temperature differences that the operation phase entails, the distance at which the rock is affected to a critical impact is minimal.

The borehole that immediately struck the authors as most interesting was the deep borehole 4C, as it contains the most thermistors, but also transects above the water intake close to the power station. The results of these temperature measurements can be seen in Figure 21, and shows that the headrace tunnel has had effect on measurements taken above in 4C.

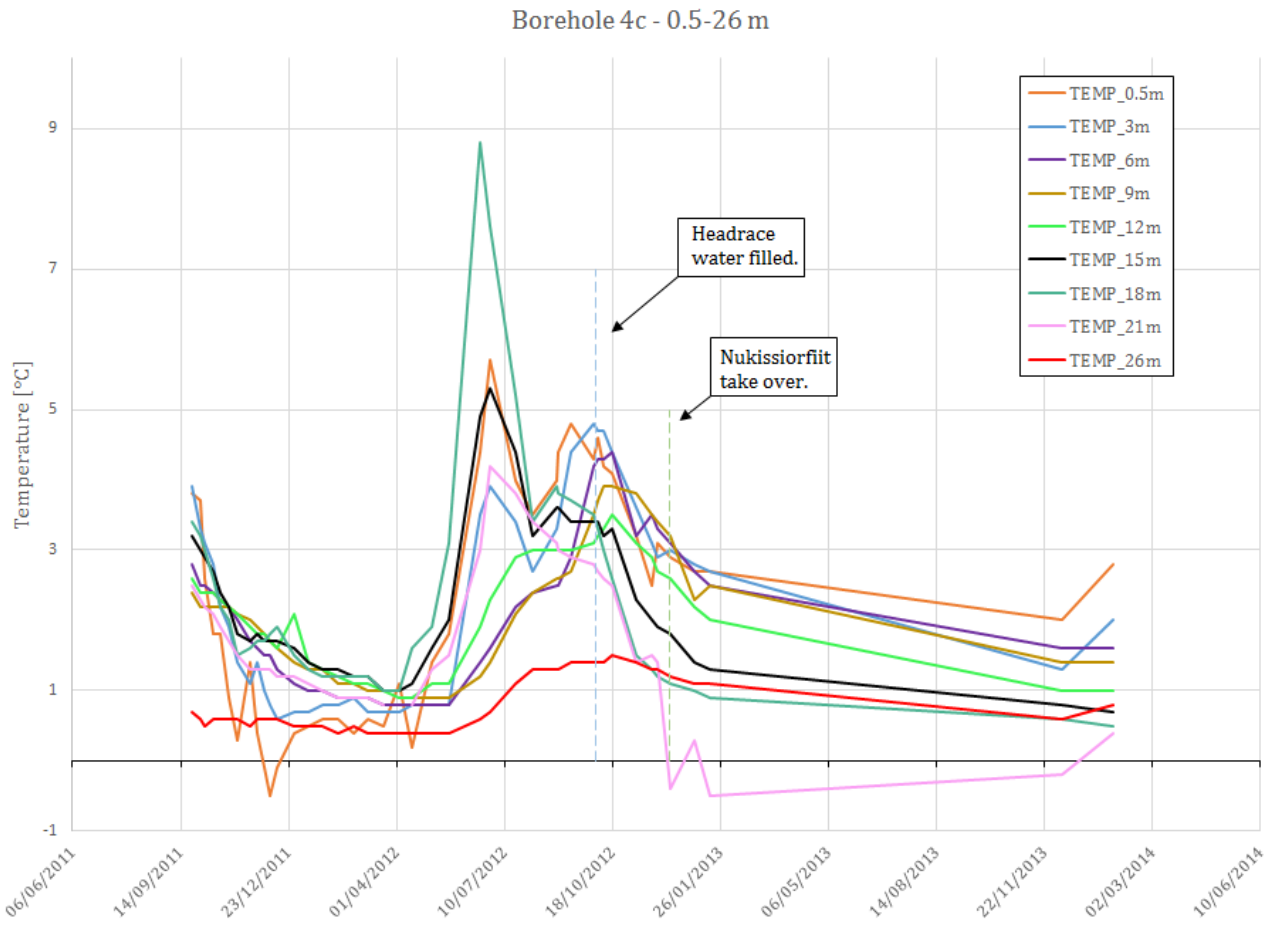

Figure 21: Temperature development of borehole 4c plotted for every depth over time.

Both Figure 20 and Figure 21 share the same lapse in temperature due to the work-stop held during the winter 2012. Another change to take in is the increase in temperature for the 15-21 meter range. Seeing as these measurement points are the ones lying above the headrace tunnel, it is likely that the fluctuations are caused by the heat coming from the work occurring in the headrace. In addition, the 21 meter measurement is shown going below zero degrees for the measurements carried out by Nukissiorfiit. The 24 meter measurement has been removed from the plot due to lacking measurement data.

12 Analytical Analysis

In the following section analytical solutions will be conducted, relevant for the progress of modelling. The main purpose of the analytical approaches in this report are to serve as control for the numerical solution.

12.1 Thaw Bulb of an Underground Pipe

The problem of a heated underground pipe, was researched primarily in the 1970s, in relations to large scale engineering projects. Amongst others this included the Trans Alaskan Pipeline, which was designed to transport crude oil from the North Slope of Alaska to Valdez. The pipeline still stands today and crosses through continuous to discontinuous, as well as sporadic permafrost zones.

One of the challenges of thawing permafrost induced by an underground pipeline is the occurrence of free water from thawing massive ice bodies and buoyancy issues. In frost susceptible soils the transition from a strong material to a liquefaction would cause differential settlements. This, in turn yields a problem with shear forces along the alignment of the pipeline. These effects were described in a preliminary study by Lachenbruch (1970).

In this report the same analytical procedure is used. According to Andersland and Anderson (1978) the thermal effects of a radial problem may be expressed by a cylinder or pipe and its thaw bulb development. Please note that the following terminology includes both frozen and unfrozen state. In thermal geotechnics regarding soil, these two states can differ significantly. However in thermodynamics regarding rock parameters, the water content marginalizes the significance of frozen/unfrozen differentiation.

The radius of thawing by an underground uninsulated pipe, is given by Equation 13:

$$2 \times \left(\frac{R}{r_0}\right)^2 \times ln\left(\frac{R}{r_0}\right) - \left(\frac{R}{r_0}\right)^2 + 1 = \frac{4k_u\,(T_s - T_f)\,t}{r_0^2 L} \tag{13}$$

where:

R = radius of thaw $[m]$
r_0 = radius of pipe $[m]$
$k_{u/f}$ = unfrozen thermal conductivity $[W/mK]$
T_s = surface temperature of pipe $[K]$
T_f = freezing isotherm $[K]$
t = time $[s]$
L = volumetric latent heat of fusion of soil $[J/m^3]$

This solution assumes an infinite domain, equivalent to having the pipe buried deep, without being influenced by seasonal fluctuations. A better approximation for the thaw radius which accounts for a non-steady temperature distribution in the inner part of the thawed zone, is given by Equation 14:

$$R_1 = R_0(1 - 0.12\,Ste)^{1/2} \tag{14}$$

Where Ste is the Stefan number, indicating the ratio between stored sensible heat and latent heat of fusion, given as Equation 15:

$$Ste = \frac{c_u \Delta T}{L} \tag{15}$$

where:

$c_{u/f}$ = volumetric heat capacity $[J/m^3K]$
ΔT = temperature difference $[K]$
L = volumetric latent heat of soil $[J/m^3]$

Preliminary calculations showed that the effect of including Equation 15, are very limited. Therefore these were not included in the onward calculations.

12.1.1 Results: Thaw Bulb of an Underground Pipe

Table 3 shows input parameters used for the analytical computation of the thaw bulb development of the tunnel. The equivalent radius (r_0) in Table 3, is calculated from Figure 22 and Table 16.

Table 3: Material Input Parameters

Material Input Parameters			
k	ρ	r_0	L
$[W/m^2]$	$[kg/m^3]$	$[m]$	$[J/kg]$
3.5	2700	2.3	333×10^3

Three analytical scenarios are taken into consideration. Scenario one deals with the thaw development in the tunnel section, when the walls have the same expected temperature as the intake water. Scenario two deals with the thaw development during construction. This scenario is also used for the access tunnel. Scenario three deals with the thaw development in the vicinity in and around the power station. The three different scenarios have been run with different initial temperatures. In scenario one the intake water temperature according to Einarsson (2011), is 0.05° Celsius. In scenario two, the temperature is in regards to the ambient air temperature during construction, which is set to 1.3°C based on the average temperature from Ístaks borehole 4B. Finally, in scenario three the ambient air temperature in the power station is set to a warm scenario, which is 16°C.

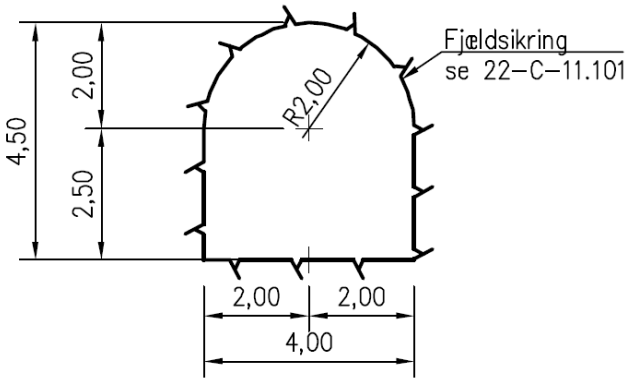

Figure 22: The actual cross sectional design from Verkís.

Because the final design of the tunnel was made as seen on figure 22, an equivalent radius for a circle has been found, by the following Equation 16:

$$r = \sqrt{\frac{A}{\pi}} = \sqrt{\frac{16.3m^2}{\pi}} = 2.3m \tag{16}$$

One parameter that has been difficult to establish, due to lacking lab testing, is the porosity of the rock. As mentioned, no samples give any information regarding porosity nor water content. Therefore the authors have turned to literature studies, trying to establish these. The papers and methods for

this background were discussed in section 10. On this background porosities of 0.3, 0.5 and 0.75 % have been chosen as representative. Furthermore it is assumed that at great depths all the pores of the rock will be filled with water.

According to Kahraman and Fener (2005) they have tested one specimen of migmatic, metamorphic rock (specimen 19), which is comparable to the rock of Paakitsoq, by its point load index. The rock specimen tested by Kahraman and Fener (2005) has an uniaxial compressive strength of 203.6 MPa. This is within the range of UCS tests conducted on the Paakitsoq rock, according to Section 7. Their results show that this rock has a porosity of 1.33 % with a water content of 0.44%. This seems to fit the expected range. However it should be noted that no examinations have been done in order to suggest the degree of saturation.

Scenario one: $\Delta T = 0.05°$

Table 4: The expected thaw distribution for the tunnel with a temperature of 0.05°

Porosity [%]	**0.3**	**0.5**	**0.75**	**1**
Time [years]	Thawing radius [m]			
1/2	3.6	3.3	3.2	3.0
1.5	4.5	4.0	3.7	3.6
5	6.1	5.3	4.8	4.5
10	7.5	6.4	5.75	5.3
50	12.9	10.8	9.4	8.5

Scenario two: $\Delta T = 1.3°$

Table 5: The expected thaw distribution for the tunnel with a temperature of 1.3°

Porosity [%]	**0.3**	**0.5**	**0.75**	**1**
Time [years]	Thawing radius [m]			
1/2	8.1	7.0	6.2	5.7
1.5	11.8	9.9	8.6	7.9
5	18.3	15.1	13.0	11.8
10	24.0	19.7	16.8	15.1
50	46.1	37.3	31.7	28.2

Scenario three: $\Delta T = 16.0°$

Table 6: The expected thaw distribution for the tunnel with a temperature of 16.0°

Porosity [%]	**0.3**	**0.5**	**0.75**	**1**
Time [years]	Thawing radius [m]			
1/2	19.9	16.3	14.1	12.7
1.5	30.7	25.0	21.3	19.1
5	50.3	40.7	34.5	30.7
10	67.5	54.3	45.8	40.7
50	135.3	108.3	90.8	80.2

As seen in Table 4, 5 and 6, the thawing radius grows with time. Additionally, as a more porous rock is introduced and more energy needed to overcome the latent heat of fusion, the thawing radius is limited. Not surprisingly, the thaw bulb development of the power station will become much greater compared to that of the tunnel on the same time scale.

With these results the authors are now able to approximate the axisymmetric distances towards the boundary conditions in 2D, thus minimizing the computation time.

13 FEM Modelling and Boundaries

13.1 A Brief Explanation of Numerical Analysis

In this report a numerical software will be used, which can model finite constitutive elements. This is called COMSOL Multiphysics. DTU has a student license for this software, which makes it optimal for the authors use. Yet, various commercial software exists today with similar capabilities.

As Peiró and Sherwin (2005) explains, in general what a FEM program does, is solve a series of PDEs (Partial Differential Equations), to a set of know boundary conditions. These PDEs are expressions of different conservation laws, as explained per section 10. The boundary conditions are what connects the discrete discontinuous problem to the rest of the physical world. In contrast to ODEs (Ordinary Differential Equations), PDEs include changing rates with regards to continuous variables. However over time these PDEs approximate ODEs, more precise after each iteration.

This is done by taking a continuous domain and subdividing it into x discrete parts - thus called a discretization scheme. By taking an infinite domain and thus defining a certain degree of resolution (dividing into elements), the model becomes finite. Constitutive finite element modelling, is called an iterative process, because it repeats its input-output. This cycle of operations is done until the result is within a predetermined margin of error.

FEM modelling is also referred to as constitutive modelling. This indicates that several physical constituents may be modelled within the same domain. For instance a soil/rock, can be a multiphase, multi constituent material i.e. including water, ice, air, and hydrocarbons.

When doing FEM, it is important to realise how the mesh affects computation time. For a user it might be of importance to increase the overall degree of detail in a certain region of a domain. Making a finer or more complex mesh in turn yields more computation time, as more iterations of PDE has to be solved. Ways of limiting the computation time includes symmetric geometries, increase of CPU power and decreasing detail of mesh. Every node in a mesh times the number of dependent variables, will give the degree of freedom of the discretization scheme. For example having a node in 3D, for a rigid body, offers a displacement vector with 6 DOF - 3 translation and 3 rotation. For every node, these may in turn be set up in local and global stiffness matrices, describing the constituent's elements.

In FEM, typically two sets of solutions exists: steady state and time dependent. When using a steady state solution, time is not regarded and the software goes directly to when no more change occur with respect to time. When using a time dependent solution (transient), the software solves an iteration for every time step, thus allowing the user to track a development over time. Thus the time dependent solution requires more iterations and occupies more memory.

Several mathematical methods of making a discretization scheme exists. Among others, these are referred to as FDM (Finite Difference Method), FEM (Finite Element Method) and FVM (Finite Volume Method). Of the mentioned methods FDM is the oldest and is based upon Taylor polynomials. Thus in FDM an approximation towards PDEs is done, with an infinite series of differential equations. This infinite series is called a Taylor series. In such a series an error is introduced. This error thus approximates the correct function. The higher order of the differential equation, the more precise the estimate. For it to be possible to solve such a series of Taylor expansions, the system has to be convergent and stabilized.

For practical use FDM operates with more simple geometries too. As stated by Peiró and Sherwin (2005): The FDM uses a topologically square network of lines to construct the discretization of the PDE. This is a potential bottleneck of the method when handling complex geometries in multiple dimensions. This issue motivated the use of an integral form of the PDEs and subsequently the development of the finite element and finite volume techniques.

13.2 COMSOL Multiphysics

Driving the system, there are a number of material parameters for the rock. These are:

- Thermal conductivity, k
- Specific heat capacity, C_p
- Density, ρ

Furthermore two boundary conditions exits, solely for the rock formation, an upper- and lower boundary:

- Upper BC, MAST (Mean Annual Surface Temperature)
- Lower BC, Local heat flux / Geothermal Gradient

These material parameters and boundary conditions have been accounted for in the previous Section 10.

13.3 2D Model - Steady State

The first model of this paper is done in order to establish the temperature distribution through the rock. In order for this process to work correctly a number of assumptions has to be made. These are listed in the following:

- The rock is homogeneous, isotropic and solid
- Only one constituent is modelled (rock) - it is not a multiphase system
- There is no pore space in the rock and thus it has no water content

These assumptions are vital for the understanding of the model and its limitations. to take into account these simplifications of an otherwise complicated physical, multi-phase, multi-constituent system.

For this model a stationary solution was chosen in COMSOL. This indicates that the authors are not interested in the time driven temperature development, but merely when the system is in a steady state condition.

The governing equation when two dimensions are involved (x,z), is given by Equation 17:

$$\frac{\delta\theta}{\delta t} = \kappa\left(\frac{\delta^2\theta}{\delta z^2} + \frac{\delta^2\theta}{\delta x^2}\right) \tag{17}$$

where:

θ = temperature [$^\circ C$]
z = depth [m]
t = time [t]
κ = thermal diffusivity = k/c [m^2/s]

When the thermal diffusivity is divided on both sides of the equal sign, the term becomes 0 and the Laplace equation is obtained (Andersland and Anderson, 1978):

$$\left(\frac{\delta^2\theta}{\delta z^2} + \frac{\delta^2\theta}{\delta x^2}\right) = 0 \tag{18}$$

13.4 Preliminary Design

13.4.1 Lower Boundary Conditions

The lower boundary condition of the 1D steady state model, is a heat flux. It is based of the geothermal gradient of borehole K85903 and the thermal conductivity of the granodiorite. It is calculated as accounted for in section **??**.

$$q = -3.5\frac{W}{mK} \times 0.0186\frac{K}{m} = -0.065\frac{W}{m^2} \tag{19}$$

The minus sign indicates the direction of the heat flow - from hot to cold, to the surface of the Earth.

13.4.2 Upper Boundary Conditions

The upper boundaries of this model has been established using borehole data assimilated by GTO during the period 1984-85 - as described in section 11.

In Figure 16 it is seen that the upper boundaries have been established along an alignment across the peninsula of Paakitsoq, from lake 187 to the fjord.

The only borehole data that has not been accessible in determining these boundaries, are concerned lake 187 and the fjord. Instead these have been determined using Verkís-reports (Einarsson, 2011). Thus a boundary temperature for the fjord bottom has been set to -0.05 ° Celsius. This has been made by a weighted average, between the dates of temperature measurement for the fjord.

This is neither fresh nor seawater, but brackish water, meaning that it has an intermediate range of salinity. This in turn will cause a depression of the freezing point.

There are available temperature measurements, conducted by Ístak from lake 187. These measurements have, to the authors knowledge, not been taken into consideration by any previous model. These profiles are shown in Figure 23.

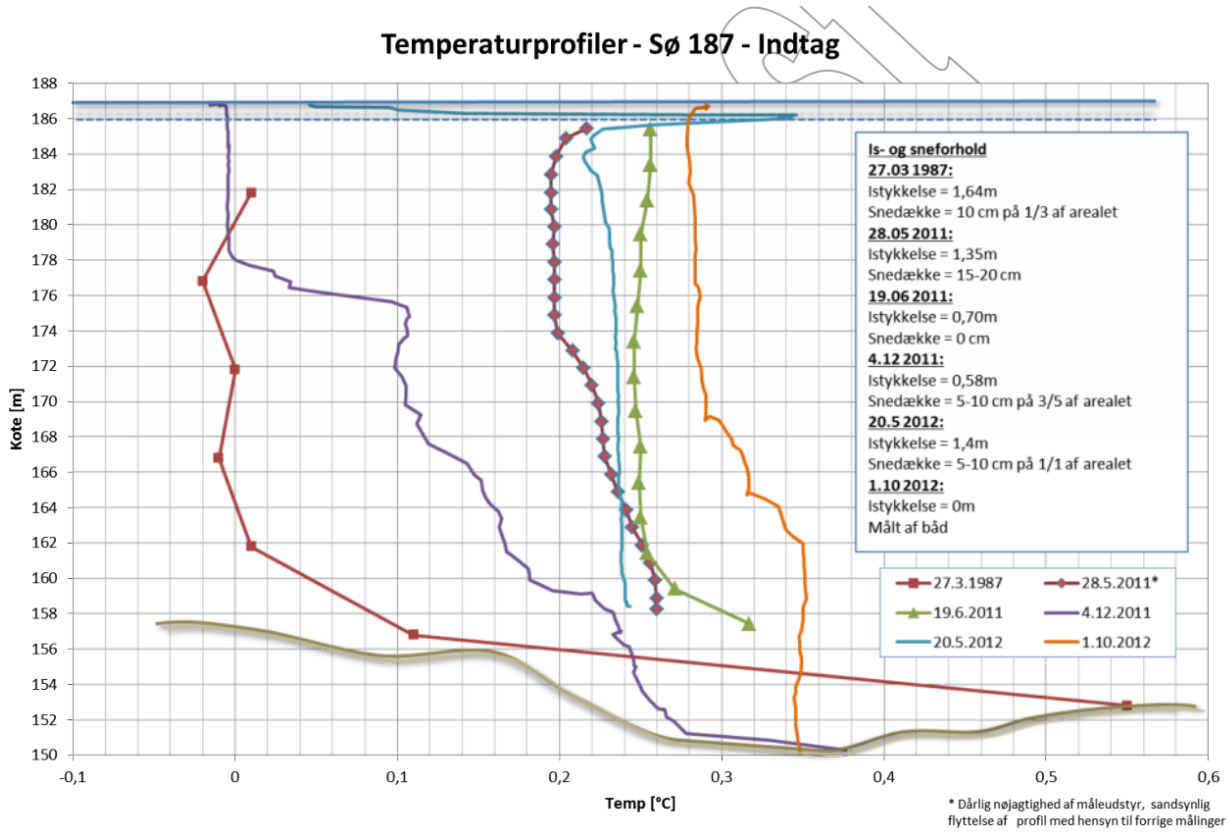

Figure 23: Temperature measurements from lake 187 taken by Istak)

As it can be seen from Figure 23, most readings have been conducted during the summer months. One reading from 1987 is from spring, while one is from the fall of 2012 and one has been conducted during wintertime of 2011. As this shows the minimum water temperature that may be expected is close to zero degrees Celsius. From these plots the authors have decided to set an overall average of the lake bottom to 0.3° Celsius. This fits well with the lake temperature expected, according to LICconsult (1985).

Furthermore access has been given to ASIAQs archives, for the K84901-903 boreholes, as described in Section 11. However faulty these are, they may offer some value in determining the upper boundaries.

Table 7: Geothermal gradient, surface temperature and joint elevation temperatures for the boreholes

Borehole	Geothermal Gradient [°C/100m]	Surface Temperature [°C]	Elevation 180 [°C]	Surface Elevation [m]
K84901	-2.30	-4.06	-4.37	42
K84902	-2.77	-2.53	-3.56	32
K84903	-2.33	-2.08	-3.04	135
K85904	-2.06	-4.79	-5.01	149
K85903	-1.86	-3.89	-3.47	241

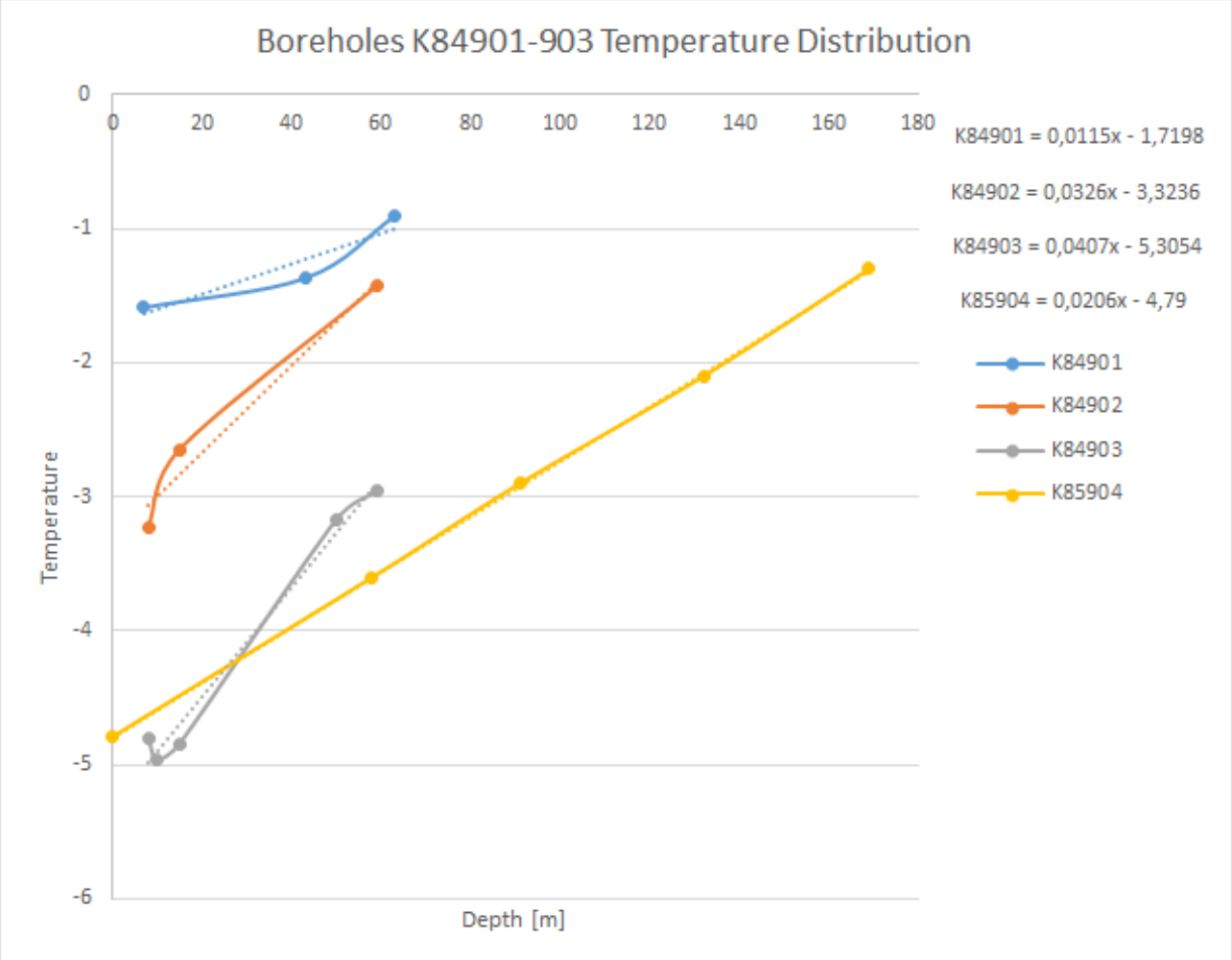

Figure 24: Three datasets of the 84-series, from ASIAQs database, together with K85904

Figure 24 shows the geothermal gradients for each of the three boreholes. In this plot an average of all temperatures in each depth, has been made. This will under all circumstances cause some error in

the top part of the borehole, which is exposed to seasonal fluctuations. To get a more exact estimate, the near surface points can be removed. This means ignoring any temperature data above the depth of zero annual amplitude. However, even when removing the first data point, closest to the surface, the geothermal gradient is still off.

Also in Figure 24 the borehole K85904 is found. As it may be seen from the three equations in the top right corner, the slopes of the graphs are extremely differentiated from each other. Furthermore non of these are close to the geothermal gradient of the main borehole (K85903), at 1.86°C/100m, except for K85904 which is at 2.06°C/100m.

Table 7 gives an overview of the geothermal gradient of K84901-903, only including the two deepest measurements, and then extrapolated with a gradient of 1.86°C/100m to the surface. In comparison with Figure 24, these data offer more realistic gradients closer to the reference borehole, K85903.

Furthermore table 7 shows the surface temperature, along with the relevant elevation of each borehole. From this it is questionable whether or not K85901 and K85903 offer reliable data, as these might be affected by topographical effects (LICconsult, 1985). These topographical effects could for instance be caused by the borhoel being drilled in a suppression of the landscape, offering shade. Also, be driven by south/north facing slopes, indicating how much direct sunlight is received each day. Thus K85901 has a relatively warm surface temperature of -4.06. This temperature would be expected lower as it is close to the fjord, where temperatures are milder than further inland.

Moreover the temperature measurements from K84903 are being rejected, as the deeper and more reliable K85904, has the same location and show much colder temperatures. Finally, Table 7 gives an overview of a joint elevation of 180m for all the boreholes. This makes comparison of the topographical effect straightforward. To obtain this value, an ambient air gradient of 0.007°C/m has been used.

The coldest surface temperatures are found in the middle of the peninsula. It gets warmer towards the lake and fjord, where more temperate conditions are found.

To summarize in accordance with Figure 16, table 8 gives the final preliminary design for the upper boundary conditions, subdivided into 6 zones. This is done in accordance with appendix (EXCEL FOR UPPER BC'S)

Table 8: Overview of upper boundary conditions

Zone:	1	2	3	4	5	6
Name:	Lake 187	K85903	Peak	K84903	K84902	Fiord
Surface Temperature [°C]	0.3	-4.46	-5.0	-4.7	-2.5	-0.05

13.4.3 Geometry of Longitudinal Profile

For establishing the geometry/topography of the cross section of the area, overview blueprints designed by Verkís have been used. This enabled the authors to cross-reference distances from lake 187 to Paakitsup fjord, with elevation and slope data.

The blueprints used can be seen in appendix 18, drawing numbers 22-C-11.041 and 23-C-11.011, respectively.

14 COMSOL Modelling

14.1 Steady State Results

It is important to note, that mean annual surface temperatures have been used as upper boundary conditions when modelling. The reason for this being that the depth is so great, that the tunnel alignment is beyond seasonal effects.

The initial results of the longitudinal profile steady state temperature distribution is shown in figure 25.

From left to right it begins with lake 187, then the peak elevation of the area, at approximately 300 m above sea level, before reaching a plateau at 30 m.a.s.l and finally ending up in the fjord at sea level.

On Figure 25 the 0°isotherm is marked by a thick black line, with a zero in the right hand side of the figure. Furthermore the legend in the right hand side, show the temperature range distribution with colour codes.

The coldest surface temperatures are found in the left side of the area. However as lake 187 convects heat, at a temperature of just 0.3°C, the cooling effect is suppressed, causing the 0°isotherm to be at a higher elevation in this area.

In the right side of Figure 25, after the peak, from 1750 m and continuous, it is the opposite case. Here the mean annual surface temperature of the rock warms. However the fjord bottom has a temperature of -0.05°C. This in turn causes the 0°isotherm to be lowered.

Figure 26 shows a temperature versus depth plot. This is taken from the model in Figure 25, where borehole K85903 is located. Figure 26 compares the gradient of the model, with measured data from other years. As seen, the general tendency is that the steady state model is a bit too cold, continuously down the borehole. However when compared to year 1986, both measured and modelled data crosses the 0°isotherm in approximately the same depth.

When looking at Figure 26, the model is most off near the surface. As discussed previously a main assumption is that the depth of zero annual amplitude is not taken into consideration in modelling, thus causing this differentiation from the measured data.

The largest deviation is located at 60 m depth, where the difference between measured monthly mean for all years and the model is 0.45°C.

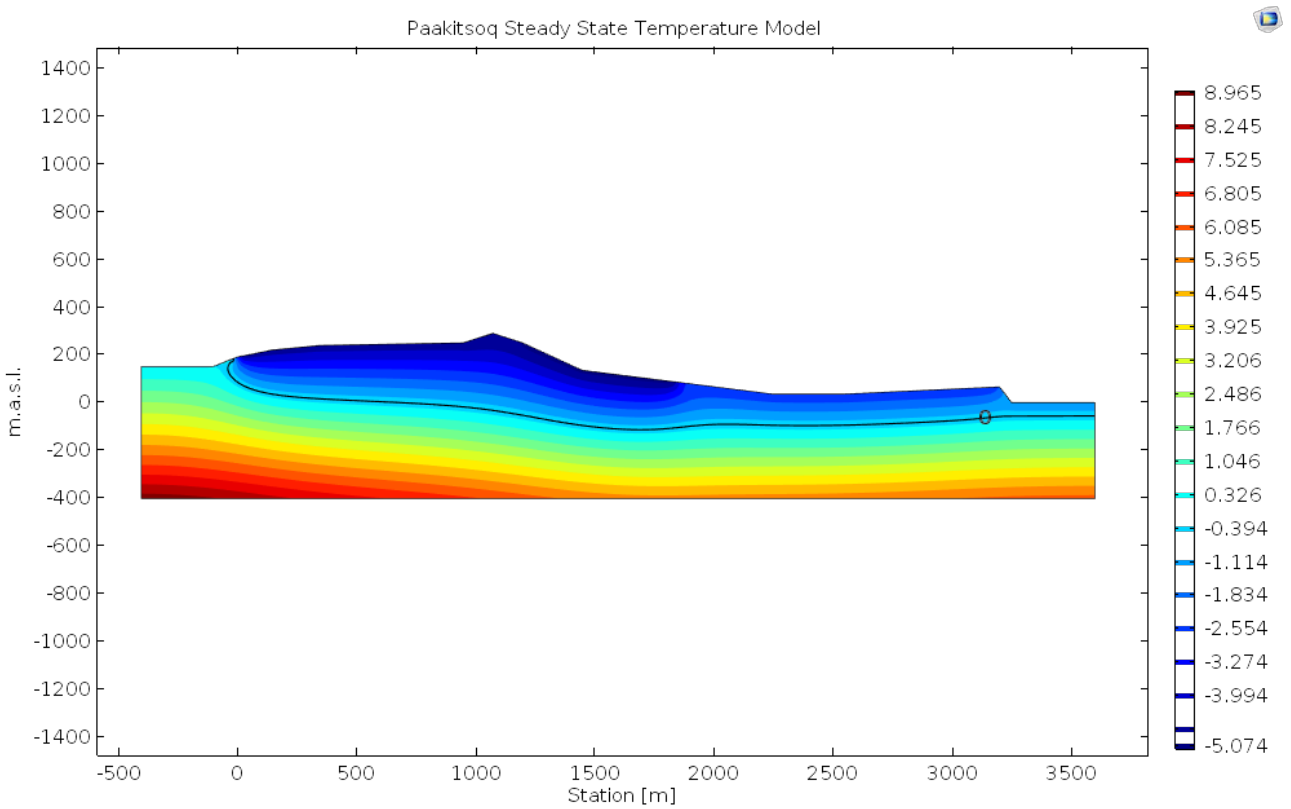

Figure 25: The final operation of the 2D longitudinal steady state profile

Table 9 compares results from the 2D steady state model with Ístaks measured data from within the tunnel. As seen in table 9, the largest deviations occur closest to lake 187 and the peak on Figure 25, (from 150 - 1185 m). These differences could be explained by the temperature of the lake bottom, which possibly could have been somewhat warmer. Furthermore a better subdivision/resolution of the boundary conditions could have been beneficial. However there is not an overall tendency, indicating that either the model is being too warm/cold. The data is deemed inconclusive, in relations to explaining these differences. However the last two comparisons of table 9, do indicate a good correlation between Istak and COMSOL data.

As the largest numeric value difference which occur between observed and modelled data is 0.84°C, the initial 2D steady state model is deemed plausible by the authors and is used as basis for further modelling.

Table 9: Comparison of steady state results from COMSOL and Istak

Elevation [m]	x-coordinate [m]	COMSOL [°C]	Istak [°C]	Difference [°C]
-13	2935	-1.26	-1.30	0.04
-27.5	1850	-1.41	-1.40	0.01
-0.7	1185	-0.92	-0.30	0.62
5.0	736	-0.14	0.70	0.84
12.5	460	-0.04	-0.30	0.26
51.5	150	-0.34	0.10	0.44

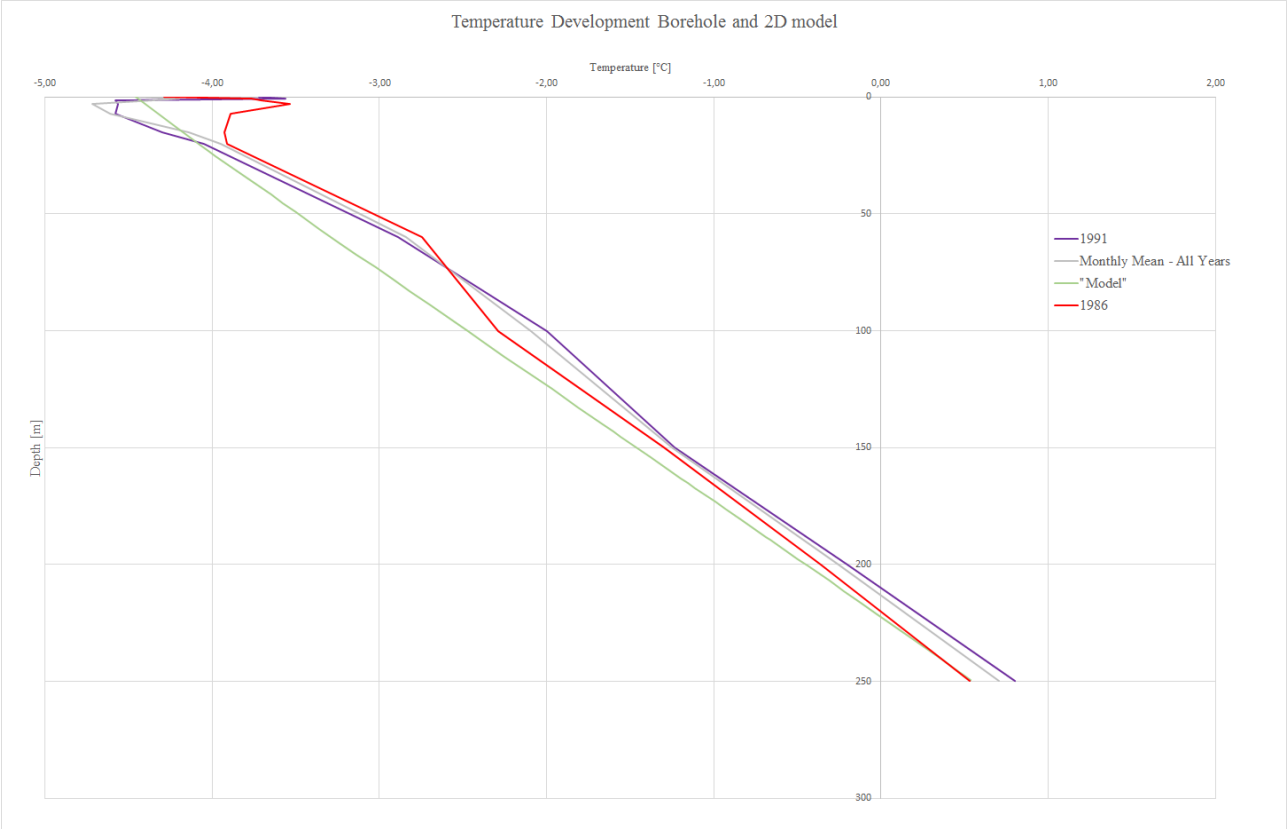

Figure 26: Initial temperature distribution for borehole K85903, in comparison with year 1986, 1991 and monthly mean of all years available.

14.2 3D Modelling

In order to increase the complexity of the model, the authors began the design of a 3D model. The earliest model was a 50 m segment of the intake tunnel, set before the power station, close to the temperature borehole 4b. This was done in order to verify results and compare with the previously calculated analytical solutions. Furthermore it would give the authors an idea as to the complexity of COMSOL's 3D capabilities.

The first model attempt was a steady state solution and with a transient model of the construction period. A more detailed CAD model of the power station was then constructed. Similar to the former model, the initial temperature regime was calculated for the solid rock mass as a steady state problem. Thereafter, with the initial temperature defined, a 1.5 year working period was simulated. Finally, with the results from the construction period, a transient model involving the operational period was simulated.

The following statement has previously been made concerning the choice of material parameter, regarding thermal conductivity.

The thermal conductivity, which has been measured on core samples at NTH (The Norwegian Technical University), is within the range of 1.5 and 1.7. This has to be seen in relations to Kappelmeyer (1974). Here it is stated that it should be between 2.5 and 3.8, with a tendency towards higher values for larger quartz content. Furthermore the conductivity is larger parallel with the foliation compared to perpendicular on the plane. Until further verification and evaluation of NTH's test results, a value of 3.5 has been chosen (LICconsult, 1985).

14.2.1 Simple Model

The model will be dealt with as air filled for 1.5 years during construction, the effect of this heating could then be continued onto the operational phase of the model. Thus, the effects of the temperatures; the construction period and the operational period can be obtained.

Once a simplified 3D model had been drawn, the steady state solution with the regular boundary conditions was made. This can be seen in Figure 27. The results of this solution, were then defined as the initial conditions for the transient model.

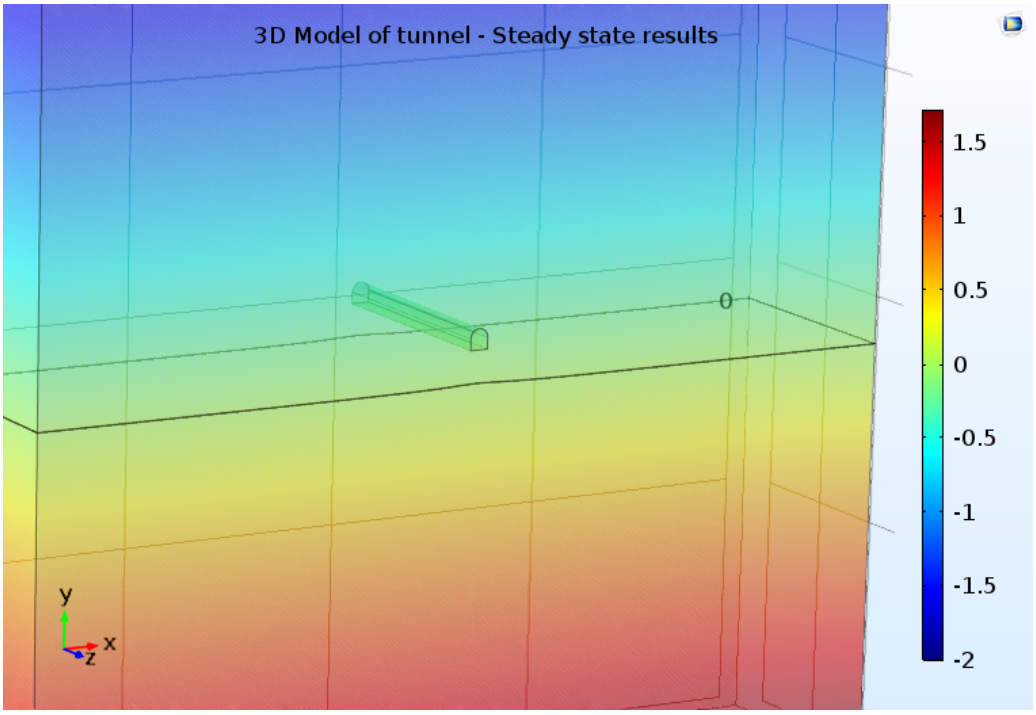

Figure 27: The result of the 3D steady state model is shown. The model displays 50 meter length of tunnel, surrounded by 100x100 meters of rock mass, legend displaying °C. The 0°C isotherm is shown as a black frame.

In the transient model, the intake-tunnel is included, which contains a fluid flow of air. Initially the scope of interest was the effect that a warm cavern during a one and a half year working period would implement, but also to find the necessary horizontal limitation of model. The result of the model can be seen in Figure 27.

A horizontal cut-line was drawn 50 meters in length from the middle of the tunnel. This cut-line was used to create the plots in Figure 28. These give an indication of the effect the construction period has had on the temperature development. Furthermore these plots help as before mentioned in establishing a limitation in the horizontal extent.

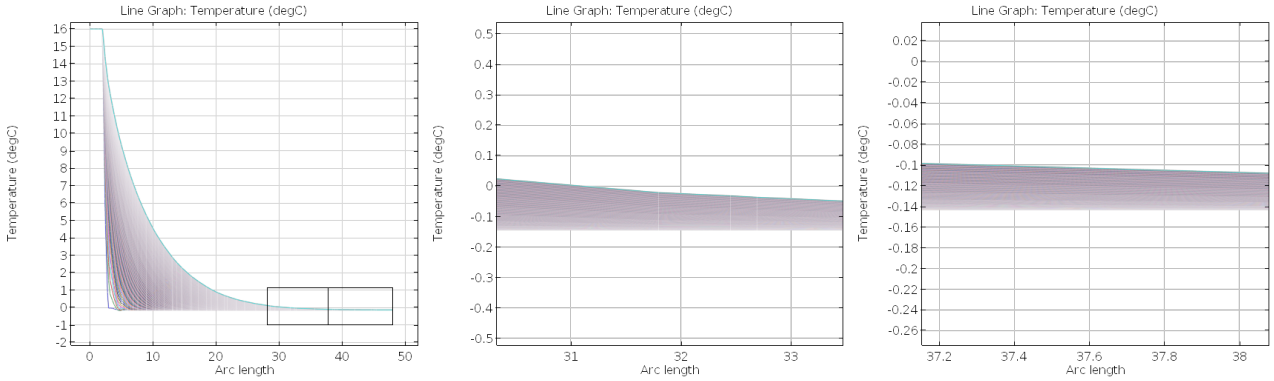

(a) Overview (b) Crossing 0°C isotherm (c) Zoomed to limit

Figure 28: The results from modelling for the width of interest are shown here, an overview to the left and zoomed in at the furthest distance to the right. Each line represents a day, with the top line being the temperature after 1.5 years.

The temperature of the tunnel was set to 16°C, as this is found to be a maximum value based on Ístaks temperature data from construction. In addition, the temperature chosen is relatively high, as a conservative value will better represent the maximum temperature development. As seen in Figure 28(c), zoomed in at the last meters of the cut-line, one can see that the variation around 37 meters is equal to 0.04 °C.

Looking at Figure 28(b), zoomed into the point where the 0°C isotherm is crossed after the work period, the distance from the tunnel wall corresponds to a thaw bulb of 29 meters horizontally (tunnel wall starts at 2 m). This is in excellent correspondence with the analytical solution, which calculated a thaw bulb of 30.7 m, for a 0.3% porosity, water saturated rock. This concludes that the analytical approach validates the modelling.

14.3 Complex Model

Initial modelling was performed in order to test the capabilities, and confirm that the functions of COMSOL were fully understood.

The next phase was to model the actual power station. The 3D geometry of the station were modelled in CAD-software and then exported to COMSOL. The model was drawn based on the GPS-positions of know points along the tunnel and power station (Figure 29(a)).

However, the model proved to be too complex and required too much editing in COMSOL in order to add the physics for simulation. Therefore, a simplified geometry was drawn up - where the access tunnel was drawn as a rectangle, also removing the differences in height (Figure 29(b)).

Furthermore, the intake tunnel was extruded to reach the boundary of the model. The boundary between station and intake tunnel inside the station was isolated, as data is available for the station temperature, which is a sum of contributions from the water and station. To increase simplicity the height differences between access tunnel and intake tunnel was also removed, resulting in the entire model constructed on one horizontal axis. The resulting models are seen in Figure 29.

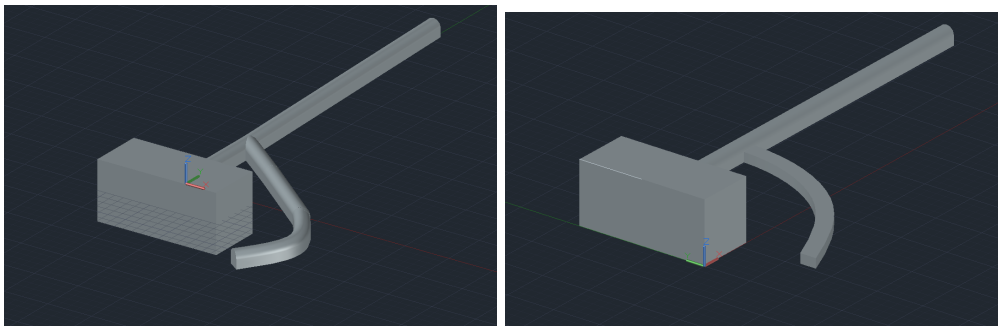

(a) Discarded CAD-model. (b) CAD-Model used for simulation.

Figure 29: Two CAD-models created.

The width of the model was based on the warmest analytical solution which saw a maximum thaw bulb radius of nearly 150 meters in a 50 year period.

The mesh used for the calculations were handled by COMSOL physics. As the contact between the tunnel face and the rock mass was the coupling between the physics the highest resolution was focused on this connection. A plane view of the mesh can be seen in Figure 30. On the far right of the figure, the maximum element size is displayed. In physical terms the size of one of the tetraheads

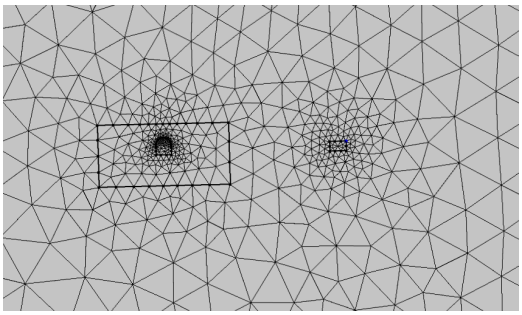

Figure 30: Mesh size displayed, power station and access-tunnel outlined.

14.3.1 Complex Model - Construction

The first phase of modelling regarded temperatures during construction. Firstly the boundary conditions were interpreted from the 2D steady state model mentioned in section 14.1. The input parameters can be seen in Table 10.

Table 10: List of model parameters.

Material Input Parameters Transient Model								
k	ρ	C_p	L	v_{air}	v_{water}	T_{intake}	$T_{accesstunnel}$	$T_{powerstation}$
$[W/m^2]$	$[kg/m^3]$	[J/°C]	$[J/kg]$	$[m/s]$	$[m/s]$	$[°C]$	$[°C]$	$[°C]$
3.5	2700	730	333×10^3	1	0.02	0.05	1.3	16

The construction period lasted approximately for two years. However, the intake tunnel of the area in question was constructed in one and a half years time, before becoming water-filled. Therefore, modelling of the construction phase lasts for 1.5 years. Based on the temperature measurements from Ístak, the average temperature during construction phase was measured to 1.3 °C in this region, this value was used for the entirety of the construction period.

The model itself was calculated for 550 days total with time steps of 1 day. This was possible with acceptable calculation time, as the previous modelling was used to find the necessary simplifications.

14.3.2 Complex Model - Operation

The operational phase of the model was built on the temperatures calculated after the 550 day construction phase. In order to be able to run this simulation, the step had to be increased and half year steps were taken to a ten year solution. Finally, a 50 year calculation was run with one year steps.

14.4 Results

In order to view a broad comparison of the resulting simulations, several different methods of visualizing the results were put in use. They included cross sections, cut-lines and 3D visualization. All results were analysed in COMSOL.

14.4.1 2D Planes

2D planes were drawn through the power station, to show temperature development horizontally and vertically surrounding it. One plane cut through the station horizontally whilst another cut through the middle of the station vertically. Both planes are displayed in Figure 31.

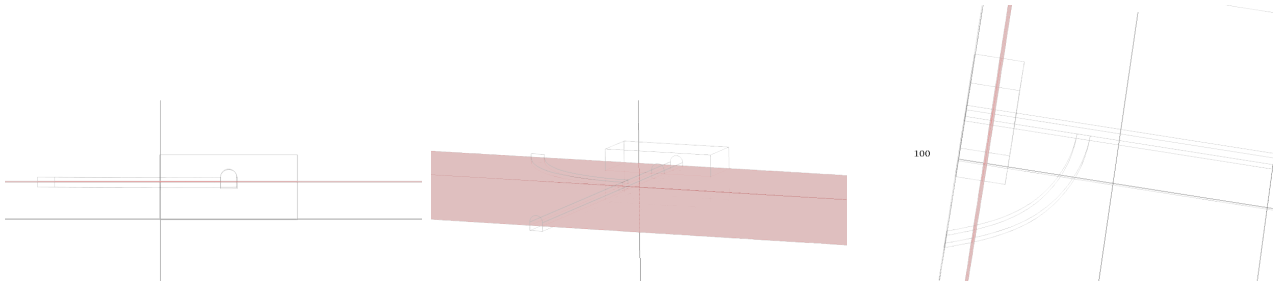

(a) Cut-plane position. (b) Plane 1 - horizontal. (c) Plane 2 - vertical.

Figure 31: Planes used to see 2D cross sections.

The results of the construction period simulations can be seen in Figure 32. The result shows effect of a 1.5 year construction period, with a 1.3°C temperature, which is the basis for the initial conditions of the operations model which is seen in the following figures.

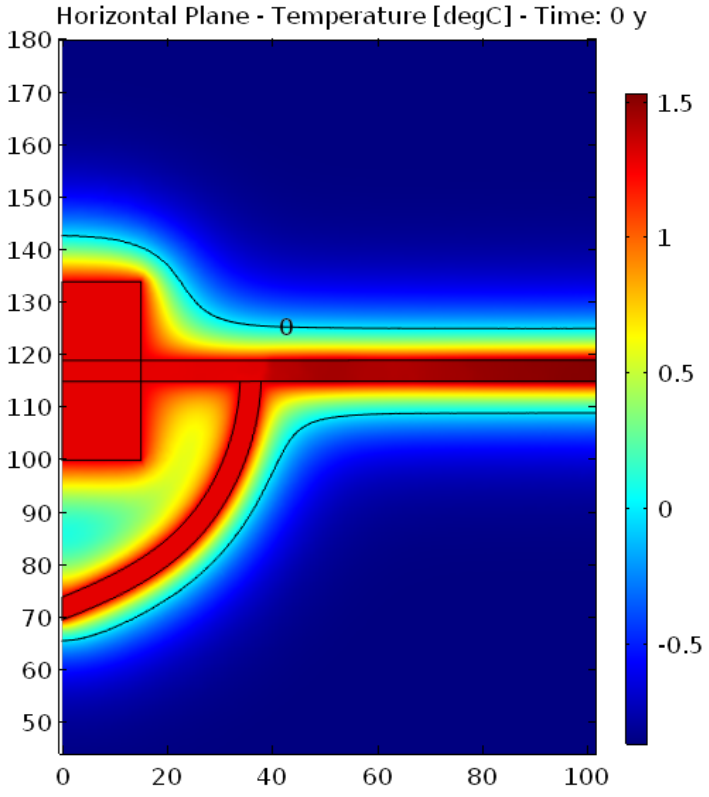

Figure 32: Temperature regime after construction period of 1.5 years.

In the following Figure 33, the temperature development during the operational phase can be seen through the horizontal plane over 10 years.

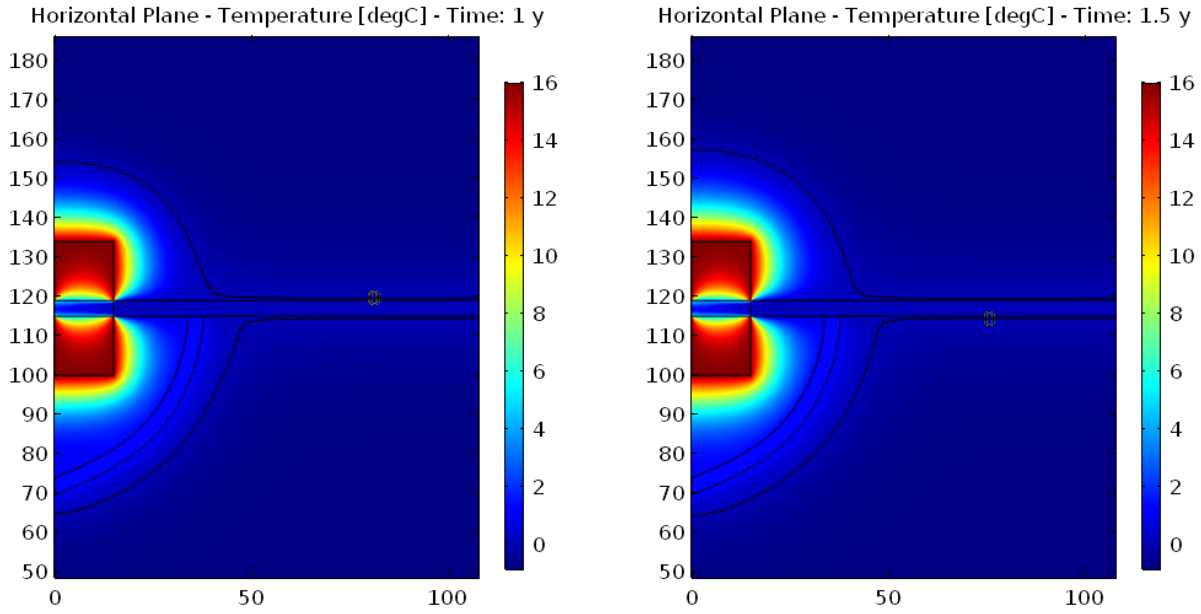

(a) Temperature regime after 1 year.

(b) Temperature regime after 1.5 years.

(c) Temperature regime after 5 years.

(d) Temperature regime after 10 years.

Figure 33: Temperature development on horizontal plane.

In Figure 33(a) and 33(b) one can see that the access tunnel has effect on the 0°C isotherm, as its position is slightly further along the x-axis compared to the other side of the intake tunnel. However on Figure 33(c) the isotherm has equalled and the access tunnel no longer bears significant effect after 5 years of operations. Lastly, the final overview of the horizontal plane taken after 50 years of operation is seen in Figure 34. According to Figure 34 the maximum thaw bulb will thus be 180 m in diameter.

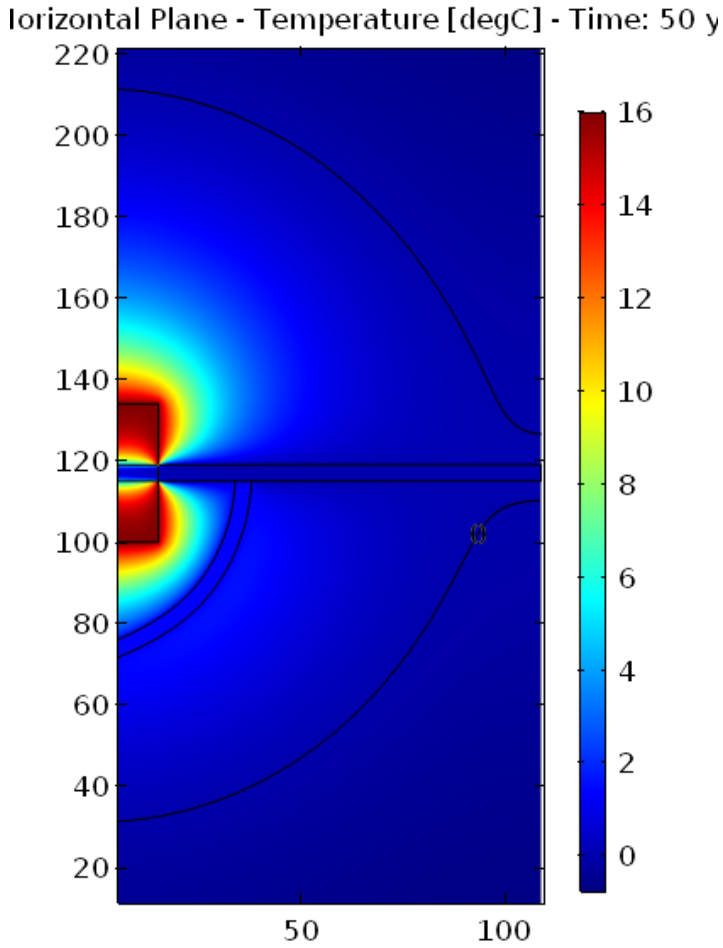

Figure 34: Temperature regime after operation period of 50 years.

The same procedure was carried out for the vertical cut-plane (Figure 31(c)). The temperature after the construction period was set as initial temperatures for the operational phase, with the result visible in Figure 35. In Figure 35 the occurrence of both the global and local 0°isotherm can be seen. However at this point they have not merged yet.

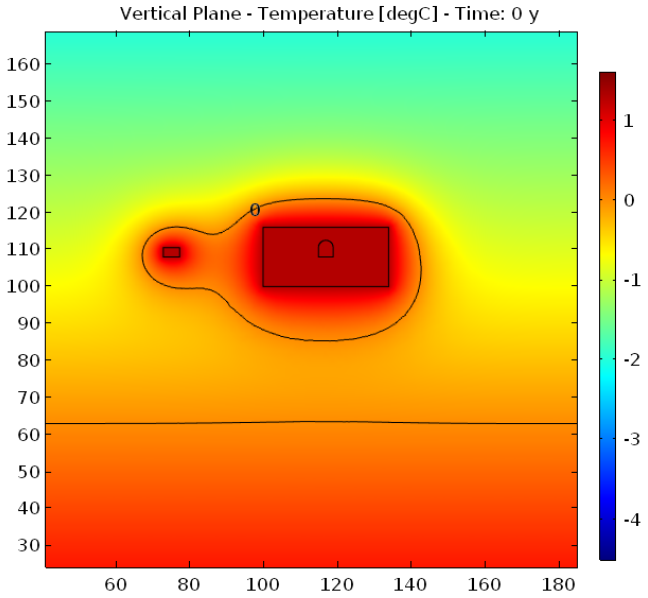

Figure 35: Temperature regime after construction period of 1.5 years.

The following figures plot the temperature development (Figure 36). However, a slightly different time step was chosen in order to show the thaw bulb connect with 0°C-isotherm in the underlying rock mass, seen between Figure 36(a) and 36(b).

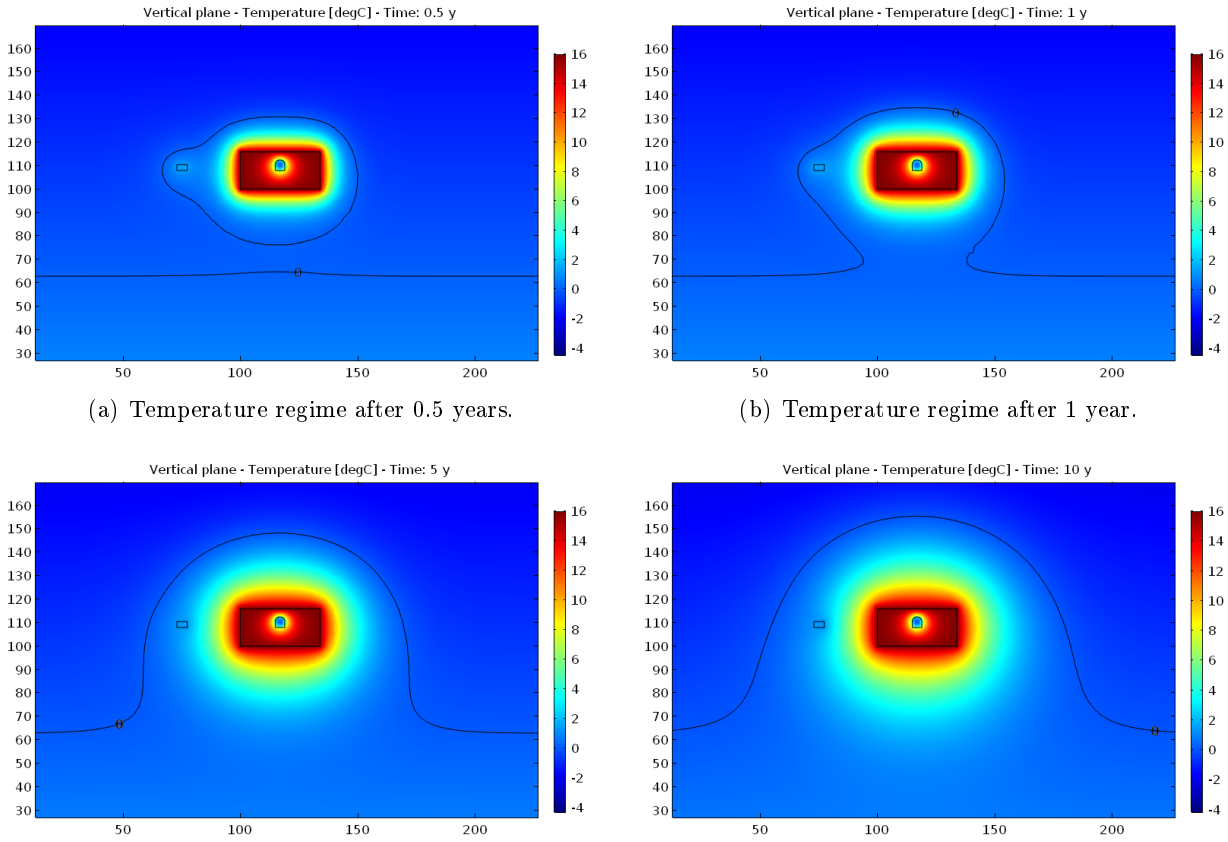

(a) Temperature regime after 0.5 years.

(b) Temperature regime after 1 year.

(c) Temperature regime after 5 years.

(d) Temperature regime after 10 years.

Figure 36: Temperature development on vertical plane.

As with the horizontal plane, a final 50 year plane is plotted in Figure 37.

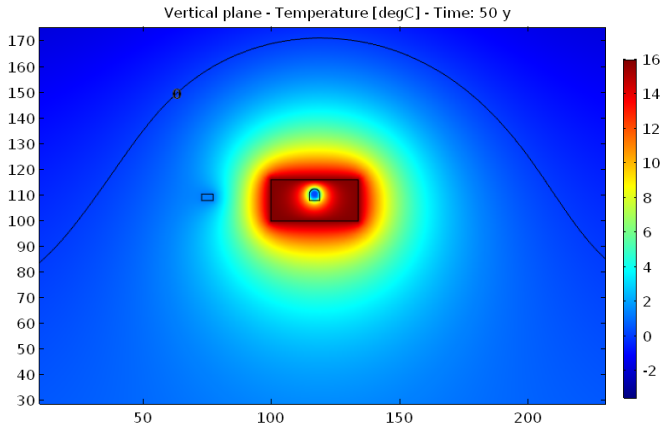

Figure 37: Temperature regime after operational period of 50 years.

14.4.2 Line Plots

In addition to the 2D-planes, two cut-lines were drawn along the power station. One is displaying the vertical temperature development under the power station. The other cut-line displays the temperature development horizontally from the station. These cut-lines can be seen in Figure 38. The cut-lines give an easily comparable development of the 0°C isotherm, as the arc length grid lines state the distances specifically.

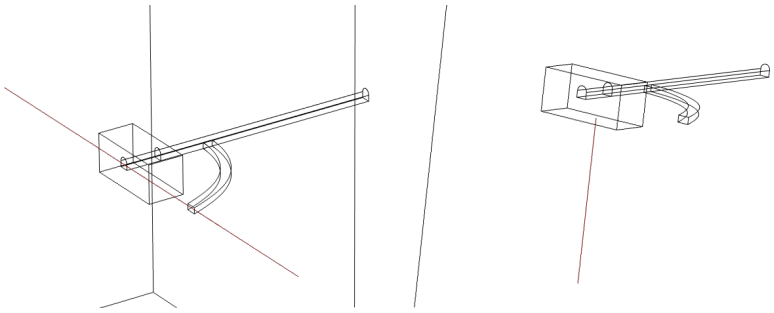

(a) Line 1 - horizontal. (b) Line 2 - vertical.

Figure 38: Position of cut-lines used to plot line graphs.

Firstly, the temperature development along the cut-lines were plotted in half year intervals for the construction period, with the steady state temperatures being plotted as the 0 year line. The results can be seen in Figure 39. Figure 39(b), shows the left side of the power station, as the access tunnel is located on this side and carries effect on the temperature regime.

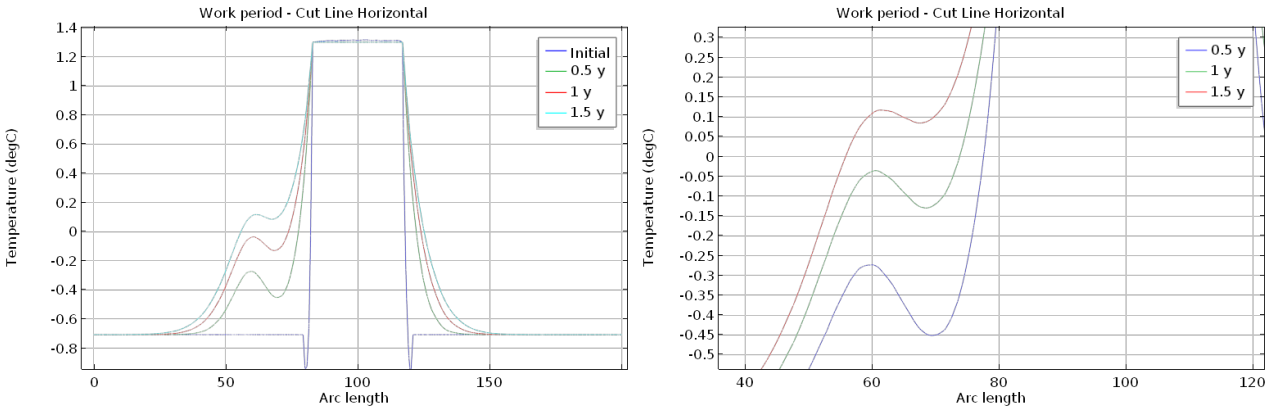

(a) Horizontal cut-line. (b) Access-tunnel side zoomed in.

Figure 39: Horizontal cut-line results for construction period.

Following the horizontal cut-lines, the results for the vertical cut-line of Figure 38(b) are plotted in Figure 40, the arc length equals the depth from the bottom of the power station. Here, one can see the heat dissipating from the power station, thawing the surrounding rock mass, before displaying a pocket of frozen rock until the gradient climbs above 0°C.

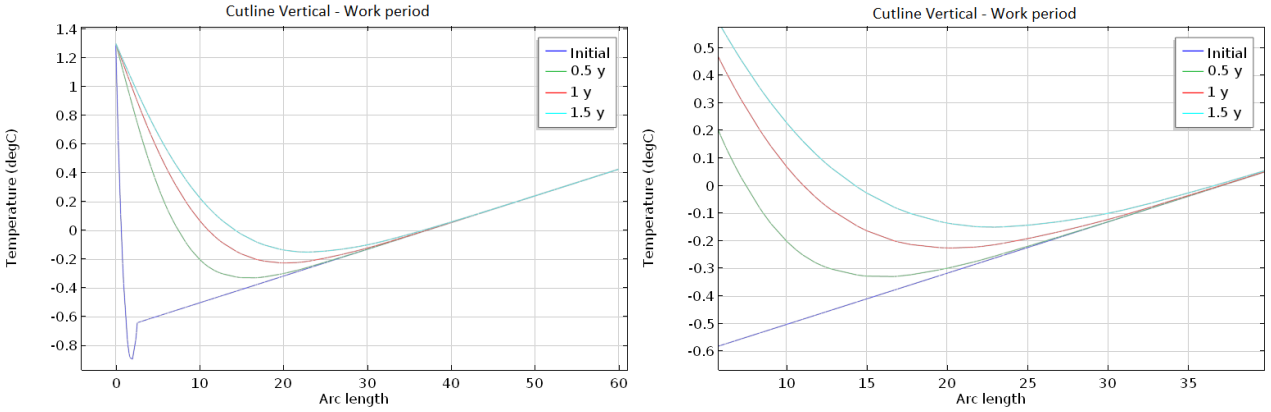

(a) Vertical cut-line results - overview. (b) 0°isotherm zoomed in.

Figure 40: Vertical cut-line results for construction period.

As the operational period is commenced, the horizontal cut-line for the first ten years can be seen in Figure 41. Again, one can see an effect on the left side of the power station, due to the access tunnel. In Figure 42, the area in question is zoomed in. As shown here, the effect of the access tunnel is practically nullified after only one year. The first line - representing half a year, shows a clear wobble of the curve as it passes the warmer access tunnel. However the next line, one year curve is hardly as bent.

If one then looks at the last two curves (ten and five years operation time), on the overview Figure 41, they assume nearly symmetrical values on either side of the power station. Thus yielding that equilibrium is almost reached.

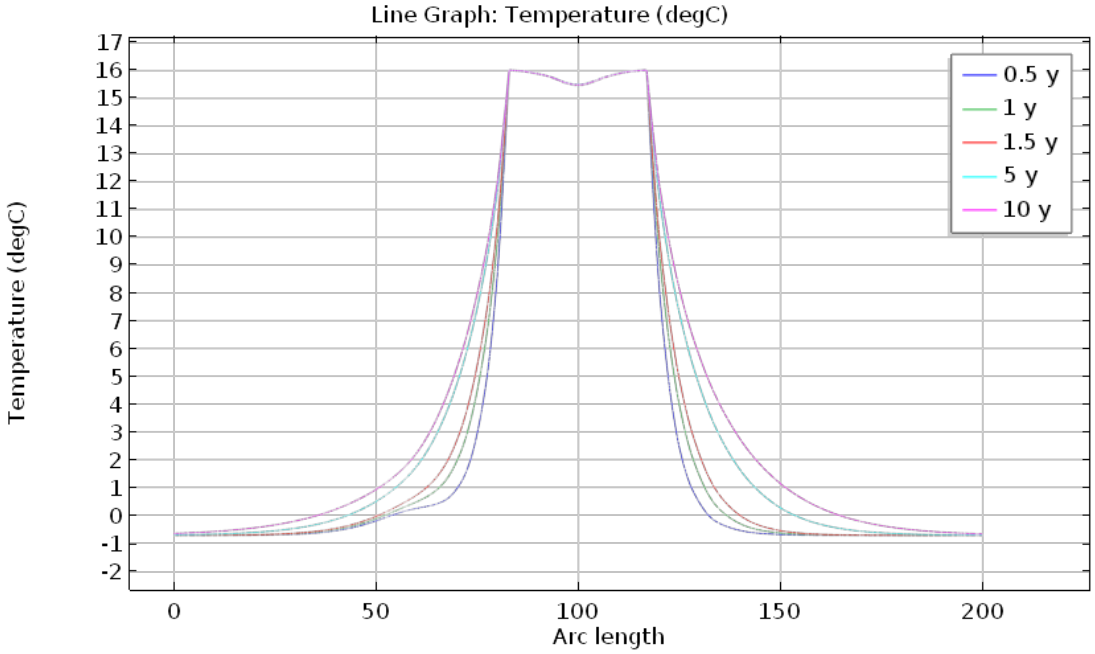

Figure 41: Results for horizontal cut-line. Power station lies in middle domain.

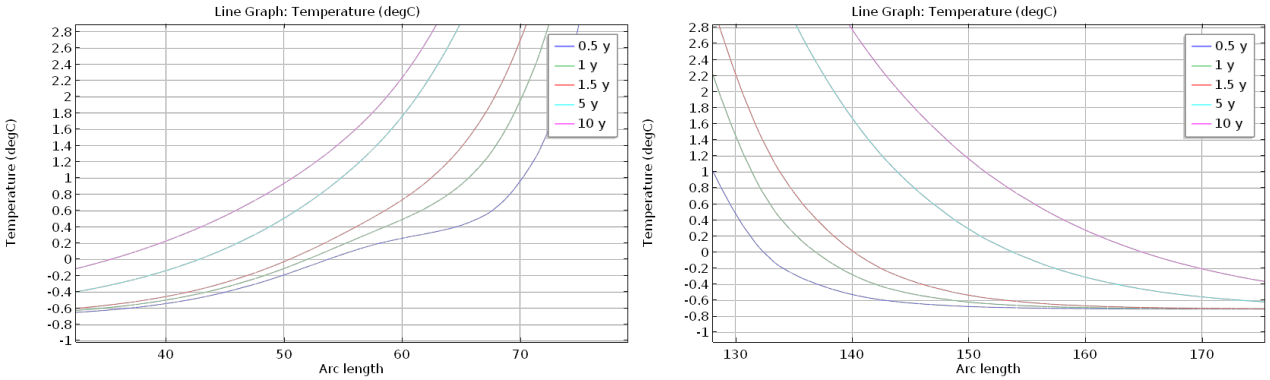

(a) Zoomed to the left side of power station - access tunnel side.

(b) Zoomed to the right side of power station.

Figure 42: Horizontal cut-line results for 10 year operation period.

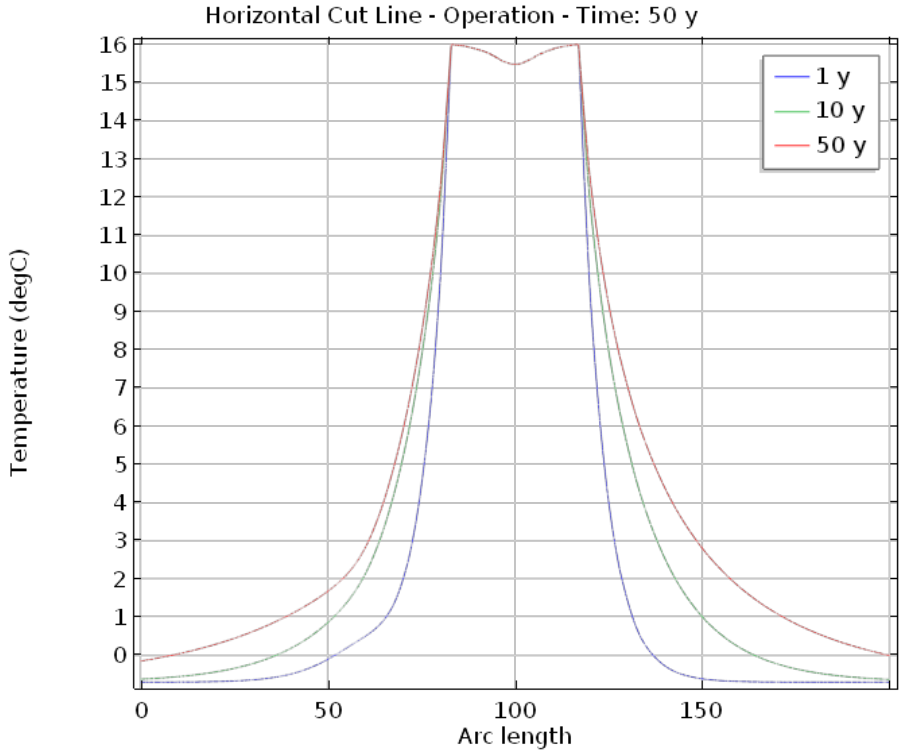

Figure 43: Results for horizontal cut-line after 50 years of operation.

The 50 year result is shown in Figure 43. It is evident that the maximum thaw after 50 years is in a magnitude of 80 m on each side of the power station. Thus the fit the corresponding analytical solutions, which according to Table 6 is in the range 80.2-135.3 m, depending on porosity.

One cut-line was drawn as a copy of the Borehole 4C (Figure 44). This way, a comparison between the measured temperatures from Nukissiorfiit and the results of COMSOL model can be made.

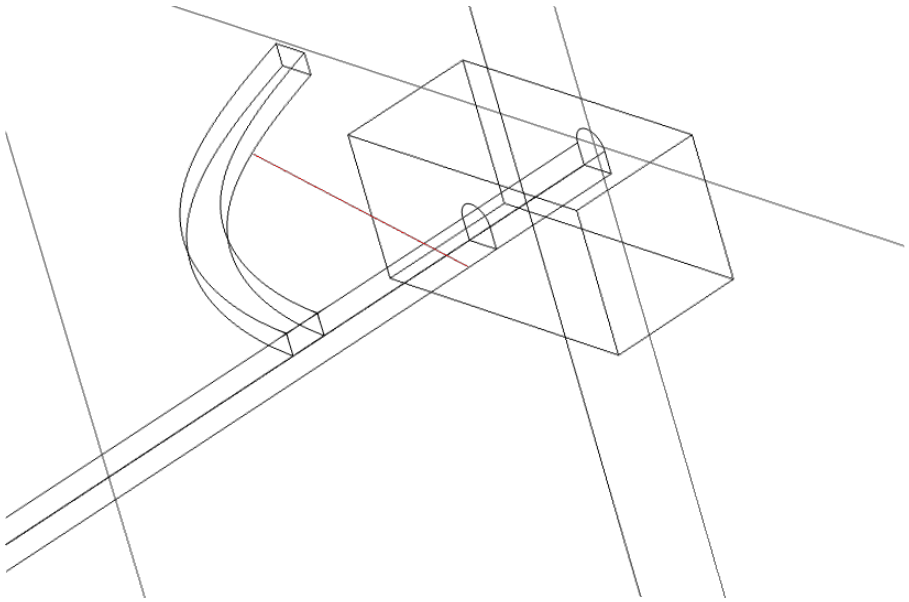

Figure 44: Cut-line shown as red line, approximately the position of borehole 4C.

The results during operation are shown in Figure 45. Beginning at the access tunnel on the left hand side, and directed over the intake tunnel towards the right. The result displays an increase in

temperature as the arc length located above the water intake is reached. Whilst the fluctuations are dampened as time is increased from a half year up to three years operation time, the curve over the intake is still visible. Specifically the one and a half year mark is interesting, as this is the limit to which Nukissiorfiit have continued their measurement data.

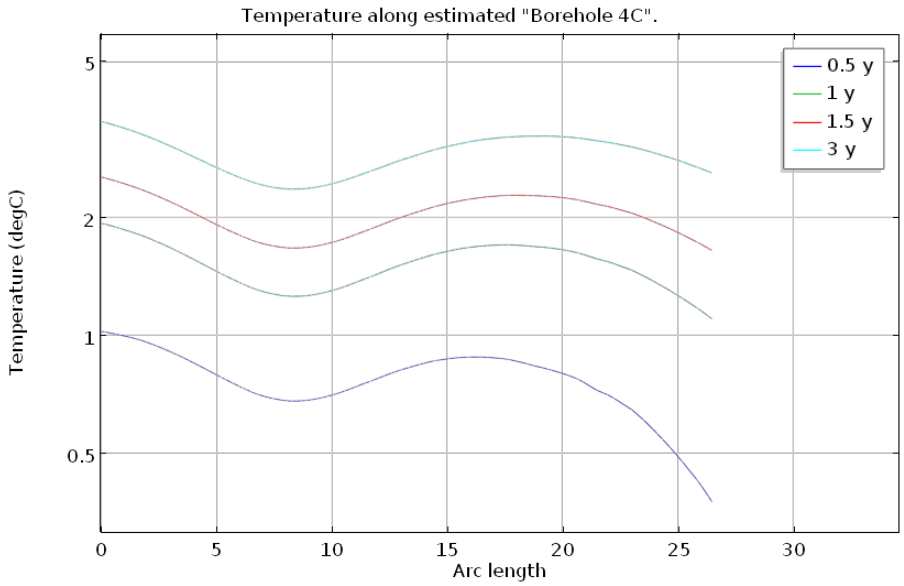

Figure 45: The modelled results of the 4C cut-line shown for different operational periods.

By comparing the modelled and measured borehole 4C results, on Figure 45 and 46, it is clear that the temperature distribution throughout the borehole follows the same trend. However the results do clearly differ from each other.

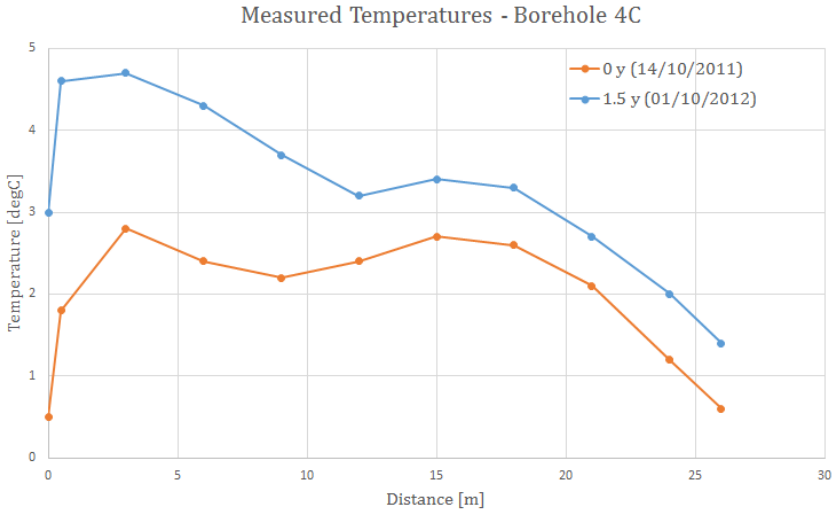

Figure 46: The measured results of the 4C cut-line shown for initial case and 1.5 years of operation.

Therefore statistical analysis between two samples assuming unequal variances has been made (t-test), testing for the probability that the means of the two are the equal. The t-test has been made with a 95% confidence interval, meaning that the true mean according to the null-hypothesis with 95% certainty is obtained.

The main assumption being done here, is that both samples approximate a normal distribution.

The null-hypothesis is thus postulated:

H_0: There is no significant difference between measured and modelled temperatures in borehole 4C after 1.5 years.

And the alternative-hypothesis thus becomes:

H_A: There is a significant difference between measured and modelled temperatures in borehole 4c after 1.5 years.

The results of the two runs of the t-test, with respectively including and disregarding the first measured data point for borehole 4C, can be seen in Table 11 and 12. According to these results, the null-hypothesis has to be rejected for the first run (Table 11) and thus the alternative hypothesis is accepted.

However when disregarding the first measured data point and thus having unequal observations in each sample, it is a different case. The reason for disregarding the first data point in the measured temperatures of borehole 4c, is to cancel out the seasonal fluctuations, which is not regarded by the model. Thus the measured first point of borehole 4c, was taken in October. By disregarding this, the curves match and correlate better with each other. The results of this action, may be seen in Table 12. Here it is seen that p-/ and t-values are within the acceptable range. Thus the p-value has to be larger than the confidence interval error of 5%, which it is. Furthermore the t-value has to lie in the range of the critical t-value, which it also does.

Furthermore as a general comment it may be seen, that the standard deviations are closely linked, for both Table 11 and 12. Thus an overlap of the mean values are assured for both modelled and measured data.

As a more qualitative statement, it does however appear that the model is a bit too warm compared to the measured data.

Table 11: Two sided t-test analysis of two independent data sets with a confidence interval of 95%. All 6 data points included for both samples

	Measured	**Modelled**
Mean	*3.16*	*2.17*
Variance	*0.77*	*0.17*
Standard Deviation	±0.80	±0.37
Observations	*6*	*6*
t-value	***2.52***	
p-value	***0.04***	
Critical t-value	±2.37	

Table 12: Two sided t-test analysis of two independent data sets with a confidence interval of 95%. Only 5 data points included for the measured sample, while all 6 are included for modelled sample.

	Measured	**Modelled**
Mean	*3.19*	*2.17*
Variance	*0.95*	*0.17*
Standard Deviation	±0.80	±0.37
Observations	*5*	*6*
t-value	***2.19***	
p-value	***0.08***	
Critical t-value	±2.57	

The statistical analysis' performed in the above mentioned section has to criticized for its relatively small sample sizes, as well as the fact that the variances of the two samples are varies a lot from

each other. However this t-test has been performed taken into account the unequal variances, in turn calculating degrees of freedom based on the discrepancy between the two standard deviations.

14.5 3D Results

The strength of modelling the temperature development in 3D, lies within the highly visual effect with which one can analyse the process. This model was produced by allowing only the volume of the model that is warmer or equal to 0°C to be shown, for different running times. Results can be seen in Figure 47, 48 and .

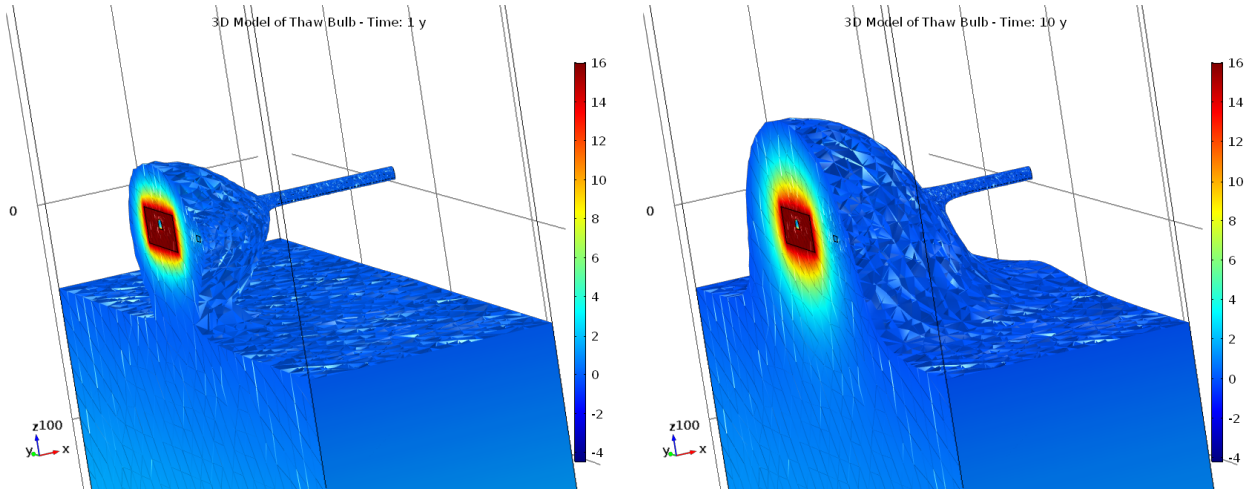

(a) Thawbulb after one year of operation.

(b) Thawbulb after ten years of operation.

Figure 47: Thawbulb development modelled in 3D.

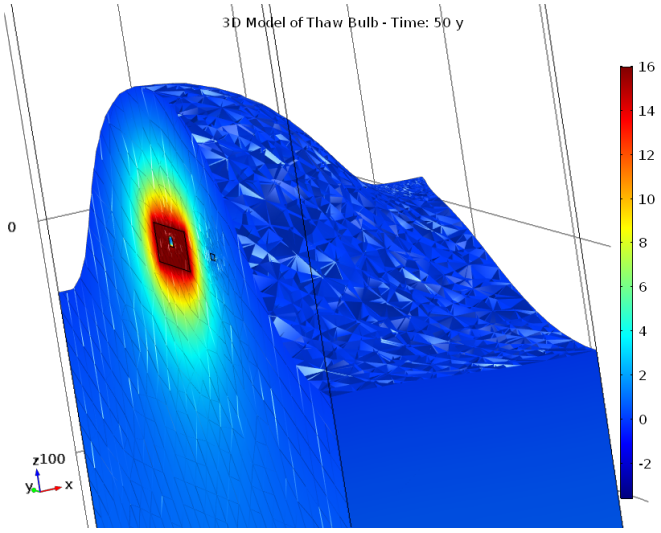

Figure 48: Thaw bulb modelled in 3D after 50 years of operation.

In Figure 48, the temperature development seen pointed to an interesting development along the intake tunnel. As the operational time gets to 50 years, the 0°C-isotherm also connects with the water intake tunnel. Seen from an alternate angle in Figure 49, one can see that the geothermal isotherm makes contact with the intake tunnel after approximately 30 years of operation.

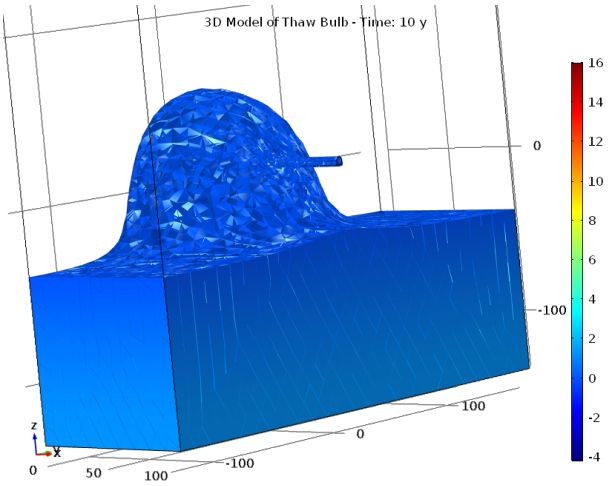

(a) Thaw bulb after ten years of operation.

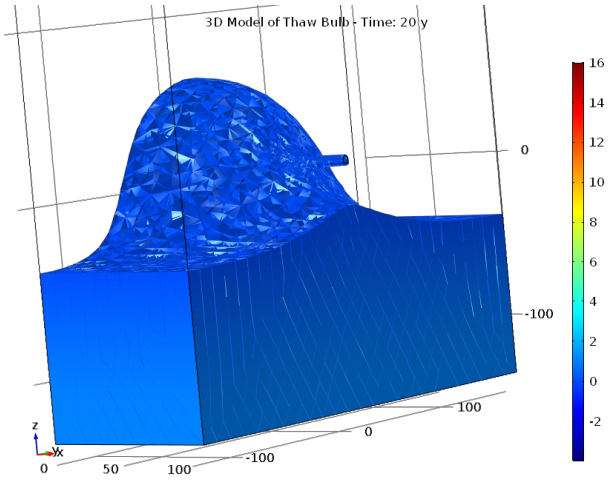

(b) Thaw bulb after 20 year.

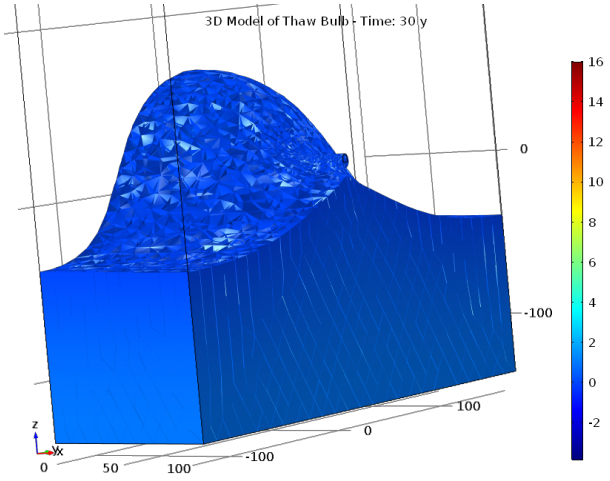

(c) Thaw bulb after 30 years.

Figure 49: Thaw bulb seen from the intake tunnel.

15 Discussion

As stated in the report, one of the key material parameters that causes some concern, in regards to validation is the thermal conductivity of the rock. To the authors knowledge no attempts have been made, trying to establish the correct thermal conductivity, via experimental work, since The Technical University of Norway did so in the 1980s. Future improvements of this study, would have to include laboratory work, re-measuring the thermal conductivity on the Paakitsoq rock. In terms of anisotropy one could also argue that it would be of value, trying to measure the thermal conductivity parallel and perpendicular to the foliations. However, in terms of realistically modelling these anisotropies in COMSOL, one must most likely be considered a senior user. Also it would be of benefit if any lab tests included determination of water content or at least porosity measurements. If this was done accordingly, a better understanding of the interaction between the constitutive elements and their effects of thermal regime, would be obtained. Furthermore it would have been good if any face logs existed, but non have been found by the authors.

The trumpet curve shown in Figure 9, is based on seven years of measurements as opposed to one year measurements, which is more common. However the authors considered it more reliable to include a wider range of data.

The next point of discussion relates to the measured temperature data. There seems to be a lack reliable data from some thermistors.

Specifically regarding the results shown in Figure 21, the authors set a question mark regarding the validity of the 21 meter thermistor seeing as it goes down to negative temperatures. This would indicate that there has developed a pocket of frozen rock mass close to the power station, which the authors consider to be highly unlikely.

It would be good if these were updated and automatic loggers were installed. Furthermore it would be beneficial for the future of the hydro power plant, if Nukissiorfiit made a scheme to take readings of each logger regularly. This way the data could be compared to a given temperature model, which in turn would give a better picture of what to expect from the temperature development in the future.

In terms of modelling, the authors have made several assumptions and simplifications, as stated previously. The results have been acceptable, however more detailed work into making the system more complex could be done. For instance a more elaborate system of boundary conditions could have been made, including using more than one heat flux or modelling the air-rock film as a convective surface, instead of taking the rock temperature directly.

Appendix 18 includes Verkís' memos in regards to establishing boundary conditions. Verkís have used the measured data from Istak to correct their boundary conditions. This method distinguishes from what the authors have done, as no subsequent corrections to boundary conditions have been made. In the last page of appendix 18, it can be seen, how both surface temperatures and heat fluxes are corrected to fit the measured data.

To summarize, Verkís' method has not been done similarly in this report. The basis of this, is to simplify the problem, but also to see exactly how much the model assumptions differentiate from the measured Istak data.

However it should be carefully considered into which of these details, it would benefit the model versus the amount of time and money spent. Another point worth mentioning is in regards to fluid flow and the assumption that it is uniform and laminar. In reality a much more complex turbulent system would exists and it is not known how this would affect the thermal regime in comparison.

Regarding the construction period little information was available. Specifically in terms of work schedules and types of work at specific positions. This would have benefited in terms of interpreting temperature development.

The results of this report include analytical, measured and modelled data. Overall the authors found there is a good correlation between the methods.

Firstly the expected ranges of thaw accounted for in the analytical section 12, correlates well with the modelled ranges of thaw, over the same time span. Comparing Table 6 for the 50 year period with Figure 43, one can see that the thaw bulb from the model is equal to 80 meter. This compares well with the 1% porosity result, which also states a thaw radius of 80.2 meters.

Moreover, the steady state results from the model and the measured data from borehole 4C, near the power station, correlates well. The first measured temperature at 4A in 26 m depth was -0.6°C. The initial temperature shown in Figure 39(a) is consistent with this, at a temperature of -0.7°C.

In terms of the thaw bulb development, the authors have chosen to focus on the power station. This was obviously done because the operational temperature was at maximum at this locality. A temperature of 16°C was chosen to represent the power station as a whole, while measurements show fluctuating temperatures varying from 12-20°C, depending on position in the power station.

One central simplification, which has been used for the modelling and will have resulted in an increased thaw bulb, is the boundary between power station and rock. The model suggests that 16°C, is directly applied to the rock, however in reality there is a concrete wall within the power station. This of course has completely different thermal characteristics.

The thaw bulb development show that a large volume will thaw. If this volume contains (as expected) ice, it will turn into free water. In the future it might be necessary to inject concrete, into the rock mass, in order to close cracks and fissures.

16 Conclusion

As a general statement, it is conclusive that this report deals with a special case, in regards to designing hydro power through permafrozen rock mass.

This report offers an overview of the theory, of which it is relevant. Through this report and its content, the theory and considerations into Arctic conditions has been made clear. This entails permafrost, glaciological, rock- and fluid mechanical theory. Moreover the basic laws of thermodynamics and its heat transfer mechanisms have been covered.

These include explanations into how the geology of the local Paakitsoq region is built up. This conclude that the geology is located within a structural fault zone, between the Rinkian and the Nagssugtoqidian mobile belts. The host rock is a migmatic orthogneiss, with a mineral composition of tonalite to granodiorite. It is concluded that the key mineral, in having high thermal conductivities is quartz.

Furthermore it is concluded that the bedrock exhibits anisotropic behaviour, due to mineral assemblage, structural damages, porosity and foliation. Via the discussion it is also noted that further laboratory test should be made into determining more exact material parameters: density, specific heat capacity and thermal conductivity.

The boundary conditions correlate well with earlier studies, which also have been the inspiration for the authors.

The steady state results in Table 9, between COMSOL and Istak correlate well, with a maximum difference of 0.84°C and the smallest difference being 0.01°C.

Results from analytical, measured and modelled data correlate fairly well with each other. Thus the expected thaw bulb after a 50 year period has a 80 m radius.

The results from the specific modelling of the construction period, are compared to the measurements conducted by Istak. Certain points correlate between measured and modelled data. However no decisive tendency, linking these have been concluded, for the entire model.

Through the modelling, it can be seen that the major thaw effects are due to the operational period and the high temperature of the power station.

The access tunnel has a large effect on the early temperature development. However after a 5 year operational period, the effects have been nullified.

The local (caused by thawing from power station) and global 0°isotherms connect in between 0.5 and 1 year of operation, as per Figure 36.

It is concluded that over time, the largest thaw bulb development, will occur around the power station. In a 50 year period a thaw bulb with a radius of 80 meters has been predicted.

With some statistical evidence, there is a correlation between the modelled and measured data. This has been proven by a t-test.

As new users of COMSOL Multiphysics, it can be concluded that it is a complex software, with a lot of possibilities. A problem with modelling, which has occured during the process, has been handling of complex geometry. However the models, which have been run, have utilize the program to good effect.

It can be concluded that the operation of the hydro power plant is not affected by seasonal conditions, as the depth of zero amplitude lies above the hydro power plant.

As described the bedrock is sound and the RQD is high, thus there is no to little chance of structural instability, as a result of freeze/thaw cycles.

From the authors point of view and the interpretation of all the data included in this study, no evidence of potential instability has been found. The hydro power plant is functioning well within the thermal regime of the rock, as it should and will continuously do so in the future.

For future references it would be interesting to make a more complex model, based on lab tested material parameters and updated in-situ temperature measurements.

References

Andersland, O. B. and Anderson, D. M. (1978). *Geotechnical Engineering for Cold Regions.* McGraw-Hill.

Andersland, O. B. and Ladanyi, B. (2004). *Frozen Ground Engineering.* Wiley.

Clauser, C. and Huenges, E. (1995). *Thermal Conductivity of Rocks and Minerals.* American Geophysical Union.

Einarsson, s. P. (2011). *Verkís Internal Memos Regarding Paaktisoq.* Verkís.

Elger, D.F., e. a. (2013). *Engineering Fluid Mechanics 10th Edition.* John Wiley & Sons, Inc.

Escher, J. C., Ryan, M. J., and Marker, M. (1999). *Early Proterozoic Thrust Tectonics East of Ataa Sund, North-East Disko Bugt, West Greenland.* GEUS.

Henriksen, N. (2006). *Grønlands Geologiske Udvikling - Fra urtid til nutid.* GEUS.

Johnston, G. H. (1981). *Permafrost - Engineering Design and Construction.* National Research Council of Canada.

Kahraman, S. and Fener, M. (2005). *The effect of porosity on the relation between uniaxial compressive strenght and point load index.* Rock Mechanics and Mining Sciences.

Kern-Hansen, C. (1990). *Data Basis for Permafrost Studies in Greenland.* Greenland Field Investigations Hydro-Technical Division.

Kothandaraman, C. P. (2006). *Fundamentals of Heat and Mass Transfer.* New Age International (P) Ltd., Publishers.

Lachenbruch, A. H. (1970). *Some Estimates of the Thermal Effects of a Heated Pipeline in Permafrost.* US Geological Survey.

Lennert, L. P. (2010). *Hydropower plant in Paakitsoq west Greenland.* The Technical University of Denmark.

LICconsult (1985). *Vandkraftværk Paaktisup Akuliarusersua Ilulissat.* GTO.

Mai, H. (2009). *Water temperatures and ice conditions in Arctic lakes and reservoirs.* Niras Greenland A/S.

Peiró, J. and Sherwin, S. (2005). *Handbook of Materials Modeling. Volume I: Methods and Models, 1-32: FDE, FEM and FVM for PDEs.* Department of Aeronautics, Imperial College.

Ístak (2012). *Ilulissat Temperatur Målinger Statusrapport - Udkast.* Ístak - Nukissiorfiit.

Yershov, E. D. (1998). General geocryology. *ARCTIC*, 53.

17 Appendix 1

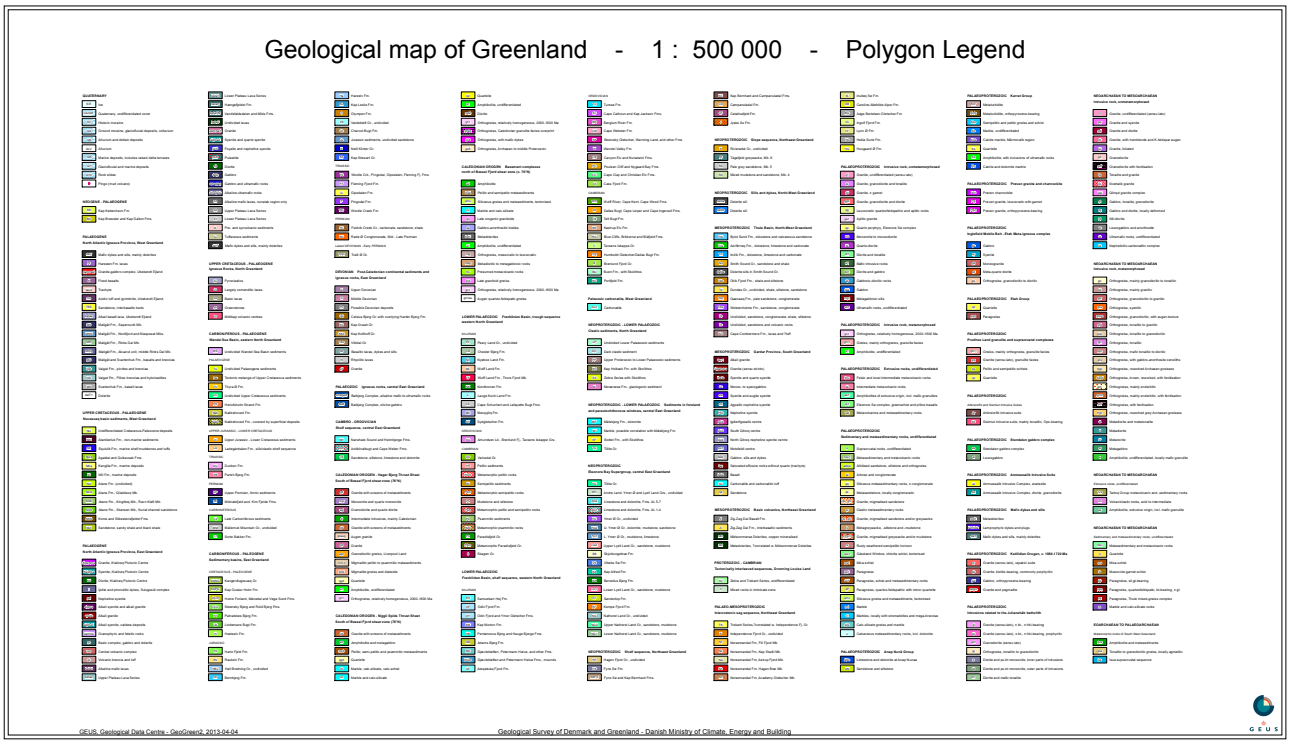

18 Appendix 2

ILULISSAT POWER PLANT

MEMO

PROJECT NO:	09304-002	DATE.:	2012-01-24
PROJECT PHASE:	41	NO.:	2363
AUTHOR:	ÓPE		
DISTRIBUTION:	ÆJ, ÞSL, EBJ/Verkís, GHG, HS/ÍSTAK		

Subject: Permafrost model, updated by new temperature measurements

Early in 2011 a study was made, where the minimum water flow required to prevent water from freezing in the main tunnels in the Ilulissat power plant in Greenland was estimated.

This was based on 25 year old temperature measurements from drilled holes in the rock in the area, estimated values of thermal properties of the rock and temperature measurements of the intake reservoir water and sea water, as well as climate data in the area ([1], [2], [3], [4]). From the known data, a three-dimensional, transient heat transfer model was developed and used to estimate the interaction between the water flowing through the tunnel and the cold surrounding rock.

The result from this study ([5]) is that 315 l/s of water flow is sufficient to prevent the water from freezing, considering a number of worst case scenarios. During plant outage, this flow can be achieved using water by-passes that consist of shut-off valves and appropriately sized orifice plates. This flow rate is considerably lower than the originally proposed 1200 l/s by-pass flow rate during outage, requiring a considerably smaller by-pass installation.

During the latter half of 2011, when the actual head- and tailrace tunnels were constructed, a number of temperature measurements ([6]) were done in the tunnel and surrounding rock over time. The result of these measurements have been used to re-calibrate the heat transfer model, where only the top and bottom boundary conditions (surface temperature and heat flux) have been modified, so that calculated and measured temperatures are in agreement.

The interaction between water flowing through the main tunnel and rock has finally been re-calculated to verify that the 315 l/s flow rate is sufficient to prevent water from freezing during outage. The location of the 0°C isotherm is also compared to the originally assumed isotherm, that was used to locate the first few hundred meters of the headrace tunnel.

1 Finite element model and boundary conditions

Finite element model

An isometric view of the three-dimensional finite element model is shown in Fig 1.

The top elevations are based on a map of the land surrounding the head- and tail-race tunnel from the reservoir to the fjord, the length of which is around 3,3 km.

The bottom elevation of the model is 200 m below the sea level. The width of the model is 400 m, i.e. 200 m from each side of the tunnel. The ends of the model reach around 100 m beyond both ends of the tunnels.

The finite element distribution along the length and height of the model can be seen in Fig 1. The mesh around the mainly unlined rock tunnel can be seen in Fig 2, where a finer mesh nearest to the tunnel is needed, due to high thermal gradients in that region compared to the rest of the model. The finite element model remains unchanged from the earlier study from 2011 ([5]).

Verkís hf.
Ármúla 4, 108 Reykjavík
+354 422 8000
verkis.is | verkis@verkis.is

Offices:
108 Reykjavík, Ármúla 4-6
108 Reykjavík, Suðurlandsbraut 4

300 Akranes, Stillholti 18
310 Borgarnes, Bjarnarbraut 8
400 Ísafjörður, Hafnarstræti 1

603 Akureyri, Austursíðu 2
700 Egilsstaðir, Kaupvangi 3b
800 Selfoss, Austurvegi 10

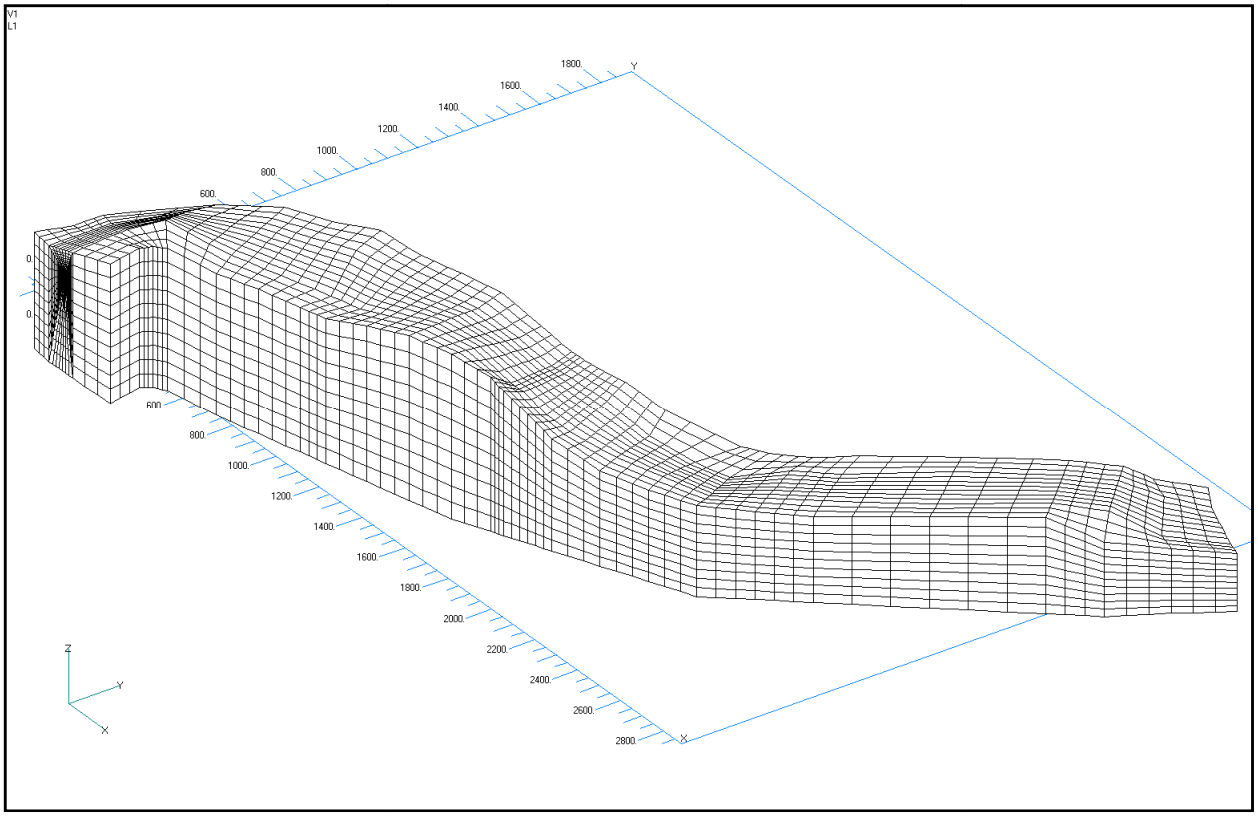

Fig 1 3D-model, isometric view showing finite element mesh on outer boundary

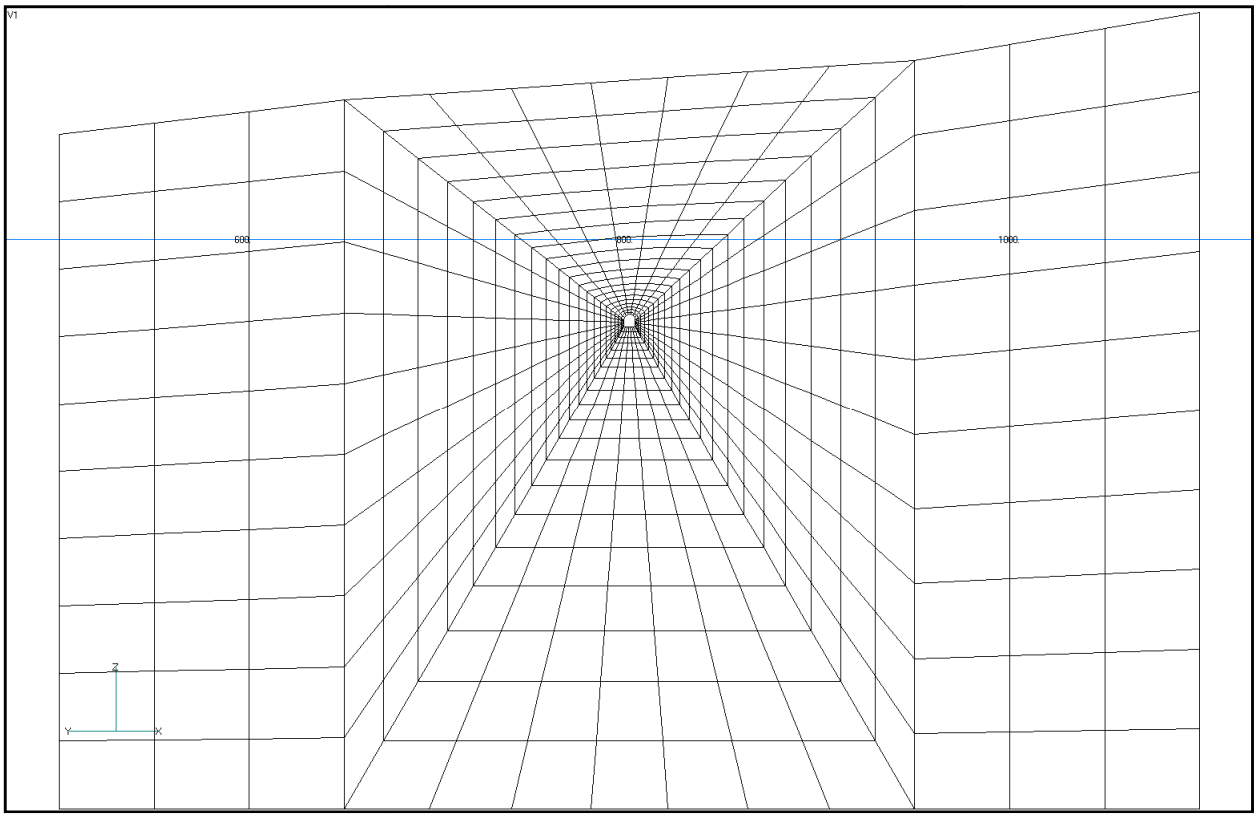

Fig 2 Finite element mesh, cross section perpendicular to tunnel

The thin line inside the model, shown in Fig 3 represents the inner boundary of the model, i.e. the inner tunnel wall. Water temperatures are imposed on this inner boundary and from temperature gradients in the surrounding rock, the heat flow from water to rock is calculated.

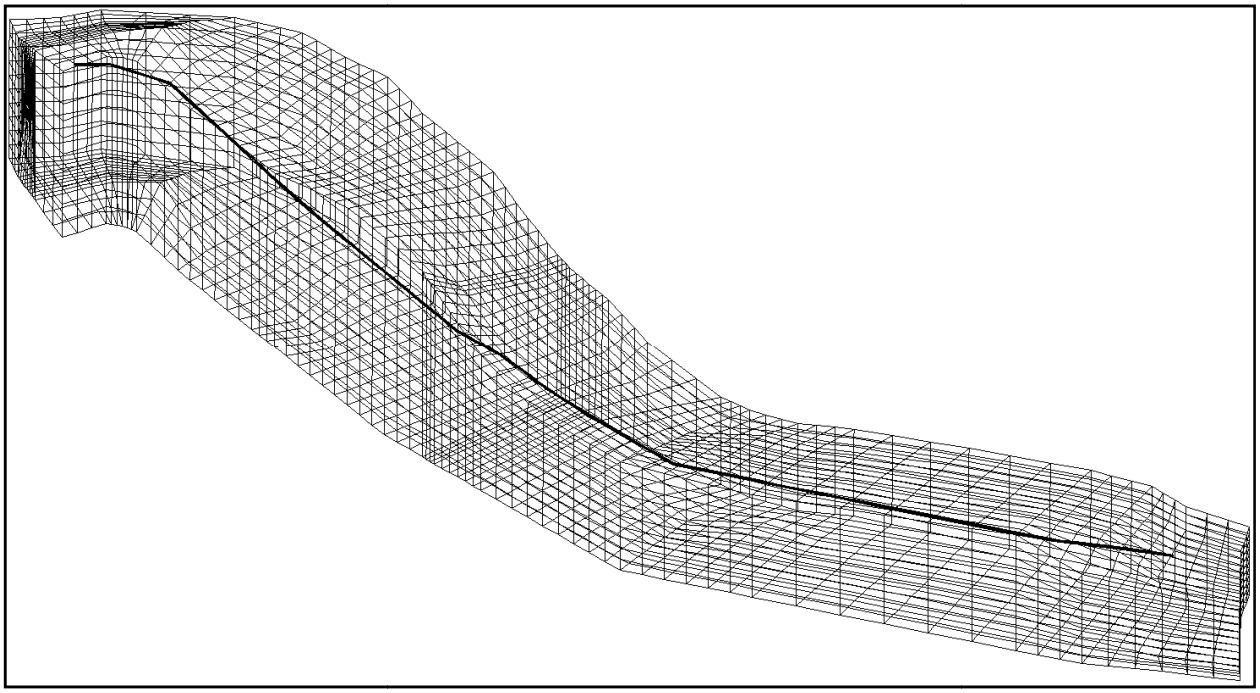

Fig 3 Inner and outer boundary of finite element model.

Thermal properties of rock

The following values from [1], page 787, are used for calculating heat conduction of the rock in the model. These values remain unchanged from the earlier study from 2011 ([5]):

- Thermal conductivity: 3,5 W/m°C
- Specific heat capacity: 730 J/kg°C
- Density: 2.700 kg/m^3

Air temperature

In the earlier study ([5]), air temperature variation with altitude was assumed to be -0.7°C per 100 m elevation ([2], page 787) and -5.0°C at sea level was used as base temperature. Different air convection parameters were then used to match model temperatures with measured temperatures. In this study, however, no combination of convection parameters with air temperature are used but instead, a constant rock surface temperature value is used at different locations on the upper surface of the model. This method is more convenient for model calibration purposes, to fit measured temperature data to the model parameters. The comparison between surface temperature in this study and the air temperature and convection used in the earlier study are shown in Fig 9, at the top of each section.

Water temperature in reservoir and fjord

Water temperatures in the fjord and reservoir are used unchanged from the earlier study ([5]) and they are:

- Fjord at 25 m depth: -0,05°C
- Reservoir Sø187 at 25 m depth: 0,84°C

These water temperatures are applied to the upper section of the model as constant temperatures, as shown in Fig 9 at the top of each section by the two tunnel ends.

Rock temperature measurements

The following measurements are taken from [6] and are shown in Fig 8 (plan) and Fig 9 (section), in relation to the heat transfer model. They are used for calibration of model by varying boundary conditions (surface temperature and heat flux from ground), until model temperatures match measured temperatures within a reasonable margin. The temperature measurements were taken over time at each location during the latter half of 2011 [6]. In all cases, the lowest measured temperature has been used, to ensure a conservative estimate of heat loss from the water flowing through the tunnels.

Table 1 Rock temperature measurements in tunnel (see Fig 8 and Fig 9)

Measuring point	Elevation	Date of measurement	Measured temperature
T8	135.5	1.10.2011	0.8
T5b	12.5	24.9.2011	0.3
T5a	5.0	3.8.2011	0.7
T4a	0.7	5.6.2011	-0.7
T2	-27.5	17.9.2011	-1.4
T1	-13.0	23.6.2011	-1.4
	m.a.sl.		°C

Zero heat flux boundary conditions

The horizontal variation of vertical heat flux is assumed to be negligible at 200 m from the side of the tunnels in the model and at 100 m from each end of the tunnel. This means that heat flux is zero through the vertical sides and vertical ends of the model (see Fig 1).

Also, during calibration of rock temperatures for steady state initial conditions, zero heat flux is assumed on the inside of the tunnel walls. This represents the assumption that no heat is added to or removed from the mountain while the tunnel is being constructed.

Calibration and resulting boundary conditions

The following table contains the boundary conditions used on the model that result in the best possible match between the temperatures calculated in the model and measured temperatures. These boundary conditions (as well as reservoir and fjord bottom temperatures by tunnel ends) are shown in Fig 9 and are compared to boundary conditions used in an earlier study ([5]).

Table 2 Boundary conditions, overview

Zone (length along tunnel)	Rock surface temperature	Heat flux from ground
1 (0-560 m)	-1.87 (0.84*)	0.082
2 (560-1150 m)	-3.86	0.058
3 (1150-1600 m)	-4.99	0.157
4 (1600-2030 m)	-5.03	0.050
5 (2030-2750 m)	-3.89	0.200
6 (2750-3380 m)	-3.92 (-0.05**)	0.151
	°C	W/m^2

* At reservoir bottom

** At fjord bottom

2 Calculations and results

The following section describes how the model results from boundary conditions are used to calculate heat loss from the water, flowing from reservoir Sø 187 to the fjord. The worst case

assumptions of water cooling are listed and finally, the estimated minimum required flow is presented and compared to an earlier study where different boundary conditions were used.

Calculated vs. measured temperatures

The following table contains measured temperatures from Table 1 and temperatures calculated from model by varying the boundary conditions.

Table 3 Calculated vs. measured temperatures

Measuring point	Measured temperature	Calculated temperature	Difference
T8	0.80	0.72	0.08
T5b	0.30	0.31	-0.01
T5a	0.70	0.53	0.17
T4a	-0.70	-0.76	0.06
T2	-1.40	-1.48	0.08
T1	-1.40	-1.44	0.04
	°C	°C	°C

Calculated values are generally slightly lower than measured values, resulting in a conservative estimate. These values are also shown in Fig 9. The agreement between measured and calculated values is fairly good, except for point T5a, where the calculated temperature is 0.17°C lower than the measured temperature. Still, the comparison results in an overall conservative estimate.

Results from steady-state calculation

The temperature profile through the model can be seen in Fig 4.

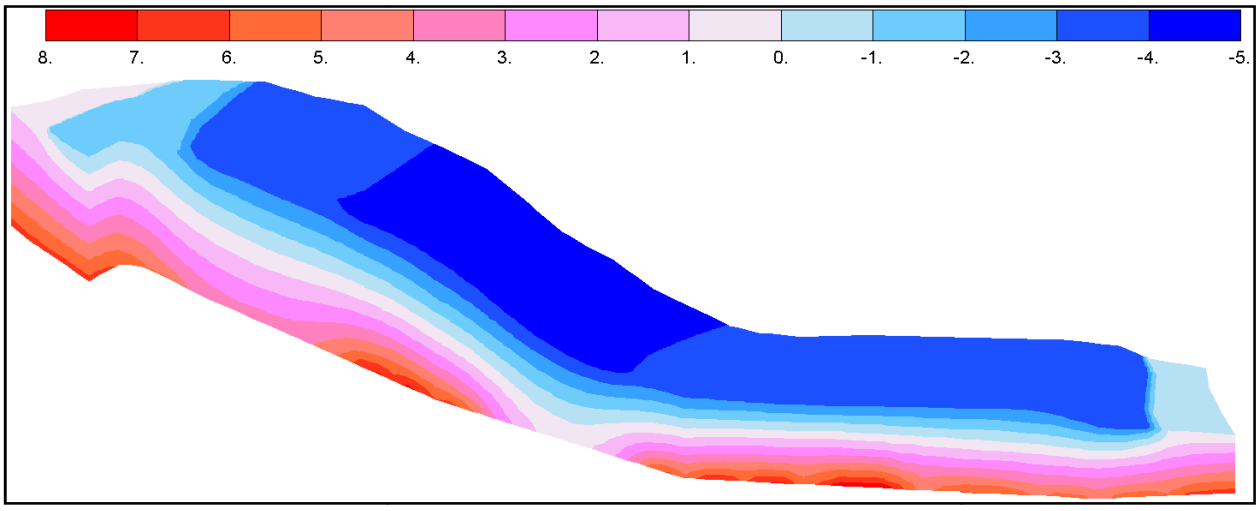

Fig 4 3D-model, isometric view showing temperature profile through rock

In Fig 9, a section is taken along the head- and tailrace tunnels through the 3D model, showing the variation of the rock temperature in the vertical plane along the tunnels. The comparison between calculated and measured temperatures is also shown in the section.

In an earlier study [5], the model was calibrated based on temperature measurements from drilled holes near the tailrace tunnel. These measurements, a total of 7 measuring points, are between 1.2°C higher and 1.0°C lower than calculated values by the current model. On average, they are 0.12°C higher than values calculated by the current model. These older temperature measurements are therefore rather scattered around the current model values and are not considered for calibration in the current model, as they are over 25 years old.

Calculation of heat loss from water

The following extreme worst conditions (identical to the assumptions from the earlier study, [5]) are assumed when calculating heat loss from water, running through the tunnel at the minimum flow rate that ensures that water temperature never goes below 0°C:

- The wall temperature is the same as the water temperature in the tunnel. This is a conservative estimate, since a film coefficient between water and rock (which is very high for water) means that rock would be at a slightly lower temperature than the water.
- Water from the reservoir is 0,01°C when entering tunnel.
- If water enters rock that is at a higher temperature than the water, it does not absorb heat from the rock. It only loses heat to colder rock. Again, this is a conservative estimate.
- When water is throttled in the water by-pass (control valve or orifice), 75% of the throttling energy (product of mass flow, gravity acceleration and head loss) is converted to heat, that increases water temperature.

The calculation is performed in the following steps, in which the tunnels are divided into 22 discrete sections, where water temperature is assumed to be constant:

- Initial temperature of water (0,01°C) is set as a temperature boundary condition on the tunnel walls. Wall temperature is equal to water temperature.
- The program calculates the heat flow through the walls, based on temperature gradient through the rock, after being exposed to constant 0,01°C water temperature for 24 hours.
- The total heat flow (q, kW) in each of the 22 tunnel sections is equal to the heat lost from water, which is the product of the water mass flow, heat capacity and temperature drop in the fluid, or $q = \dot{m} \times C_p \times \Delta T$. This quantity is always positive, i.e. temperature change is always zero or negative.
- The temperature profile of the water is calculated through each section. In the section running through the power station, the heating through throttling of water is calculated as $\dot{m} \times g \times \Delta h = \dot{m} \times C_p \times \Delta T$, or $\Delta T = g \times \Delta h / C_p$. The water mass flow, $\dot{m}$, is the product of the water density (1000 kg/m^3) and water flow, in l/s. Water heat capacity is C_p=4.224 kJ/kg°C at at 0°C, g=9,81 m/s^2 is the gravitational acceleration and the head loss through throttling (Δh) is equal to the elevation of the reservoir, 186,1 m.a.sl. Note that the temperature rise (calculated to be 0,43°C) from throttling is independent of mass flow.
- The new temperature profile of the water is added as a new temperature boundary condition (step 2 through 5 repeated) and flow is varied until water temperature is always at least 0°C and the temperature profile of water through the tunnel does not change significantly.

Results of the calculation after 24 hours can be seen in Fig 5. A slight temperature increase can be seen around the tunnel wall.

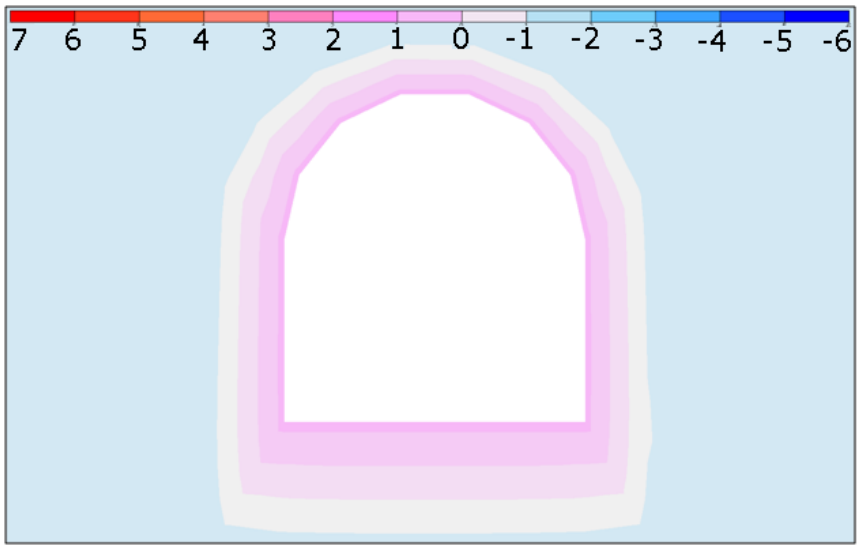

Fig 5 Temperature around tail-race tunnel after 24 hours, section.

The result from the calculation in an earlier study ([5]) was that at least 315 l/s of water flow are required for tunnel water to stay above 0°C, during worst possible conditions. The temperature profile of water and initial rock temperature is shown in Fig 6, where the water temperature actually reaches just above 0°C before entering the power station and by-pass orifice.

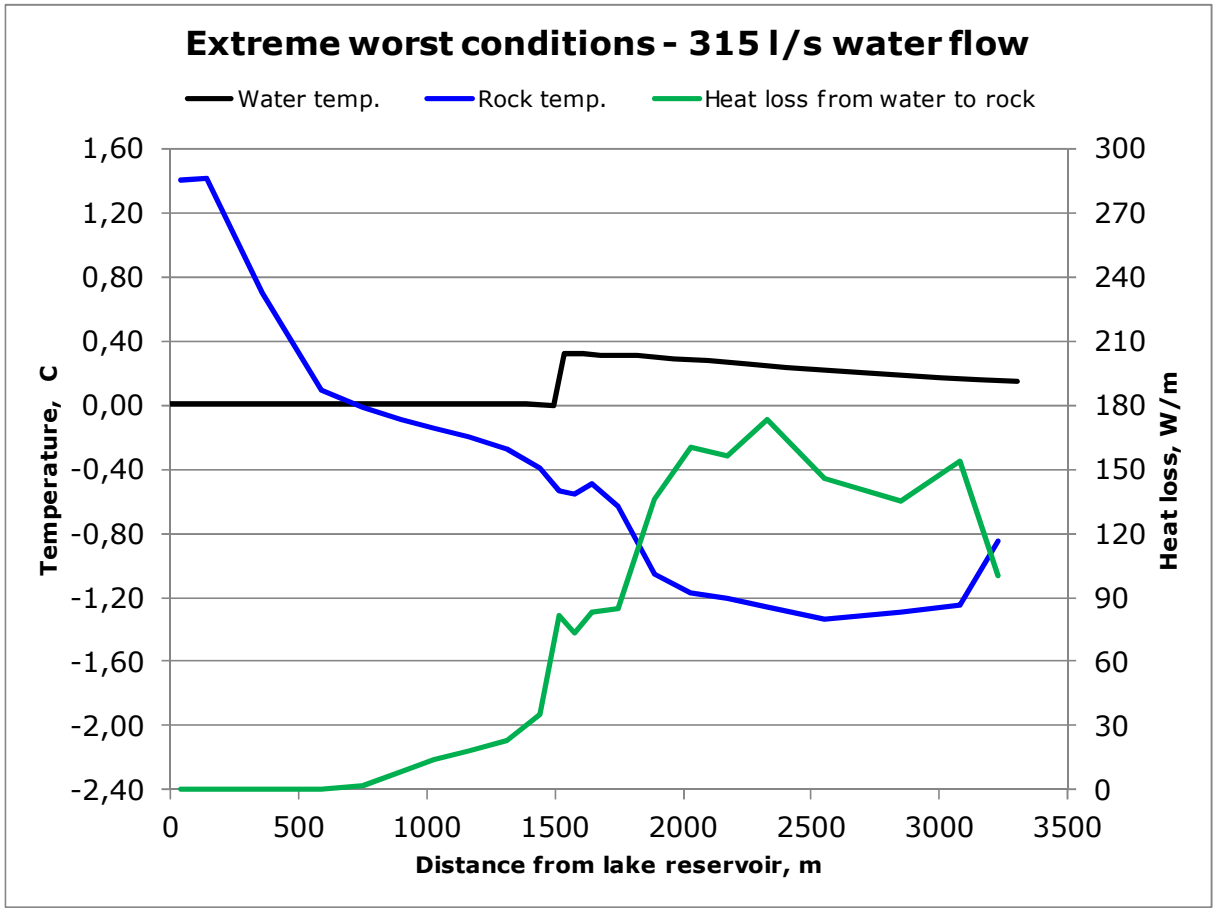

Fig 6 Temperature profile of water and rock, extreme worst conditions in earlier study.

The updated result is shown in Fig 7. The main difference is that rock temperature around the headrace tunnel is higher than was estimated in the earlier study but temperatures around the tailrace tunnel are lower than estimated in the earlier study.

Overall, the total heat lost from the water is lower than in the earlier study, so 315 l/s water flow is not strictly needed. As the by-pass installation has already been designed and tendered, there is no reason to change the specified design flow. Instead, if 315 l/s flow is maintained, it would mean that only 40% of the pressure energy needs to be converted to heat (not 75%), in order to maintain water temperature over 0°C. The water temperature after throttling through the by-pass is shown in Fig 7, both for 75% and 40% conversion of mechanical energy of water to heat in the by-pass.

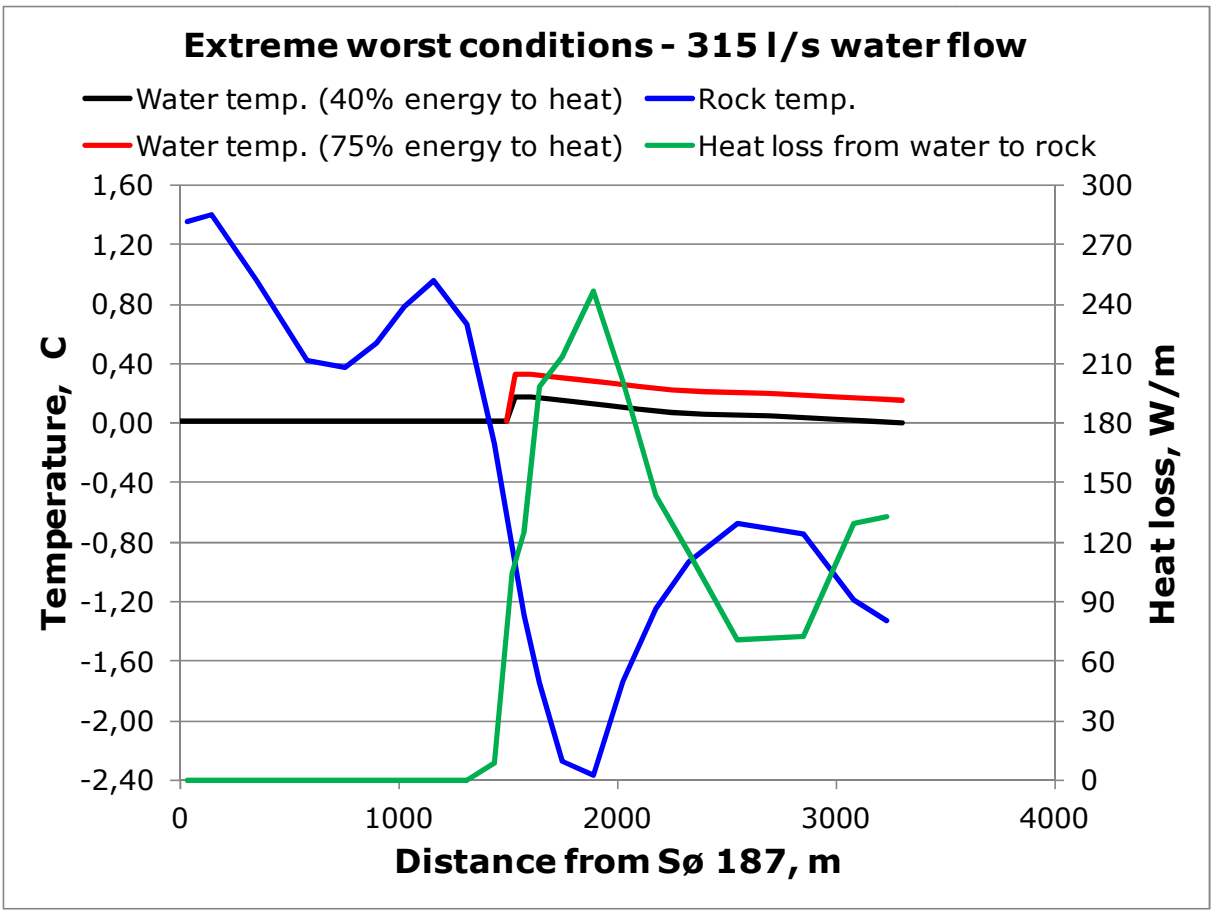

Fig 7 Temperature profile of water and rock, updated boundary conditions.

The above results are shown after the first 24 hours of operation of the tunnels, without any assumed changes in natural temperatures in the rock. After several days and weeks, the rock temperature around the tunnel will increase significantly, the heat lost from the water will reduce drastically and the water will be on the average warmer than shown in Fig 7. Also, during normal plant operation, the water flow is over 14 m^3/s, meaning that water cooling in the tunnel will be negligible.

Another significant result is shown in Fig 9. The elevation of the headrace tunnel was based on an assumed location of a 0°C isotherm, shown as a thick, dotted line in Fig 9. The new 0°C isotherm (shown as a thick, solid line in Fig 9), based on recent measurements in the tunnel and model calculations, lies significantly higher than the originally assumed isotherm. This means that the tunnel near the Sø 187 reservoir can be excavated at more shallow depth than was originally assumed. Even if the tunnel is at shallower depth than in the 3D model, rock temperatures will be higher than water temperature in both cases, so this will not affect the calculated minimum required water flow.

3 Conclusion

A 3D heat transfer model has been re-calibrated to fit recent temperature measurements and used to estimate the minimum required water flow that prevents water from freezing in the head- and tail-race tunnels of the Ilulissat power station. The

The results from an earlier study - where the same heat transfer model was used - were that 315 l/s was the minimum water flow required to prevent water from freezing. The results from the model with updated boundary conditions - where calculated temperatures are in good agreement with measured temperatures - is that lower water flow than 315 l/s would be needed, as rock temperatures are overall higher than assumed in an earlier study.

As the by-pass installation has already been designed and is currently being tendered and constructed, it is concluded that there is no reason to modify the earlier result of 315 l/s by-pass flow.

[1] Mai, Henrik. Hydropower Tunnels in Permafrost. Underground Hydropower Plants, Oslo, June 22-25, 1987.

[2] Grønlands Tekniske Organisation. Vandkraftværk Paakitsup Akuliarusersua Ilulissat/Jakobshavn, Permafrostundersøgelse, Endelig Rapport. LIC Consult Rådgivende Ingeniører. November 1985.

[3] Anlægstekniske forundersøgelser, Paakitsup Akuliarusersua. GTO. 30. September 1987.

[4] Web site: http://www.climatetemp.info/greenland/ilulissat-jakobshavn.html

[5] Einarsson, O., Permafrost Model By-Pass Flow Through Tunnels, Verkis Memo, 2011-01-25

[6] Ístak Grønland/Nukissiorfiit.gl, Ilulissat Vandkraftværk - Temperaturmålinger, Statusrapport, October 2011.

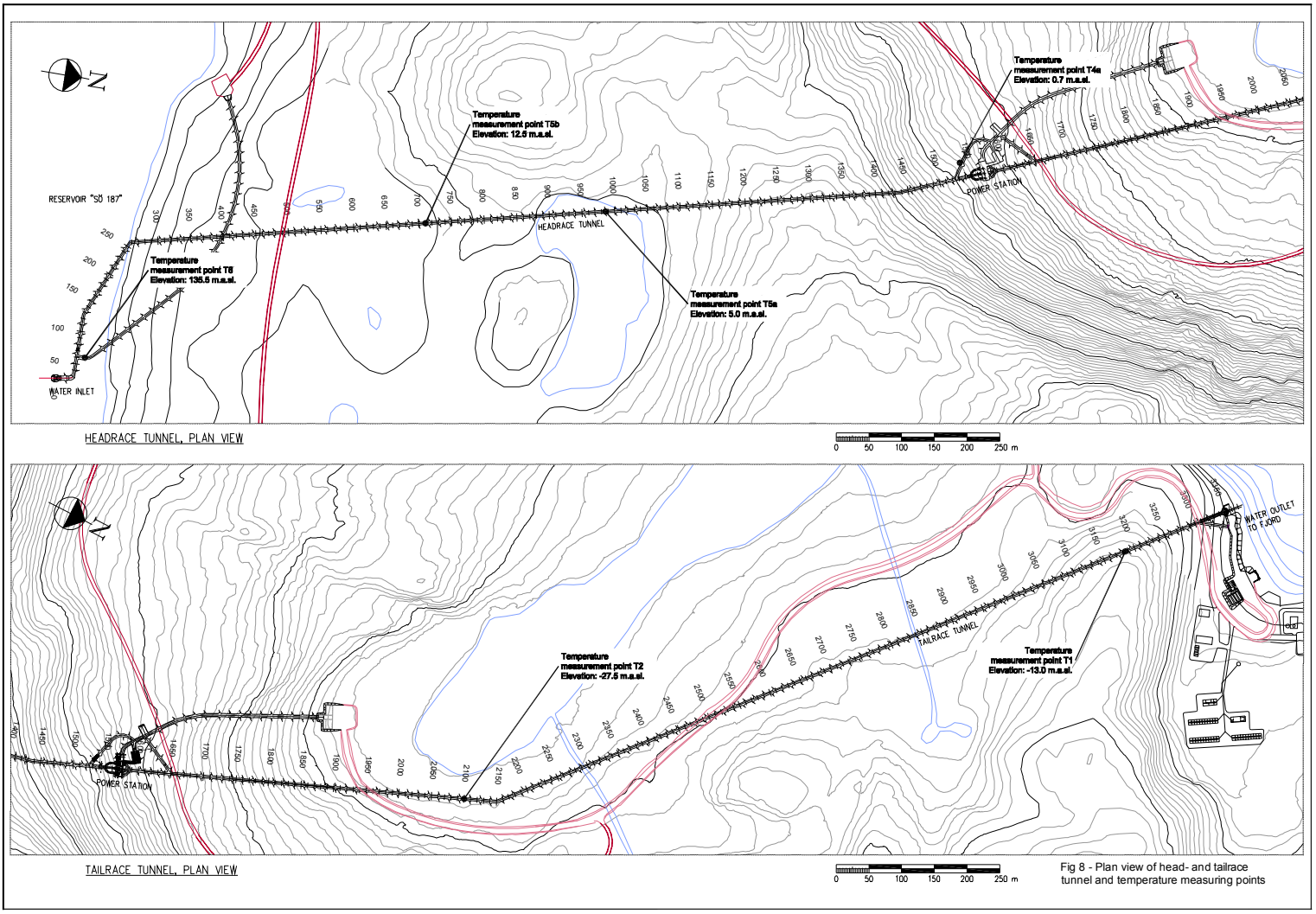

Fig 8 - Plan view of head- and tailrace tunnel and temperature measuring points

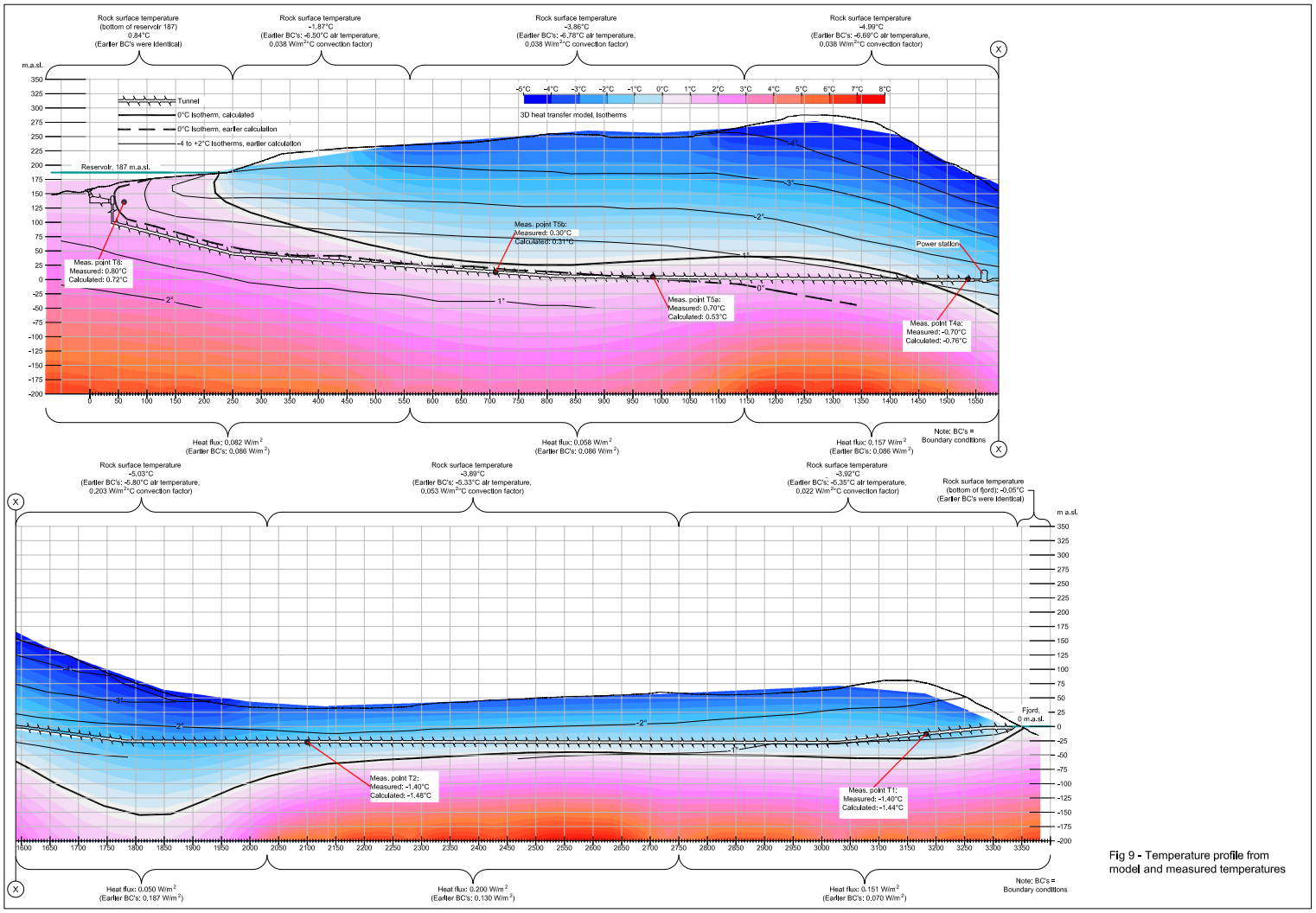

Fig 9 - Temperature profile from model and measured temperatures

ILULISSAT POWER PLANT

MEMO

PROJECT NO:	09304-002	DATE.:	2013-09-27
PROJECT PHASE:	41	NO.:	4090
AUTHOR:	ÓPE		
DISTRIBUTION:	ÆJ, ÞSL, EBJ/Verkís, GHG, HS/ÍSTAK		

Subject: Permafrost model, diversion tunnel - UPDATED

In the past years, a 3D heat transfer model has been developed to estimate the water flow through a hydropower plant head- and tailrace tunnels, situated in a permafrost rock in Ilulissat, Greenland, which is necessary to prevent the water from freezing. The latest result from this study [1] is based on temperature measurements taken through 3.3 km long head- and tailrace tunnels at various points during construction. These measurements were used to calibrate the heat transfer model and confirm earlier estimates of the minimum required flow, which was 315 l/s through a by-pass.

A similar study is presented here, for a 1 km long diversion tunnel between the upper and lower reservoirs in the hydropower plant in Ilulissat. The tunnel is situated under a mountain that reaches 340 meters above sea level (m.a.sl.), whereas the tunnel lies at an elevation of 160-180 m.a.sl. As no rock temperature measurements exist at this stage, the values obtained from the above mentioned study (heat flux from ground and estimate of rock surface temperature) will be used to estimate the possible range between maximum and minimum required flows that prevent water from freezing in the diversion tunnel.

In this updated report, the temperatures measured in the diversion tunnel during construction are compared to calculated scenarios presented earlier. The risk of freezing and an estimate of minimum required water flow through the tunnel is briefly discussed, following this comparison of model and measurements.

1 Finite element model and boundary conditions

Finite element model

An isometric view of the three-dimensional finite element model is shown in Fig 1.

The top elevations are based on a map of the land surrounding the tunnel from the upper to the lower reservoir. The tunnel length is around 1 km.

The bottom elevation of the model is 200 m below sea level. The width of the model is 400 m, i.e. 200 m from each side of the tunnel. The ends of the model reach around 50-100 m beyond both ends of the tunnel. The finite element distribution along the length and height of the model can be seen in Fig 1. The mesh around the tunnel can be seen in Fig 2, where a finer mesh nearest to the tunnel is needed, due to high thermal gradients in that region compared to the rest of the model.

Verkís hf.
Ármúla 4, 108 Reykjavík
+354 422 8000
verkis.is | verkis@verkis.is

Offices:
108 Reykjavík, Ármúla 4-6
108 Reykjavík, Suðurlandsbraut 4

300 Akranes, Stillholti 18
310 Borgarnes, Bjarnarbraut 8
400 Ísafjörður, Hafnarstræti 1

603 Akureyri, Austursíðu 2
700 Egilsstaðir, Kaupvangi 3b
800 Selfoss, Austurvegi 10

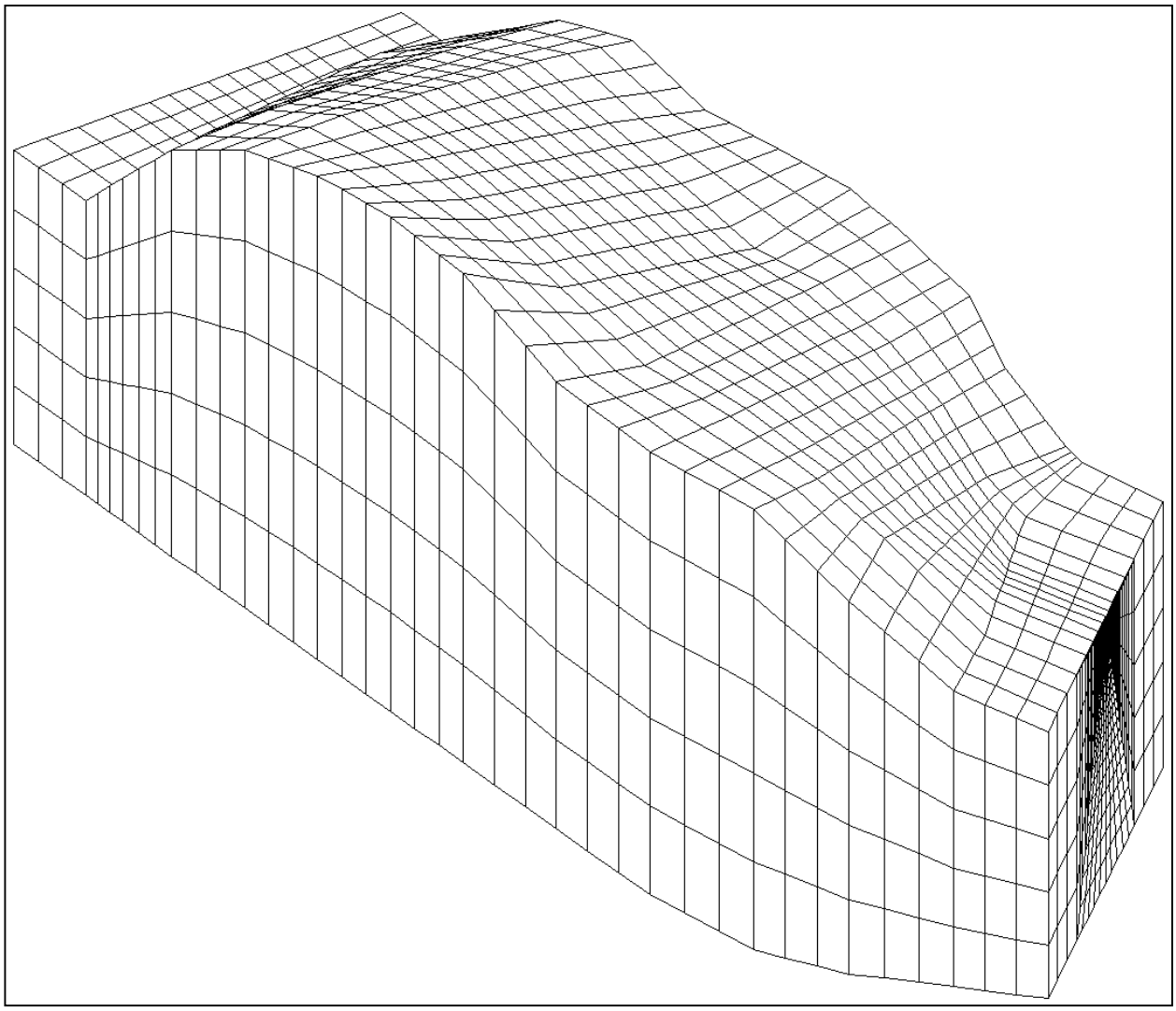

Fig 1 3D-model, isometric view showing finite element mesh on outer boundary

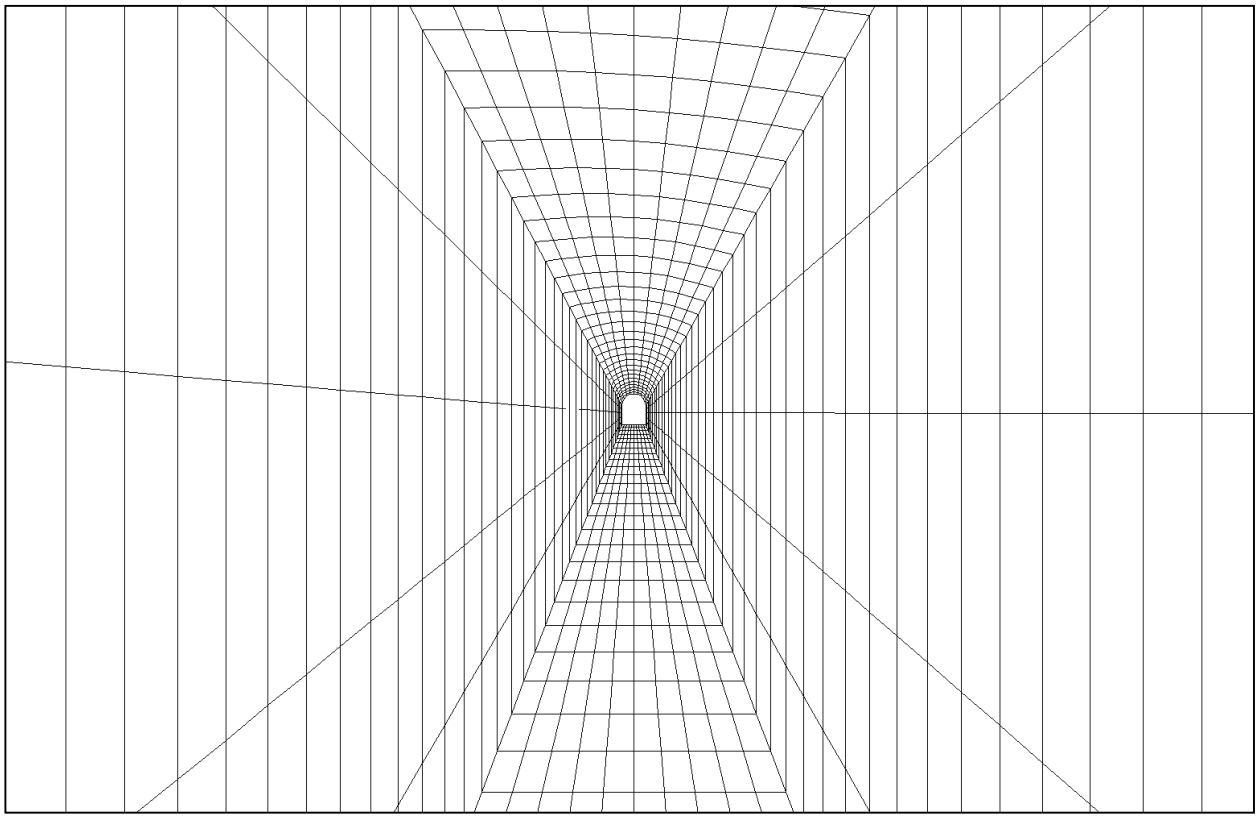

Fig 2 Finite element mesh, cross section perpendicular to the tunnel

The Thick line inside the model, shown in Fig 3 represents the inner boundary of the model, i.e. the inner tunnel wall. Water temperatures are imposed on this inner boundary and from temperature gradients in the surrounding rock, the heat flow from water to rock is calculated.

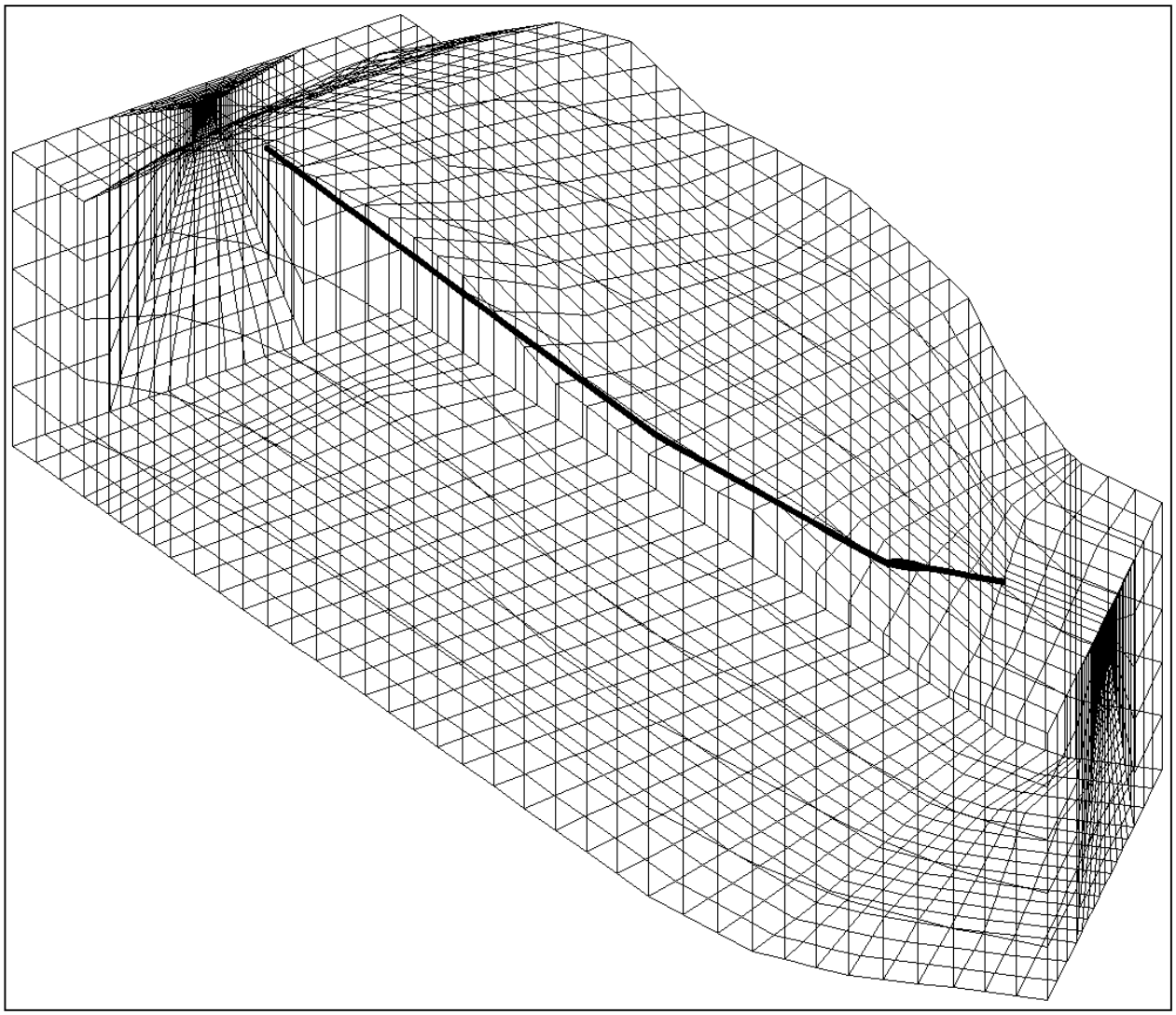

Fig 3 Inner and outer boundary of finite element model.

Thermal properties of rock

The following values are used for calculating heat conduction of the rock in the model. These values remain unchanged from the earlier study from 2012 [1]:

- Thermal conductivity: 3,5 W/m°C
- Specific heat capacity: 730 J/kg°C
- Density: 2.700 kg/m^3

Air temperature and estimated rock surface temperature

In earlier studies ([3], page 787), variation of air temperature with elevation is estimated to be 0.7°C for every 100 meters above sea level. In an earlier study for the head- and tailrace tunnels ([1]), a constant temperature was assigned to the top of the 3D heat transfer model in various locations, one of which was -5.03°C over an area at an elevation of 115 meters above sea level (m.a.sl.). This corresponds to -4.22°C rock surface temperature at sea level, the lowest value found in that study. This will be used in this calculation, where a surface temperature will be applied to the top surface of the model, which at an elevation between 198 and 361 m.a.sl. will be between -5.61 and -6.75°C, respectively.

Water temperature in reservoirs

The water temperatures in the two reservoirs are taken from an earlier study ([3]). The average water temperature in the lower reservoir is 0.84°C, while it is 2.07°C in the upper reservoir.

For calculation of heat lost from the water when it flows through the diversion tunnel, a value of 0.995°C is used for nominal conditions (water temperature at 25 m depth) but 0.210°C for extreme worst conditions (lowest temperature measured in the lake, at a depth of 10 m).

Heat flux from the ground

Two values are being considered as a possible range of heat flux from the ground.

The former (nominal conditions) is the average of various heat flux values obtained from calibration of an earlier study for the head- and tailrace tunnels ([1]), a value of 0.116 W/m^2.

The latter value (extreme worst conditions) is the lowest local value obtained from calibration in [1], or 0.050 W/m^2.

Zero heat flux boundary conditions

The horizontal variation of vertical heat flux is assumed to be negligible at 200 m from the side of the tunnels in the model and at 100 m from each end of the tunnel. This means that heat flux is zero through the vertical sides and vertical ends of the model (see Fig 1).

Also, during calibration of rock temperatures for steady state initial conditions, zero heat flux is assumed on the inside of the tunnel walls. This represents the assumption that no heat is added to or removed from the mountain while the tunnel is being constructed.

2 Calculations, results and temperature measurements

The following section describes how the model results from boundary conditions are used to calculate heat loss from the water, flowing from the upper to the lower reservoir. The nominal and worst case assumptions of water cooling are listed and a preliminary estimate of reasonable maximum and minimum water flow is presented. Finally, temperature measurements in the actual tunnel, from the last 1-2 years, are compared to model results.

Results from steady-state calculation

The temperature profile through a vertical plane lying along the tunnel is shown below, for nominal conditions (Fig 4, with 0.116 W/m2 heat flux from the ground) and extreme worst conditions (Fig 5, with 0.050 W/m2 heat flux from the ground).

It is obvious from these figures that the magnitude of heat flux from the ground has a strong influence on temperatures around the diversion tunnel. Temperature measurements in the rock surrounding the tunnel - at various locations within the tunnel - will be necessary to ascertain the heat flux and calibrate the model.

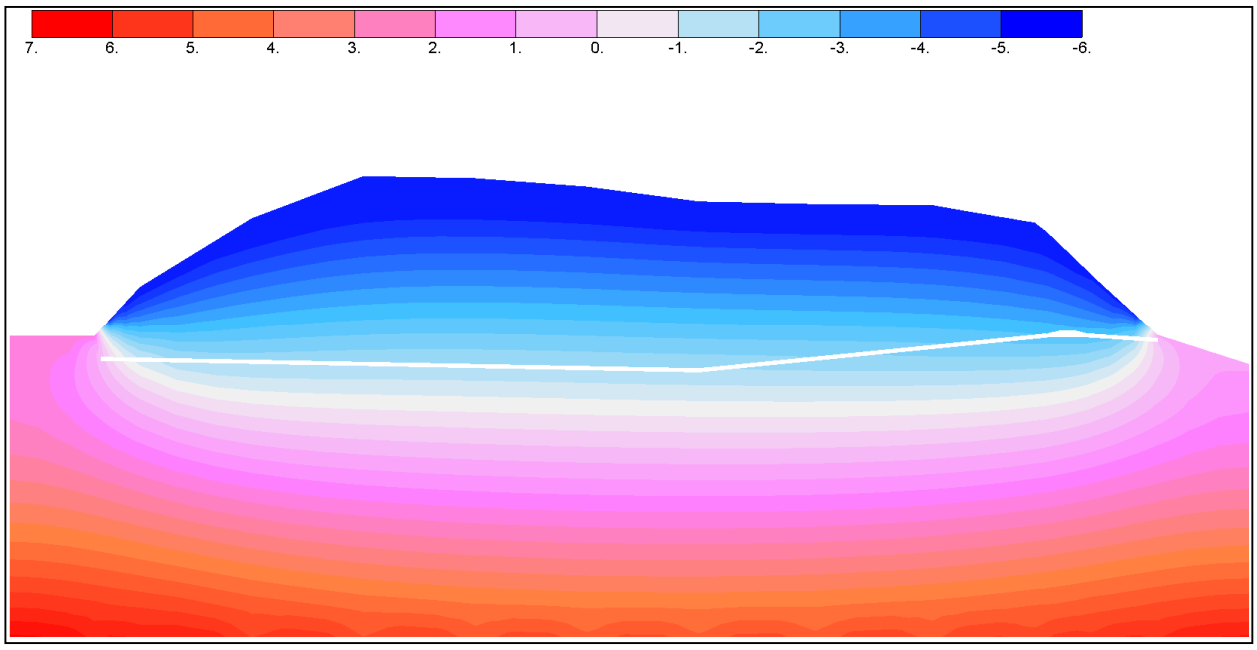

Fig 4 Temperature profile through rock, nominal conditions

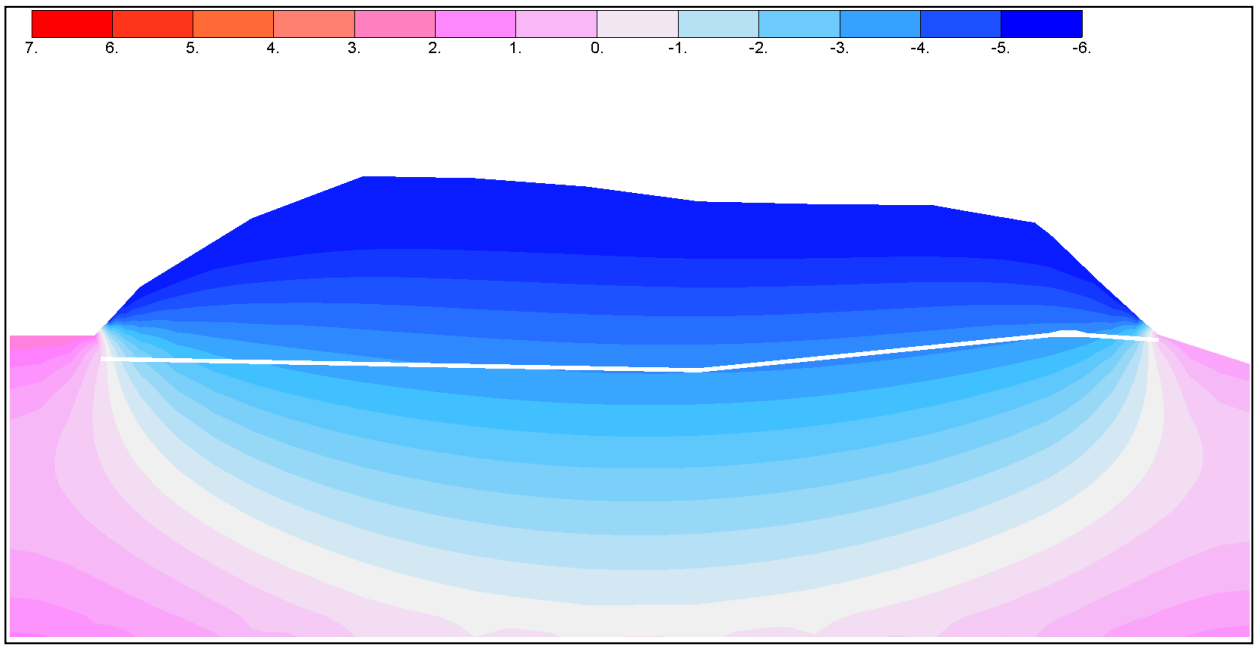

Fig 5 Temperature profile through rock, extreme worst conditions

Calculation of heat loss from water

The following conditions are assumed when calculating heat loss from water, running through the tunnel at the minimum flow rate that ensures that water temperature never goes below 0°C:

- The wall temperature is the same as the water temperature in the tunnel. This is a conservative estimate, since a film co-efficient between water and rock (which is very high for water) means that rock would be at a slightly lower temperature than the water.
- Water from the reservoir is 0.995°C (nominal conditions) or 0.210°C (extreme worst conditions) when entering tunnel.
- If water enters rock at higher temperature than the fluid, it does not absorb heat from the rock. It only loses heat to colder rock. Again, this is a conservative estimate.

The calculation is performed in the following steps, in 11 discrete tunnel sections, where water temperature is assumed constant in each section and over a period of 24 hours:

1. Initial temperature of water (0.210°C or 0.995°C) is set as a temperature boundary condition on the tunnel walls. Wall temperature is equal to water temperature.
2. The program calculates the heat flow through the walls, based on temperature gradient through the rock, after being exposed to constant 0.210/0.995°C water temperature for 24 hours. The water temperature profile changes in subsequent iterations, when cooling of water has been recalculated.
3. After the initial conditions, the total heat flow (q, kW) in each of the 11 tunnel sections is equal to the heat lost from water, which is the product of the water mass flow, heat capacity and temperature drop in the fluid, or $q = \dot{m} \times C_p \times \Delta T$. This quantity is always positive, i.e. temperature change is always zero or negative. The water mass flow, $\dot{m}$, is the product of the water density (1000 kg/m^3) and water flow, in l/s. Water heat capacity is C_p=4.224 kJ/kg°C at at 0°.
4. The temperature profile of the water (or water cooling along the tunnel) is calculated through each section.
5. The new temperature profile of the water is added as a new temperature boundary condition on the tunnel wall (step 2 through 5 repeated) and flow is varied until water temperature is always at least 0°C or does not change significantly between iterations.

Results of the calculation can be seen in Fig 6 (nominal conditions) and Fig 7 (extreme worst conditions).

The minimum flow required for the nominal condition is 93 l/s, where the water cools from 0.995 to 0°C, while flowing through rock that is initially at a temperature of -2 to -3°C.

The minimum flow required for extreme worst conditions is 656 l/s, where the water cools from 0.210 to 0°C, while flowing through considerably colder rock, initially at -3 to -4°C.

Both results, based on the first 24 hours of operation of the tunnel are highly uncertain at this point, as the temperatures inside the mountain over the tunnel are unknown and require some local temperature measurements for more accurate results.

It should be noted that if water flows through the tunnel over a longer period of time than 24 hours, the surrounding rock will heat up even further and the need for minimum flow of 0.2-1.0°C water will decrease rapidly. Also, during construction of the tunnel, some heat from machinery and equipment will heat up the rock above the present temperature.

At this stage, no measurements of rock exist around the diversion tunnel. During construction, temperatures of rock around the tunnel will be measured and compared to the calculated temperatures, as shown in Fig. 6 and Fig. 7 (blue line). If these measured temperatures are above -3 to -4°C throughout the tunnel, the model calculations and results should be on the safe side, in regards to minimum required flow.

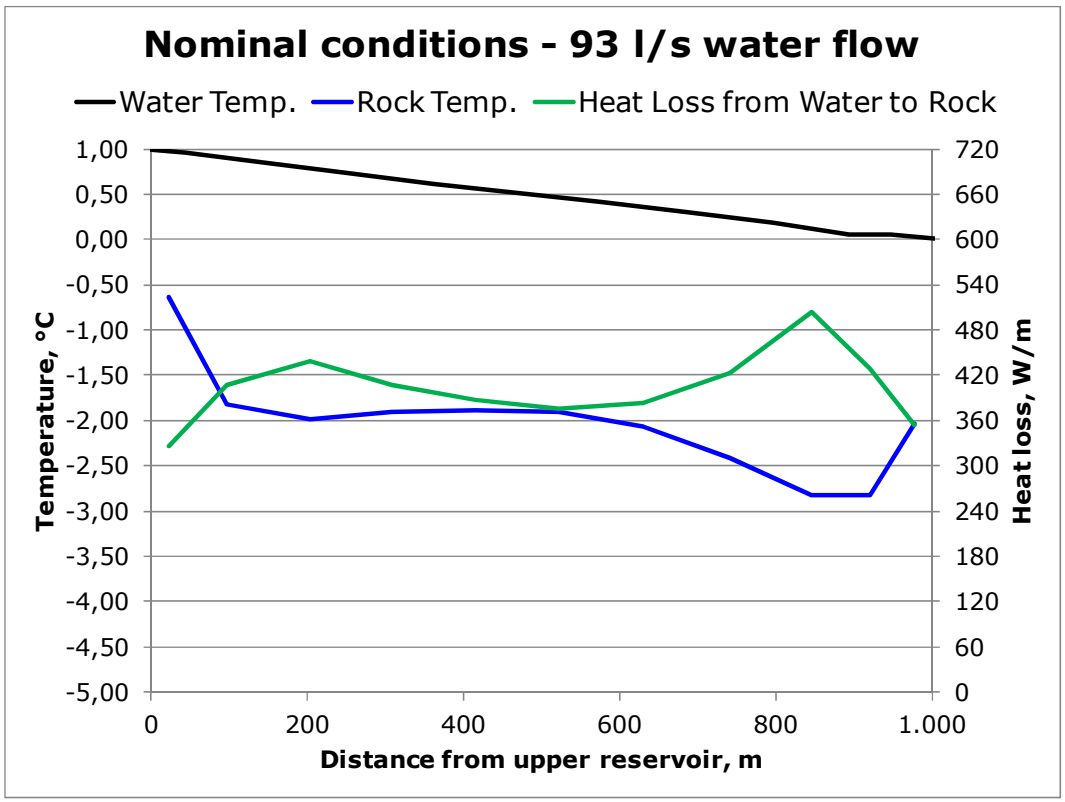

Fig 6 Temperature profile of water and rock, nominal conditions.

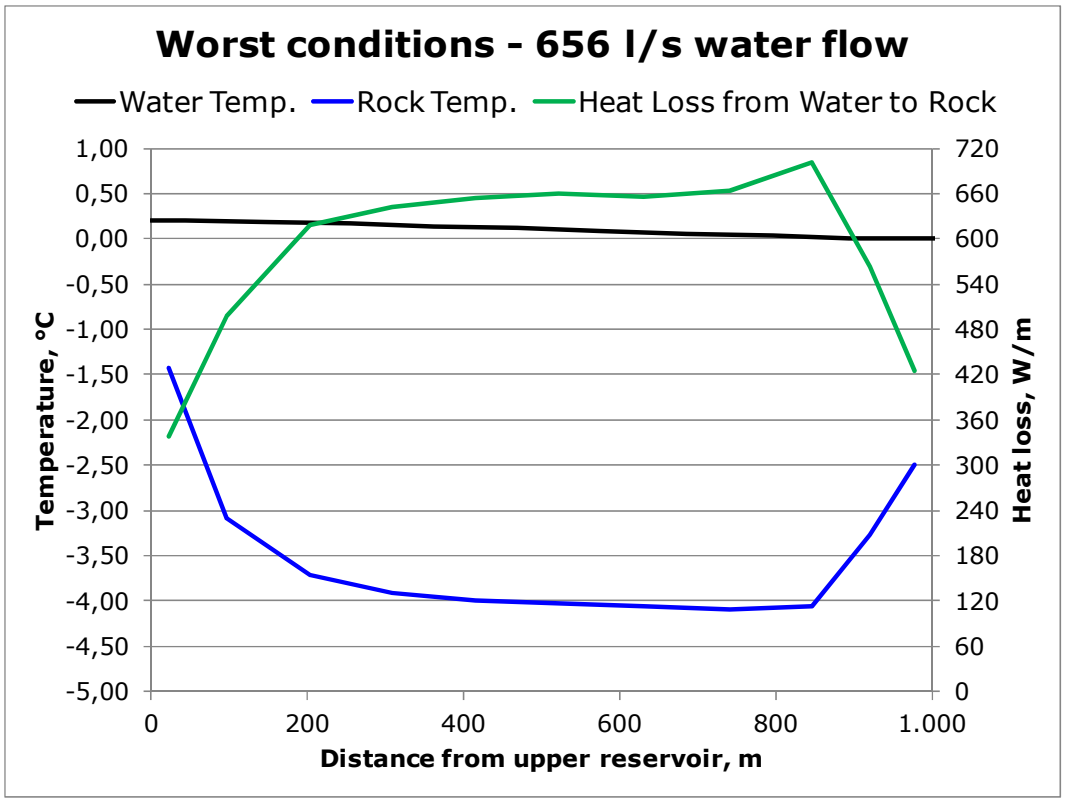

Fig 7 Temperature profile of water and rock, extreme worst conditions.

Temperature measurements in diversion tunnel – comparison to model

Temperatures in the diversion tunnel were measured in three locations in the period of November 2012 through May 2013 ([7]). The rock temperature was measured at depths of up to 6 meters in boreholes perpendicular to the tunnel walls.

The deepest measurements (6 m) are considered here as a realistic comparison to initial rock temperatures in the heat transfer model, as air temperature fluctuations have the least effect at this depth. The results from these three measurements are shown below, along with nominal and extreme worst conditions as predicted by the model.

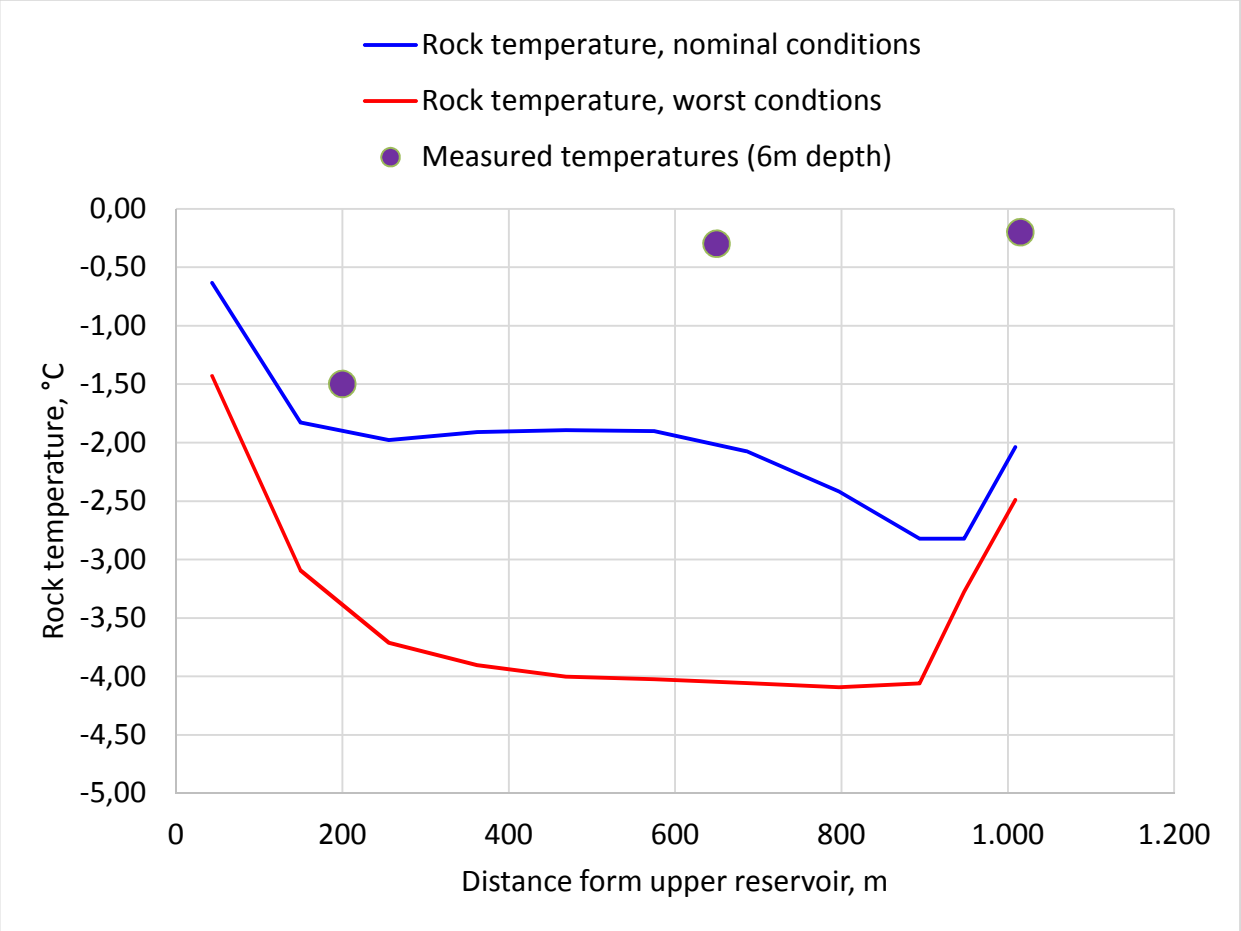

Only near the 200 meter mark of the tunnel is there some similarity between measured and predicted values (nominal conditions in model), as the measured temperature is less than 0,5°C higher than predicted. The two values measured at approximately 650 and 1000 meters from the upper reservoir, however, are between 1,5°C and 2,0°C higher than predicted by the nominal conditions. Furthermore, the measured values presented here are the lowest values measured during several time periods – they are actually higher in other cases. They do, however, remain fairly constant over time at this depth in the tunnel wall (6m).

3 Conclusion

A 3D heat transfer model has been developed to estimate the minimum water flow through a diversion tunnel between the upper and lower reservoir at the hydropower plant at Ilulissat, Greenland. Currently, very little temperature data exists to ascertain an accurate estimate of this flow, which currently is thought to lie between 93 and 653 l/s.

Temperature measurements have now been taken at three locations within the tunnel. The measured values are at least 0,5 to 1,5°C higher than predicted by the nominal conditions (resulting in minimum flow of 93 l/s). It can be concluded that all assumptions done by the

model have turned out to be very conservative, resulting in less than 93 l/s minimum theoretical flow to prevent freezing.

The recommended operation of the diversion has been proposed in [6]. In the memo it is recommended that during the first 2 to 4 years after installation, at least one of the two diversion pipes shall be in operation 24 h for 365 days per year. This provides 2 m^3/s to 4 m^3/s minimum discharge through the tunnel. This is not considered to reduce the energy production potential of the system significantly, see [6]. During these first years it is important to have the smaller pipe open through the whole summer when the water temperature is expected to be higher than 2 °C. The inflow to the upper reservoir during the summer is much more than needed to fill the reservoir even during the driest summers. A lot of warm water is therefore available to heat up the rock mass around the tunnel. If it would become necessary to stop the flow it can be done for a limited time. If the water temperature of the still-standing water in the tunnel becomes close to 0 °C, the coldest water will accumulate at the highest part just upstream of the valve chamber where accurate temperature meters will be located. Before the measured temperature reaches 0 °C a discharge through the tunnels must be re-established. The length of such a stop can be days and even up to weeks depending on the initial water temperature and how much the rock has been warmed by the warm summer flow. No separate by-pass system to obtain minimum flow is therefore necessary.

[1] Einarsson, O., Permafrost Model, Updated By New Temperature Measurements, Verkis Memo no. 2363, 2011-01-24

[2] Mai, Henrik. Hydropower Tunnels in Permafrost. Underground Hydropower Plants, Oslo, June 22-25, 1987.

[3] Grønlands Tekniske Organisation. Vandkraftværk Paakitsup Akuliarusersua Ilulissat/Jakobshavn, Permafrostundersøgelse, Endelig Rapport. LIC Consult Rådgivende Ingeniører. November 1985.

[4] Anlægstekniske forundersøgelser, Paakitsup Akuliarusersua. GTO. 30. September 1987.

[5] Web site: http://www.climatetemp.info/greenland/ilulissat-jakobshavn.html

[6] ÞSL. Forbedret design af overføringstunnel, beregninger angående gennem-strømningen og drift strategier. Memo, 1–MB-1980, from Verkis. 2011-11-04

[7] Temperature measurements carried out by Ístak in 2012 and 2013 (Excel sheets "Tunneltemp-pt100_7-10 130520.xlsx" and " Tunneltemp-pt100_11.xlsx").

19 Appendix 3

TEMPERATURMÅLINGER - BOREHULLER

BORING Nr: K84901

Etableret: 26/8 -1984

PAAKITSOQ

OVERFLADEKOTE: 42,4

Hældning med vandret: 60°

FØLERE Nr.	Lodret Dybde	Kote	25.9.84	6.12.84	1.5.85	18.5.85	30.7.85	14.8.85	13.9.85	10.12.85	2.5.86	16.9.86	10.11.86	17.88	11.8.88	28.9.88			
'8'	6,9	35,5	-1,54	-1,35	-5,44	-4.87	-1,56	-0,81	-0,04	-0,41	-4,14	+0,62	+0,28	-2,64	-0,82	+0.46			
'50'	43,3	-0,9	-1.79	-1,17	-1,20	-1,28	-1,23	-1,19	-1,21	-1,36	-1,53	-1,44	-1,44	-1,47	-1,39	-1,43			
'73'	63,2	-20,8	-1,54	-0,79	-0,78	-0,80	-0,80	-0,79	-0,79	-0,87	-1,04	-0,89	-0,86	-0,92	-0,86	-0.90			
m.	m.	m.							°C										

NUNA.TEK FORUNDERSØGELSER
HYDRO-TEKNISKE UNDERSØGELSER

TEMPERATURMÅLINGER · BOREHULLER

BORING Nr: K 84902

Etableret: 69-1984

PAAKITSOQ

OVERFLADEKOTE: 31,9

Hældning med vandret: 90°

FOLERE																		
Nr.	Lodret Dybde	Kote	25.9.84	6.12.84	1.5.85	18.5.85	30.7.85	14.8.85	13.9.85	10.12.85	2.5.86	16.9.86	10.11.86	4.7.88	11.8.88	28.9.88			
'8'	8	23,9	-3.85	-3.17	-3.38	-3.50	-3.56	-3.49	-3.35	-2.84	-2.85	-2.91	-2.66	-3.35	-3.23	-3,02			
'15'	15	16,9	-2.82	-2.17	-2.66	-2.66	-2.69	-2.72	-2.80	-2.79	-2.63	-2.63	-2.61	-2.59	-2.62	-2,66			
'59'	59	-27,1	-1,54	-1.41	-1.41	-1.40	-1,38	-1,39	-1.43	-1.43	-1.43	-1.43	-1.44	-1.44	-1,42	-1,44			
m	m	m							°C										

NUNA.TEK FORUNDERSØGELSER
HYDRO-TEKNISKE UNDERSØGELSER

TEMPERATURMÅLINGER - BOREHULLER

BORING Nr: K84903

Etableret: 29-1984

PAAKITSOQ

OVERFLADEKOTE: 135,3

Hældning med vandret: 90°

FØLERE																			
Nr.	Lodret Dybde	Kote	21.9.84	25.9.84	6.12.84	1.5.85	18.5.85	30.7.85	14.8.85	13.9.85	10.12.85	2.5.86	15.9.86	10.11.86	4.7.88	11.8.88	28.9.88		
'8'	8	127,3	-4.62	-5.00	-4.27	-6.93	-6.99	-5.25	-4.75	-4.10	-3.28	-5.84	-3.64	-2.87	-5.35	-4.35	-3.34		
'10'	10	125,3	-5.13	-5,38	-4,58	-5.93	-6.09	-5.58	-5.24	-4.79	-3.83	-5.16	-4.23	-3.59	-5.29	-4.75	-4.02		
'15'	15	120,3	-4.87	-5,38	-4,97	-4.87	-4.97	-5.21	-5.08	-5.11	-4,64	-4.44	-4.63	-4.38	-4.60	-4.62	-4.54		
'50'	50	85,3	-3.33	-3.33	-3,10	-3,10	-3.09	-3.09	-3.00	-3.11	-3.16	-3.30	-3,19	-3.18	-3.21	-3.18	-3.22		
'59'	59	76,3	-3.08	-3.08	-2,95	-2.93	-2.89	-2.92	-2.82	-2.92	-2.96	-2.96	-2.97	-2.99	-3.01	-2.99	-3.04		
m.	m.	m.							°C										

NUNA.TEK FORUNDERSØGELSER
HYDRO-TEKNISKE UNDERSØGELSER

20 Appendix 4

TEMP UDVIKLING

BOREHUL **4b**

ISTAK

Dybde / Dato	Luft	Væg	0.5	2.0	4.0	6.0	
17/05/2011	3.5	3.6	2.1	0.9	-0.1	-0.3	No ventilation
19/05/2011	1.5	5.4	2.3	1	0.2	0	
22/05/2011	1.5	4.4	2.1	0.8	0.1	-0.2	
24/05/2011	2	2	2	0.9	0.1	-0.2	
25/05/2011	4.5	5.8	2	1	0.1	-0.3	
27/05/2011	1.5	3.4	2.1	1	0.2	-0.3	
30/05/2011	0	3.8	1.9	0.9	0.2	-0.3	
01/06/2011	3	0.4	1.9	1	0.2	-0.3	
05/06/2011	13	3	2.1	0.9	0.3	-0.2	
10/06/2011	14	6.4	2.4	1.1	0.3	-0.2	
13/06/2011	12	4.6	2.7	1.1	0.4	-0.2	
20/06/2011	7	4	3	1.4	0.4	-0.1	
29/06/2011	13	5.8	3.5	1.6	0.5	0	
07/07/2011	12	6	4.6	2	0.7	0	
11/07/2011	14	6.2	4.5	2.2	0.7	0.1	
14/07/2011	11	6	4.9	2.3	0.8	0.1	
18/07/2011	13	6.4	4.7	2.5	0.9	0.1	
28/07/2011	12	9.2	5.6	2.9	1.2	0.3	
03/08/2011	14	8.2	5.9	3	1.3	0.4	
10/08/2011	13	7.8	6.3	3.2	1.5	0.5	
19/08/2011	7.5	7	5.6	3.4	1.7	0.6	
26/08/2011	9	6.2	4.9	3.3	1.7	0.7	
01/09/2011	5.5	6.2	4.9	3.2	1.8	0.8	
14/09/2011	5	4.4	4.5	3.2	1.9	0.8	
02/10/2011	0	3.4	3.4	2.6		1	
07/10/2011	0	0.8	2.6	2.5		1	
14/10/2011	-4	0.6	2	2.3	1.5	1	

21/10/2011	-7	0.2	1.8	1.8	1.4	1	
29/10/2011	-10	-1.4	1	1.5	1.2	0.9	
06/11/2011	-12	-1.4	0.6	1.2	1.1	0.9	
18/11/2011	4	0.4	1.1	0.9	0.9	0.8	Sensor at 6m damaged
24/11/2011	-14	-1.4	0.9	1	0.8	0.8	
30/11/2011	-15	-1.2	0.4	0.9	0.8	0.7	
06/12/2011	-20	-1.6	0.2	0.8		0.7	
13/12/2011	-11	-0.6	0.3	0.5	0.7	0.7	
28/12/2011	-10	0.8	0.4	0.4	0.5	0.5	
10/01/2012	-16	2.4	0.5	0.4		0.5	
24/01/2012	-9	2.4	0.5	0.4		0.4	
07/02/2012	-10	0.6	0.6	0.3			
21/02/2012	-24	-0.4	0.5	0.4		0.3	Injection around plug
06/03/2012	-22	0.2	0.6	0.3		0.3	
20/03/2012	-21	2.2	0.5	0.4		0.3	
03/04/2012	5	1.8	0.7	0.3		0.3	Waterfilling started 1.10 2012,
15/04/2012	5	1.6	0.4	0.4	0.4	0.2	
03/05/2012	4	1.2	0.4	0.4		0.1	
20/05/2012	2	3.6	2.4	1.1		0.2	
17/06/2012	8	4.6	4.2	2.2		0.3	Injection around plug
26/06/2012	16	7.2	4.2	2.6		0.5	
20/07/2012	14	6.4	3.7	2.5		0.7	
05/08/2012	16	4.2	3.4	2.5		1	
09/09/2012	3	4.8	3.7	2.2		0.6	
MIN	-24	-1.6	0.2	0.3	-0.1	-0.3	
MAX	16	9.2	6.3	3.4	1.9	1	
AVE	1.265	3.286	2.500	1.522	0.776	0.350	

TEMP UDVIKLING
4c)

	Dybde Dato	Luft	0	0.5	3.0	6.0	9.0	12.0	15.0	18.0	21.0	24.0	26.0	
ISTAK	25/09/2011	3	3.2	3.8	3.9	2.8	2.4	2.6	3.2	3.4	2.5		0.7	
	02/10/2011	0	3.2	3.7	3.3	2.5	2.2	2.4	3	3.2	2.3		0.6	
	07/10/2011	0	1.1	2.6	3.1	2.5	2.2	2.4	2.9	3	2.2		0.5	
	14/10/2011	-4	0.5	1.8	2.8	2.4	2.2	2.4	2.7	2.6	2.1	1.2	0.6	
	21/10/2011	-7	0.2	1.8	2.2	2.3	2.2	2.3	2.4	2.2	1.9	1.2	0.6	
	29/10/2011	-10	-0.6	0.9	1.9	2.2	2.2	2.2	2.2	2	1.7	1.1	0.6	
	06/11/2011	-12	-1.6	0.3	1.4	2	2.1	2.1	1.8	1.5	1.5	1.1	0.6	
	18/11/2011	4	-0.8	1.4	1.1	1.7	2	1.9	1.7	1.6	1.3	1	0.5	
	24/11/2011	-14	-1.8	0.4	1.4	1.6	1.9	1.8	1.8	1.7	1.3	0.9	0.6	
	01/12/2011	-11	-1	-0.1	1	1.5	1.8	1.8	1.7	1.7	1.3	0.9	0.6	
	06/12/2011	-20	-2.2	-0.5	0.8	1.5	1.7	1.7	1.7	1.8	1.3	0.9	0.6	
	13/12/2011	-11	-0.8	-0.1	0.6	1.3	1.6	1.6	1.7	1.9	1.2	0.9	0.6	
	28/12/2011	-10	0	0.4	0.7	1.1	1.4	2.1	1.6	1.5	1.2	0.8	0.5	
	10/01/2012	-16	0.5	0.5	0.7	1	1.3	1.4	1.4	1.3	1.1	0.8	0.5	
	24/01/2012	-9	1.4	0.6	0.8	1	1.3	1.3	1.3	1.2	1	0.9	0.5	
	07/02/2012	-10	0.6	0.6	0.8	0.9	1.1	1.2	1.3	1.2	0.9	0.7	0.4	
	21/02/2012	-24	-0.4	0.4	0.9	0.9	1.1	1.1	1.2	1.2	0.9	0.7	0.5	
	06/03/2012	-22	0.4	0.6	0.7	0.9	1	1.1	1.2	1.2	0.9	0.7	0.4	
	20/03/2012	-21	1.2	0.5	0.7	0.8	1	1	1	1	0.8		0.4	
	03/04/2012	5	1.2	1.1	0.7	0.8		0.9	1	1		0.6	0.4	
	15/04/2012	5	1.4	0.2	0.8	0.8	0.9	0.9	1.1	1.6	0.8	0.6	0.4	
	03/05/2012	4	1.2	1.4	0.8	0.8	0.9	1.1	1.6	1.9	1.3		0.4	
	20/05/2012	2	2.8	1.8	0.8	0.8	0.9	1.1	2	3.1	1.5	0.5	0.4	
	17/06/2012	8	4.2	4.4	3.5	1.4	1.2	1.9	4.9	8.8	3		0.6	
	26/06/2012	16	8.8	5.7	3.9	1.6	1.4	2.3	5.3	7.6	4.2	1.4	0.7	
	20/07/2012	14	5.2	4	3.4	2.2	2.1	2.9	4.4	5.2	3.8	2	1.1	
	05/08/2012	16	3.8	3.5	2.7	2.4	2.4	3	3.2	3.4	3.4	2	1.3	
	27/08/2012	3	5.2	4	3.3	2.5	2.6	3	3.6	3.9	3.1	2.1	1.3	Concrete work in
	28/08/2012	4	2.8	4.4	3.4	2.5	2.6	3	3.6	3.8	3	2.1	1.3	plug started 1 hr.
	09/09/2012	3	4.8	4.8	4.4	2.9	2.7	3	3.4	3.7	2.9	2	1.4	
	01/10/2012	0	3.8	4.3	4.8	4.2	3.5	3.1	3.4	3.5	2.8	2.1	1.4	
	05/10/2012	0	3	4.6	4.7	4.3	3.7	3.2	3.4	3.3	2.7	2	1.4	Chemical injection aro
	10/10/2012	-8	3	4.2	4.7	4.3	3.9	3.3	3.2	3	2.6		1.4	Headracetunnel water
	18/10/2012	-3	3.8	4.1	4.4	4.4	3.9	3.5	3.3	2.6	2.5	1.9	1.5	
	09/11/2012	-9	2.8	3.2	3.6	3.2	3.8	3.1	2.3	1.5	1.4	1.7	1.4	El.production started
	23/11/2012	-16	2.6	2.5	3.1	3.5	3.5	2.9	2	1.3	1.5	1.6	1.3	
	29/11/2012	-4	3.6	3.1	2.9	3.3	3.4	2.7	1.9	1.2	1.4	1.5	1.3	
NUKIS.	10/12/2012	-9	0.4	2.9	3.0	3.1	3.2	2.6	1.8	1.1	-0.4	0.1	1.2	
	02/01/2013	-15		2.7	2.8	2.7	2.3	2.2	1.4	1	0.3	-0.9	1.1	
	16/01/2013	-7	0.8	2.7	2.7	2.5	2.5	2	1.3	0.9	-0.5		1.1	
	08/12/2013	-8	1.2	2	1.3	1.6	1.4	1	0.8	0.6	-0.2	-0.2	0.6	
	25/01/2014	-18	-0.2	2.8	2.0	1.6	1.4	1	0.7	0.5	0.4	-0.1	0.8	
	MIN	-24	-2.2	-0.5	0.6	0.8	0.9	0.9	0.7	0.5	-0.5	-0.9	0.4	
	MAX	16	8.8	5.7	4.8	4.4	3.9	3.5	5.3	8.8	4.2	2.1	1.5	
	AVE	-5	1.69	2.24	2.3	2.1	2.1	2.1	2.3	2.4	1.7	1.1	0.8	